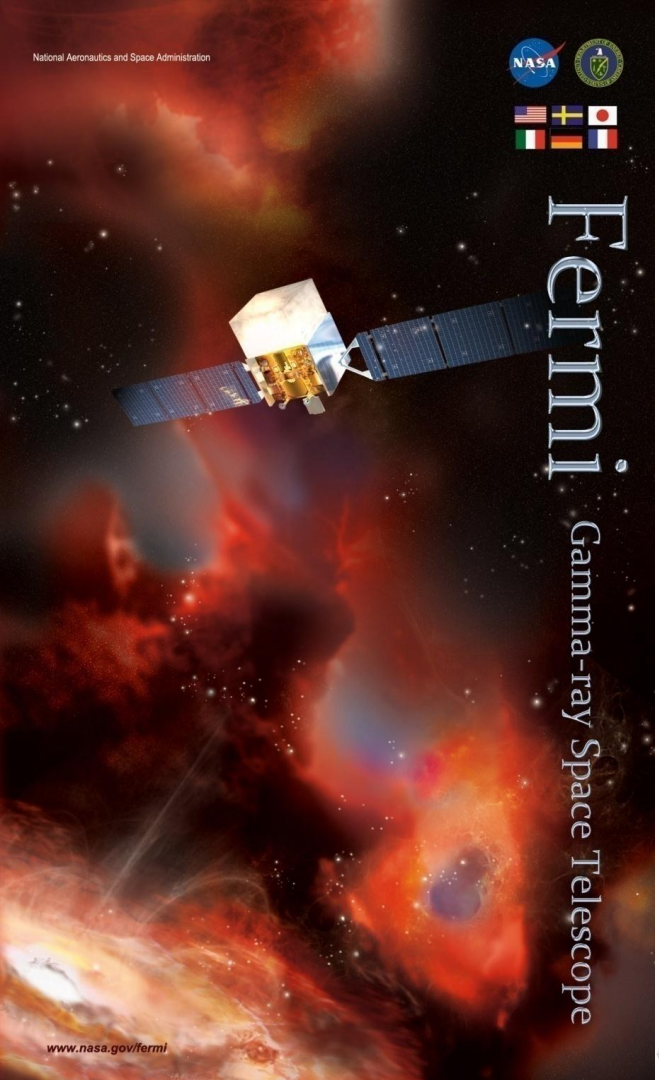

The Fermi-LAT Light Curve Repository and AGN variability

Janeth Valverde
Marquette University

What is an AGN?

- A few % of galaxies.
- Activity centered in the galactic nucleus.
- Rapid variations => extremely compact source.
- Central supermassive black hole (SMBH) $\gtrsim 10^9$ solar masses, surrounded by accretion disk.
- Strong twisted magnetic fields (B), possibly confine particles in the jet (Blandford & Znajek 1977, Blandford & Payne 1982).
- Billions of light years away => possibly an early stage in development.

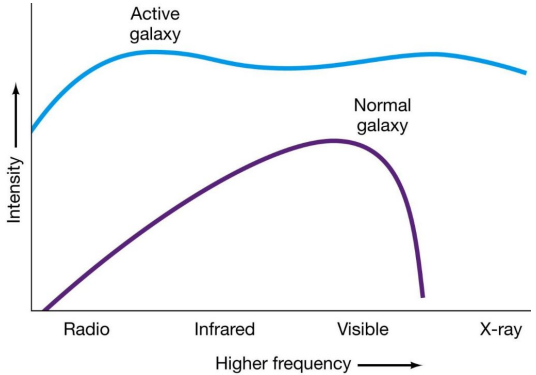

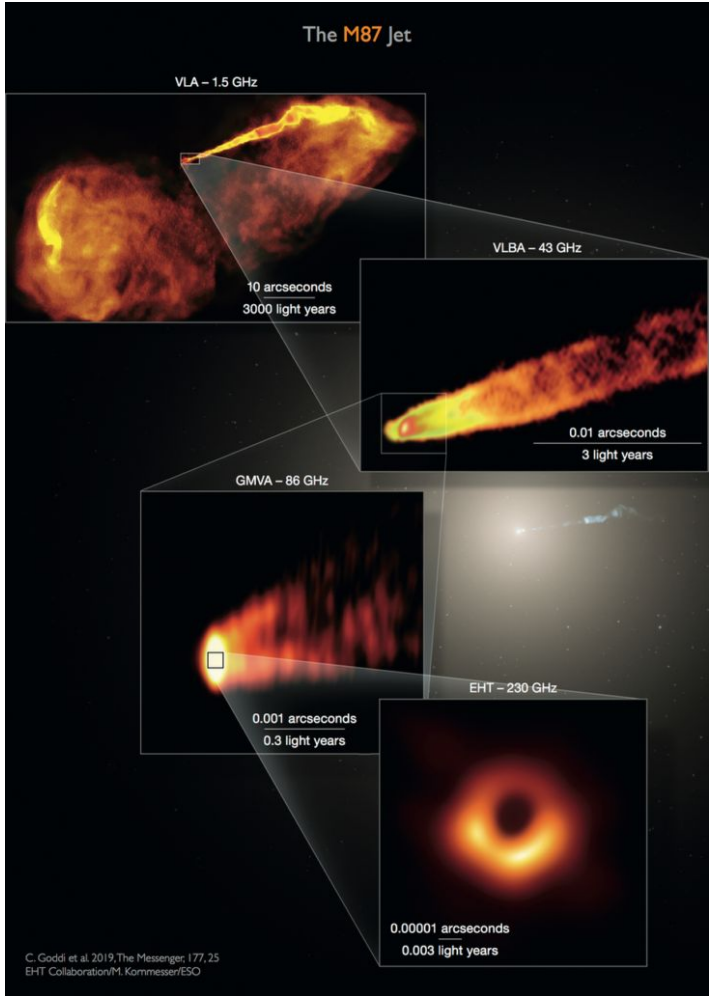

What we see depends on how we see it

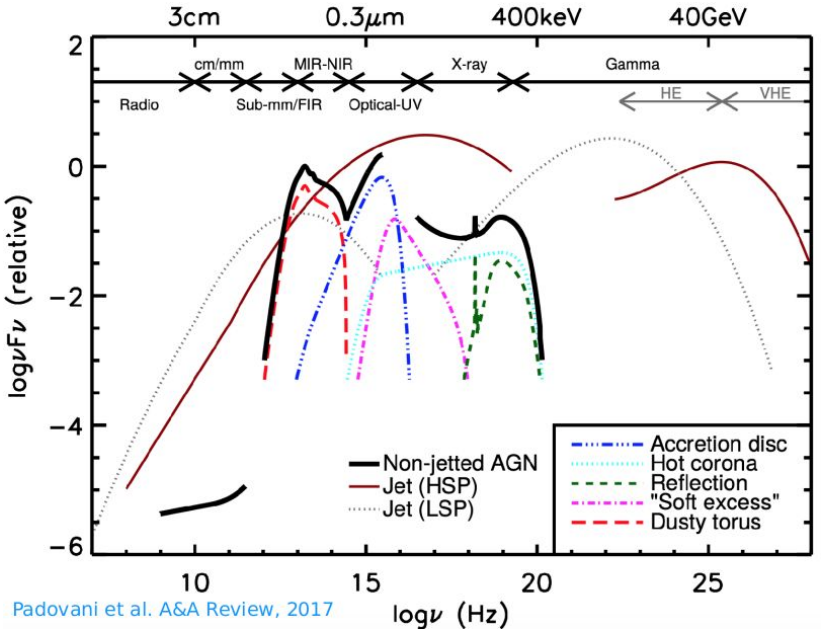

Padovani et al. A&A Review, 2017

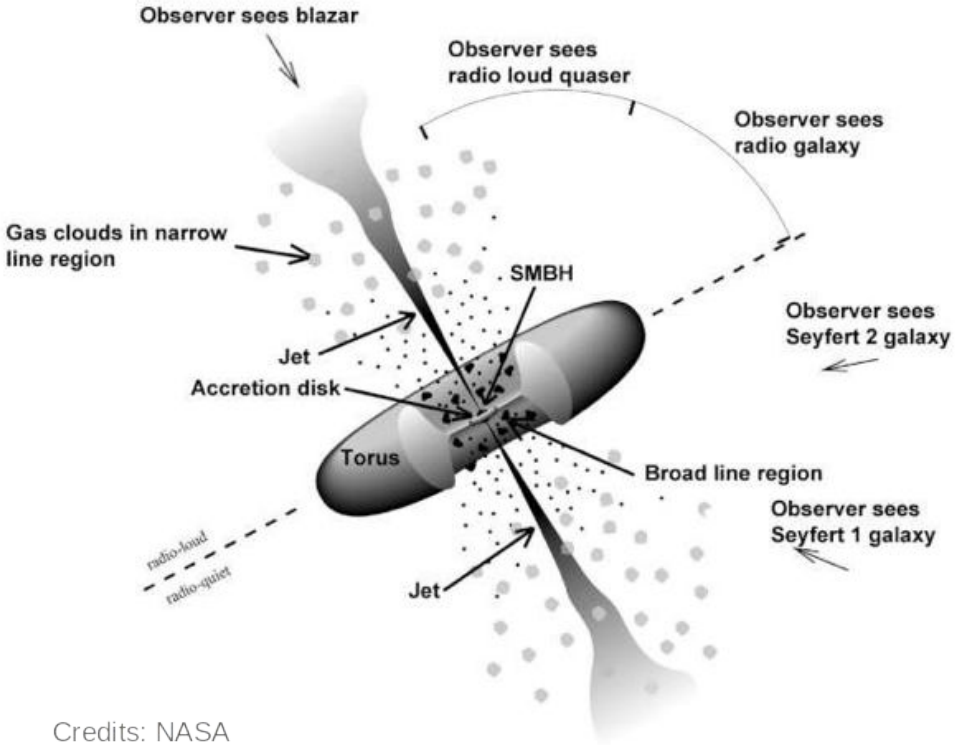

Credits: NASA

Blazars

- A few % of AGNs, radio loud.
- Jet points at us (animation).
- Can be flat spectrum radio quasars (FSRQs, broad emission lines) or BL Lac objects with weak or no emission or absorption lines.
- Large amplitude variability.
- Polarization.
- Relativistic beaming, Doppler factor:

$$\delta = \frac{1}{\gamma(1 - \beta\ \cos(\theta))}, \qquad \gamma = (1 - \beta^2)^{-1/2}$$

- Characteristic spectral energy distribution (SED).

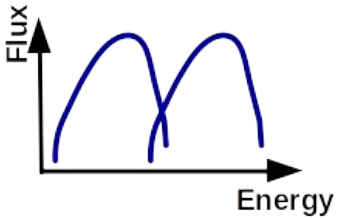

FSRQs

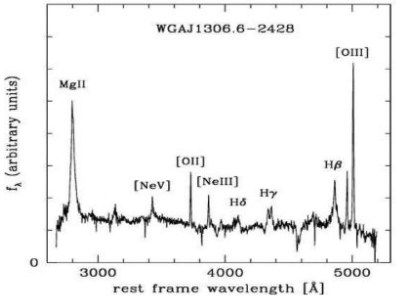

BL Lacs

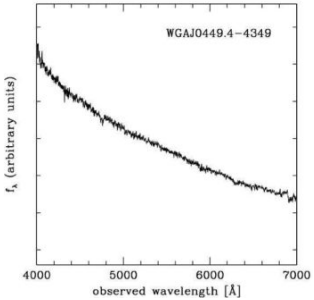

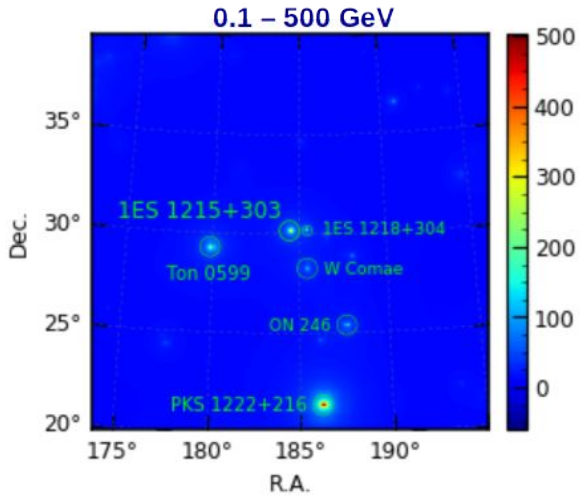

Blazar classification

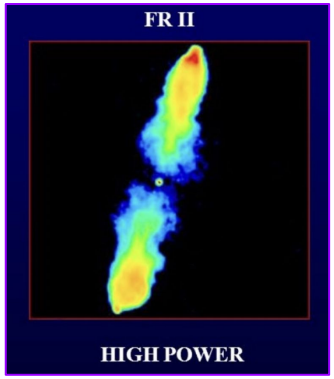

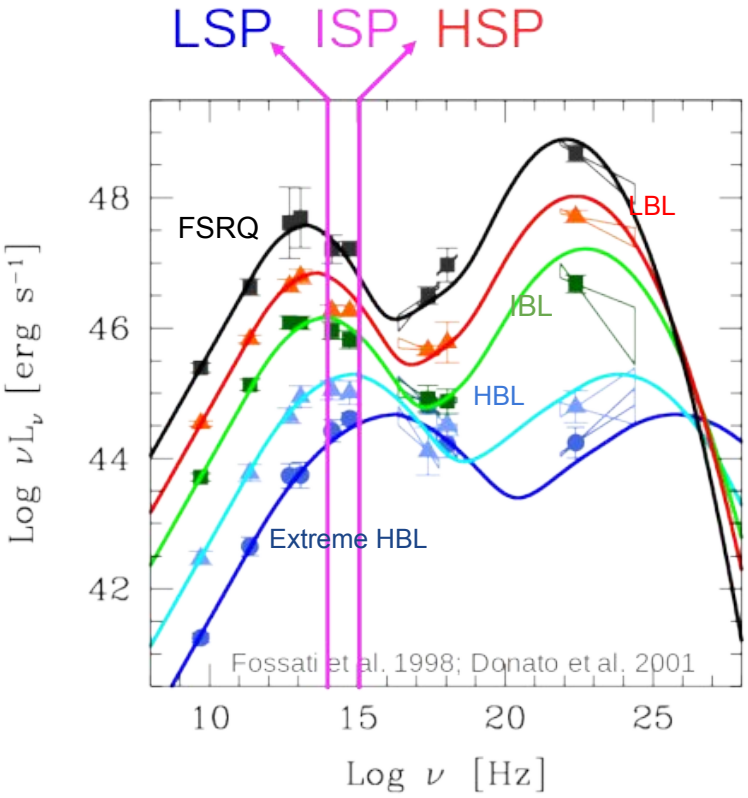

- BL Lacs subtypes: Low-, intermediate- or high-synchrotron-peaked (LSP, ISP, HSP; Abdo et al. 2010).
- Based in Padovani & Giommi (1995; ratio 5 GHz/1 keV flux) for BL Lac objects: LBL, IBL, HBL.

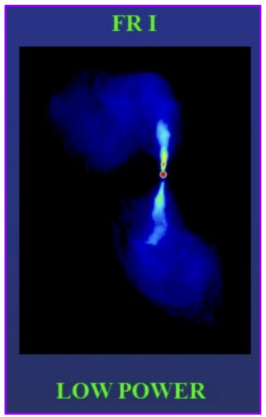

Models of blazar emission

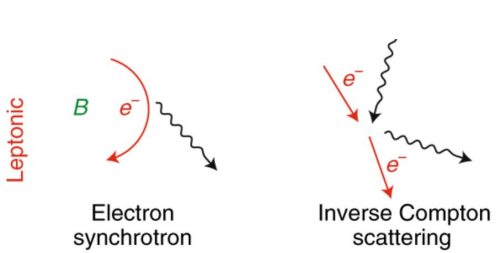

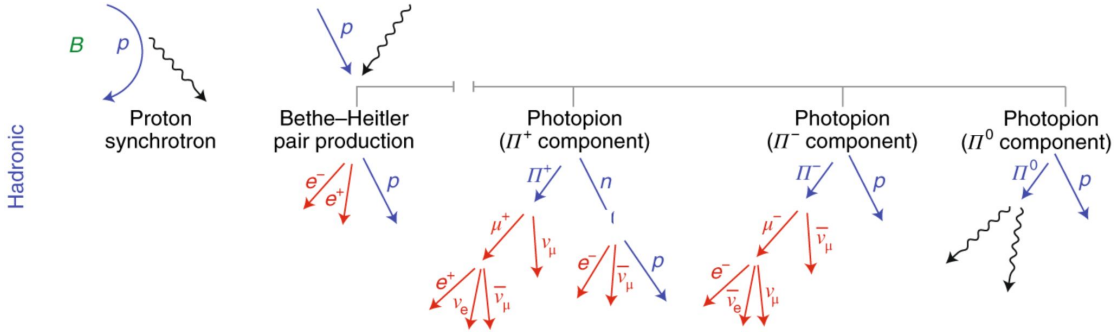

Leptonic

- HE emission likely from inverse Compton scattering by same e-/e+ that emitted synch: synchrotron self-Compton (SSC).
- Upscatter of low-energy photons from broad-line region, disk or torus: external inverse Compton (EIC).
- Synch. & Compton variations correlated.

Hadronic

- HE emission from ultra-relativistic e-/e+ & protons.
- γ-ray emission via e.g. proton synchrotron or photo-pion prod.
- Synch. & Compton emission from secondary products of π±.
- Production of neutrinos.

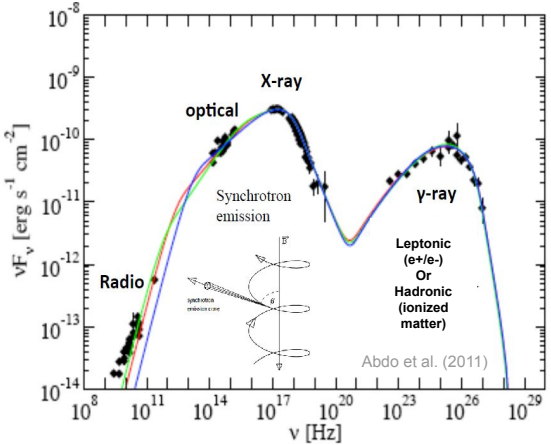

Motivation

- To understand the physics that underlies variations:
  - Unobservable activity in accreting objects.
  - Precession of collimated relativistic plasma.
  - Nature of the parent particle population.
  - Changes in the field strength.
  - Particle acceleration in the emission zone.
  - Characteristics per source class
- Time-domain and multi-messenger (MM) astrophysics:
  - Correlations with gamma-rays.
  - Real time alerts in different timescales and levels of activity.
  - Duty cycles.

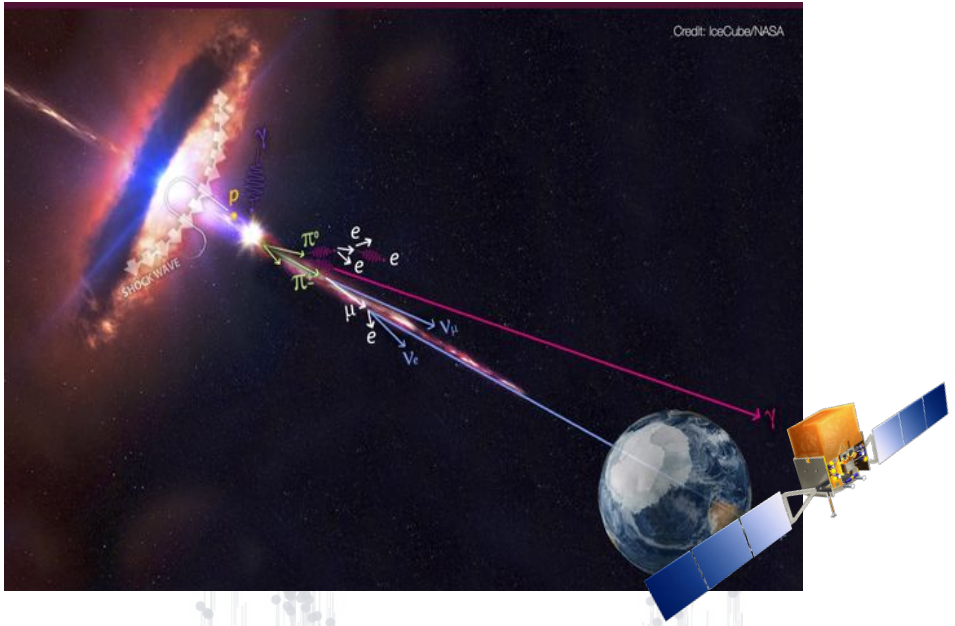

Generating mission-long well-sampled Fermi-LAT light curves of steady sources is computationally expensive
➥ Use of the publication-quality, mission-long, continuously updated Fermi-LAT Light Curve Repository (LCR) data.

Gamma Flare Timescales

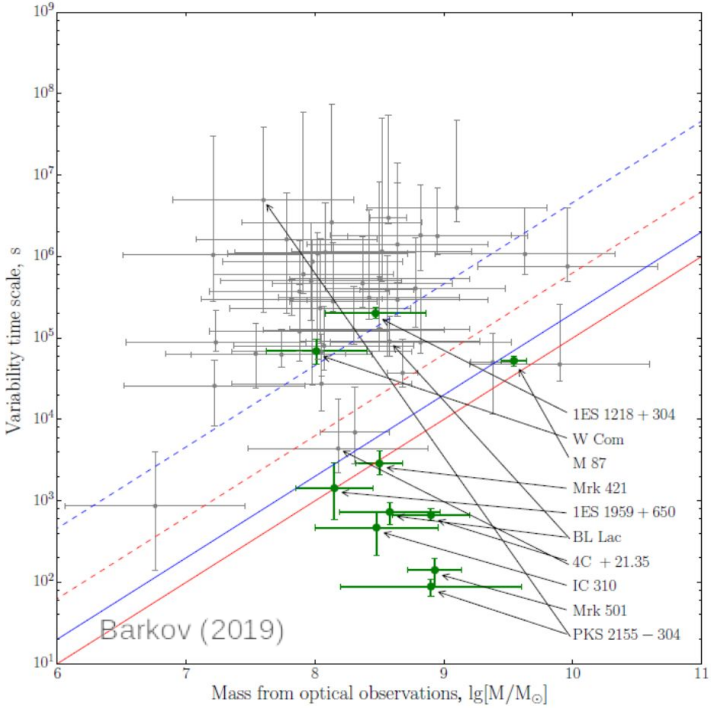

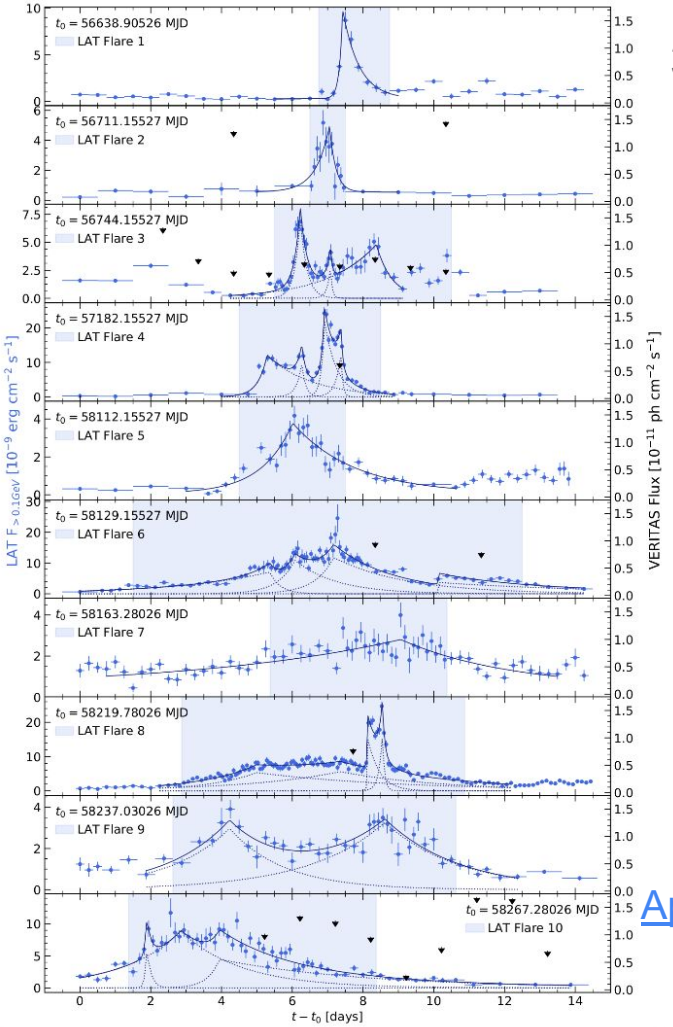

3C 279

[ApJ 924 (2022) 95]

Long-term GeV-optical flux increase: Flare?

ApJ 891 (2020) 170

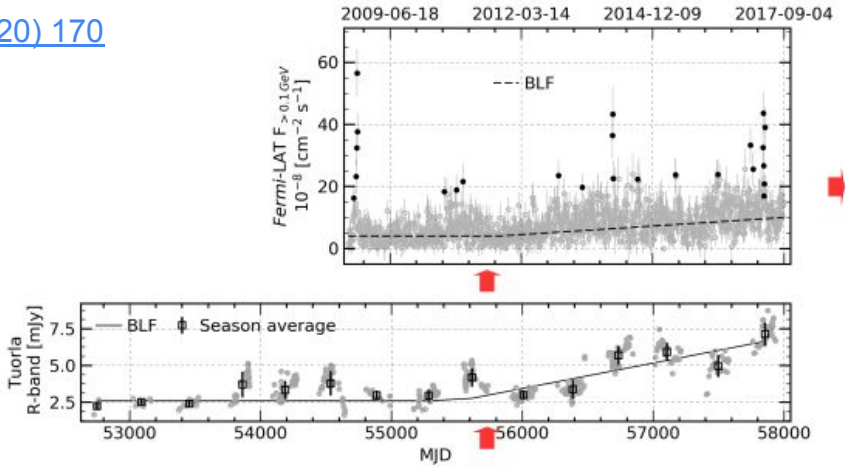

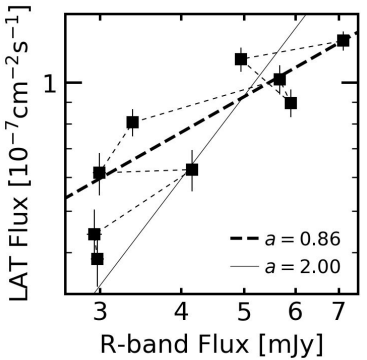

LAT: linear increasing trend
inconsistent with stochastic modeling
@ ≈ 3.3σ (from simulated LCs).

Continuous increase since 2011

Jet precession: X

No strong radio-knot oscillation/ shift
No clear increase of radio luminosity
No jet broadening from stacked VLBI images

Accretion process: ~ V

Timescale consistent with the falling time considering the SMBH mass and an ADAF disk

$$\tau_{ff} = 4.63\times10^{-5}\left(\frac{r}{1.0\times10^{3}r_g}\right)^{3/2}\left(\frac{M_{\rm BH}}{10M_\odot}\right)\text{days} \simeq 8.7\ \text{years}$$

A&A 503, 797–799 (2009)
DOI: 10.1051/0004-6361/200912303

Astronomy & Astrophysics

Lognormal variability in BL Lacertae
(Research Note)

B. Giebels and B. Degrange

Laboratoire Leprince-Ringuet, École polytechnique, CNRS/IN2P3, 91128 Palaiseau, France
e-mail: berrie@poly.in2p3.fr

Received 8 April 2009 / Accepted 15 June 2009

ABSTRACT

Context. The characterization of a time series is a powerful tool for investigating the nature of mechanisms that generate variability in astrophysical objects. Blazar variability across the entire electromagnetic spectrum is a long-standing puzzle, and it has been difficult to ascertain the mechanisms at play.
Aims. Lognormal variability in X-ray light curves, probably related to accretion disk activity, has been discovered in various compact systems, such as Seyfert galaxies and X-ray binaries. Identifying a similar behaviour in blazars would establish a link between them.
Methods. Public X-ray data from the blazar BL Lac are used to investigate the nature of its variability, and more precisely the flux dependency of the variability and the distribution of fluxes.
Results. The variations in the flux are found to have a lognormal distribution and the average amplitude of variability is proportional to the flux level.
Conclusions. BL Lac is the first blazar in which lognormal X-ray variability is clearly detected. The light curve is orders of magnitude less variable than other blazars, with few bursting episodes. If this defines a specific state of the source, then the lognormality might be the imprint of the accretion disk on the jet, linking for the first time accretion and jet properties in a blazar.

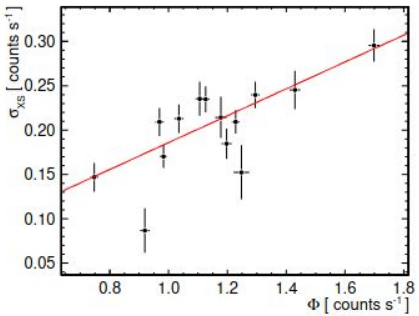

Fig. 3. Scatter plot of the excess variance versus the average of the fluxes for which the excess was determined. The line is a linear fit showing $\sigma_{XS} \propto (0.15 \pm 0.02)\,\Phi$.

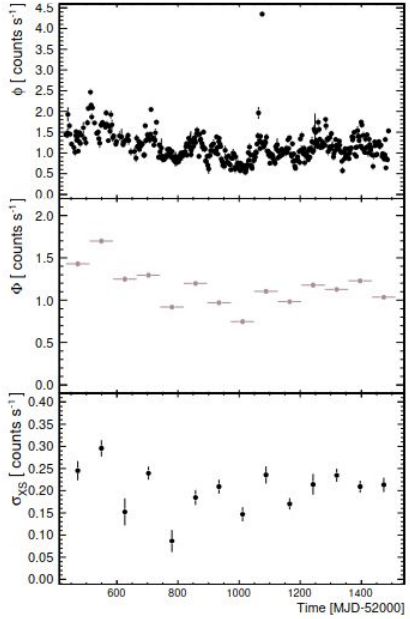

Fig. 1. Top panel: PCA flux light curve (in units of counts s^{-1}) of BL Lac with bins of 1 day. Middle and bottom panel: PCA mean flux and excess rms measured from 77 day segments (see text).

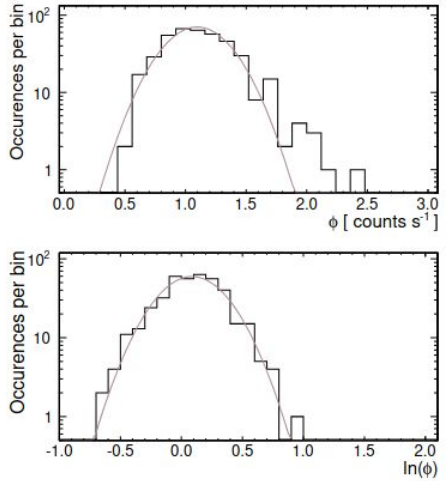

Fig. 2. Distribution of the fluxes for the considered period (top) and the distribution of the logarithm of the fluxes (bottom). The lines are the result of a Gaussian fit to the data. The improvement to the fit provided by the logarithmic function is clearly apparent in that it reproduces more successfully the steeper-than-Gaussian left-hand part of the distribution, as well as the broader, tail-like right hand part, which are characteristic of the lognormal distribution. The single flux estimation of the flare on MJD 54075 has been excluded so as not to favour the logarithmic fit.

Biteau & Giebels 2012: mini-jets-in-a-jet model as additive process.

A&A 503, 797–799 (2009)
DOI: 10.1051/0004-6361/200912303

Lognormal v
(R

B. (

Laboratoire Leprince-Ringuet, École polytechnique, (
e-mail: berrie@poly.in2p3.fr

Received 8 April 2009 / Accepted 15 June 2009

Context. The characterization of a time series is a pow
astrophysical objects. Blazar variability across the ent
to ascertain the mechanisms at play.
Aims. Lognormal variability in X-ray light curves, pr
systems, such as Seyfert galaxies and X-ray binaries.
Methods. Public X-ray data from the blazar BL Lac
dependency of the variability and the distribution of fl
Results. The variations in the flux are found to have a
to the flux level.
Conclusions. BL Lac is the first blazar in which logno
less variable than other blazars, with few bursting epi
be the imprint of the accretion disk on the jet, linking

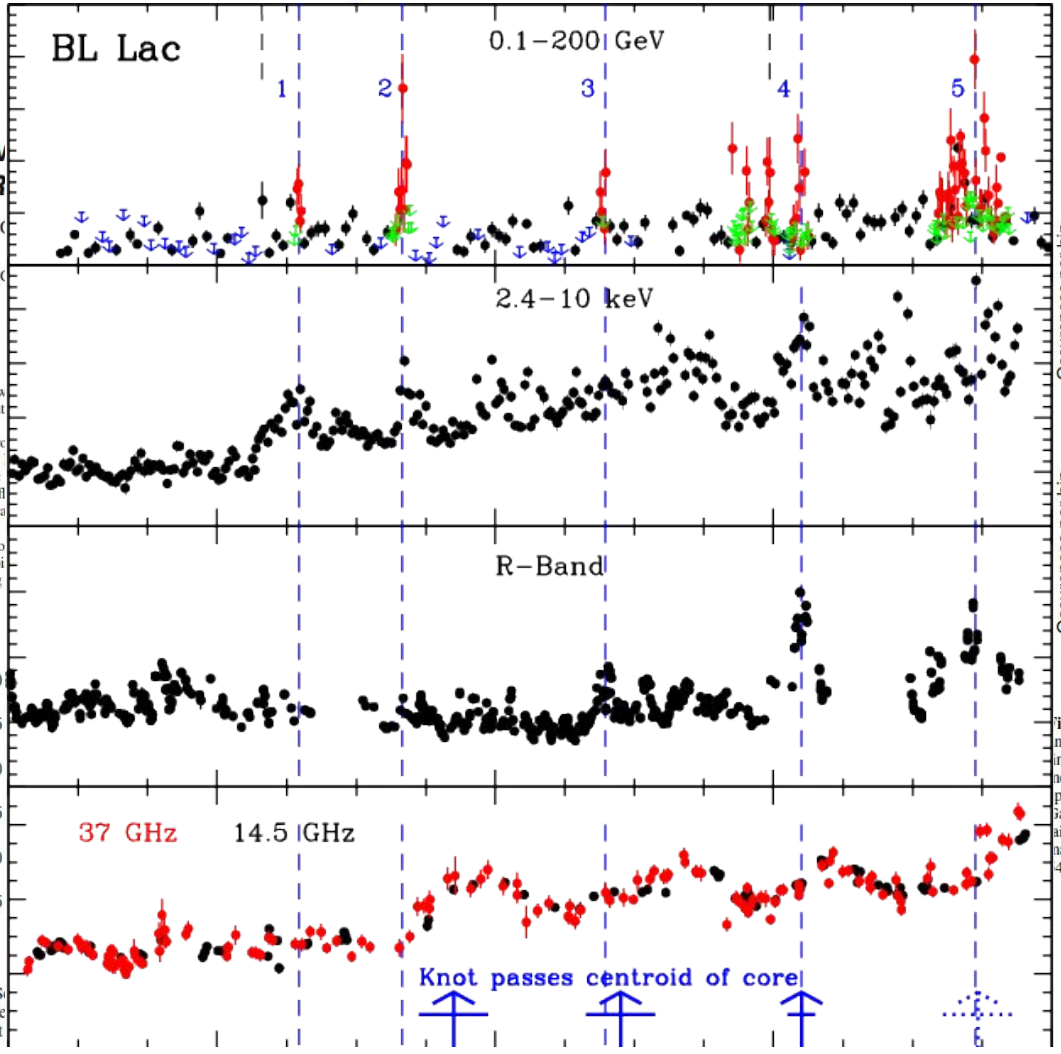

Fig. 3. S
the fluxe
linear fit

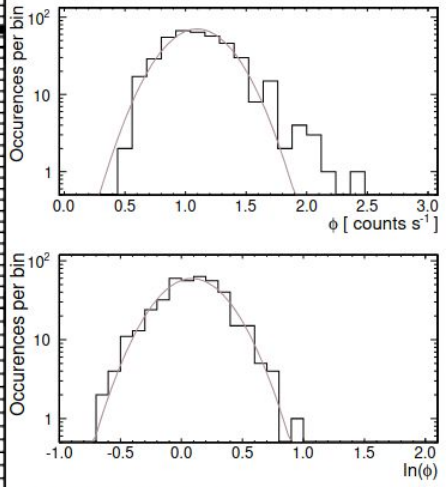

Fig. 2. Distribution of the fluxes for the considered period (top) and the distribution of the logarithm of the fluxes (bottom). The lines are the result of a Gaussian fit to the data. The improvement to the fit provided by the logarithmic function is clearly apparent in that it reproduces more successfully the steeper-than-Gaussian left-hand part of the distribution, as well as the broader, tail-like right hand part, which are characteristic of the lognormal distribution. The single flux estimation of the flare on MJD 54075 has been excluded so as not to favour the logarithmic fit.

Duty cycle: BL Lac object

[ApJ 891 (2020) 170]

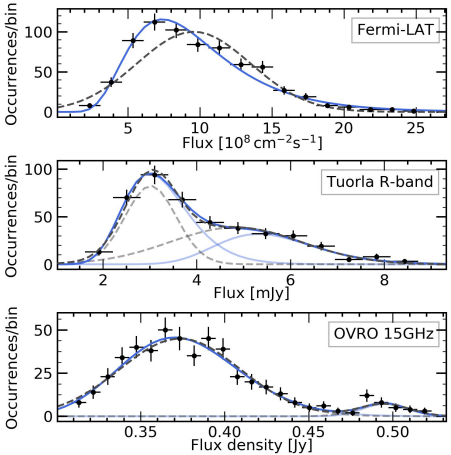

- TeV γ-rays
- GeV γ-rays
- X-ray
- UV-Optical
- Optical
- Optical polarization
- Radio

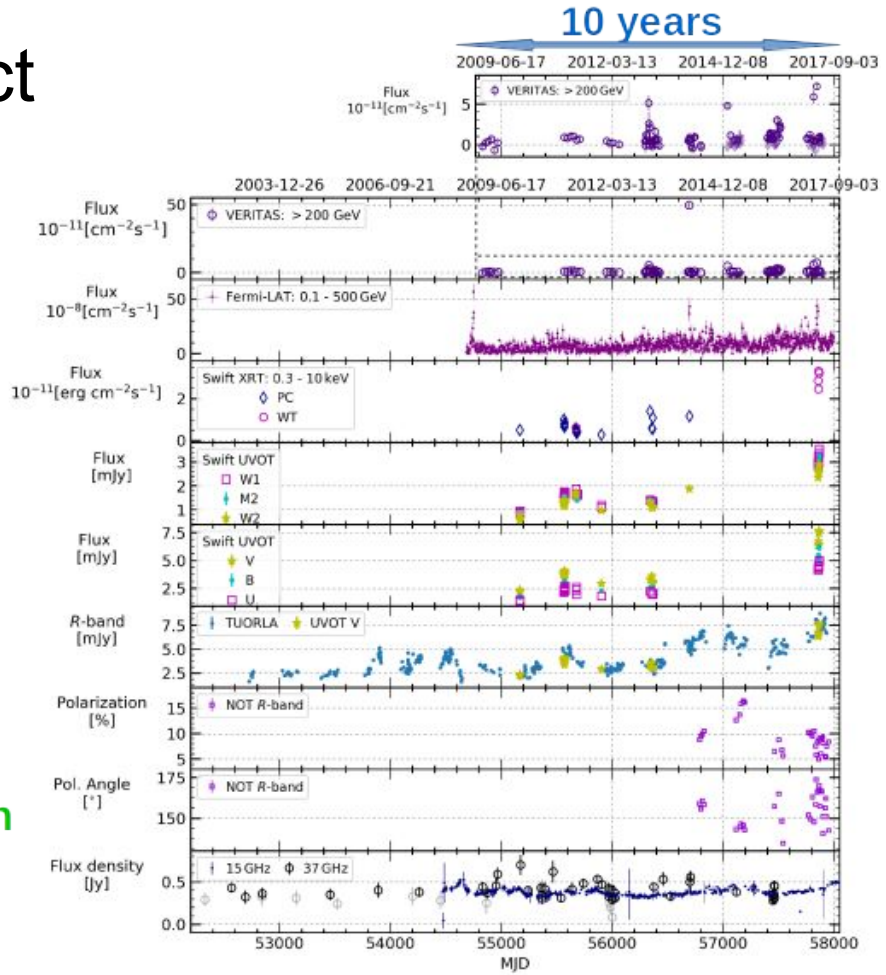

Search for multiplicative processes

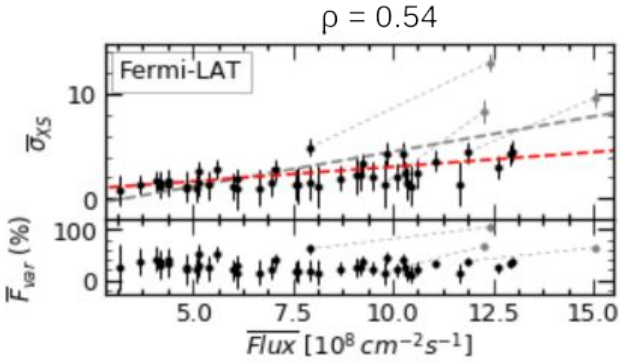

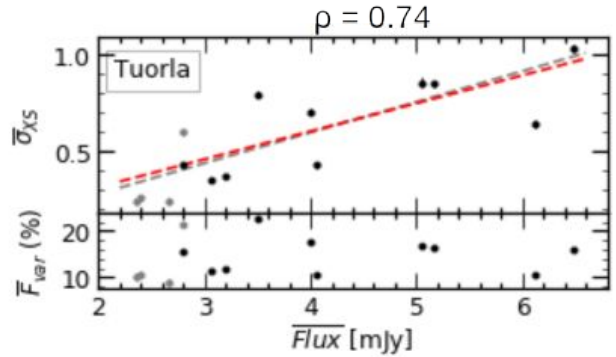

- rms ∝ $\overline{Flux}$ observed in X-ray binaries and AGNs (Uttley & McHardy 2001, MacHardy 2008).
- Possible long-time-scale energy releases caused by accreting variations (Liubarskii 1997)
- rms ∝ $\overline{Flux}$ means log-normal distribution, i.e. multiplicative processes
- Excess variance (Vaughan et al. 2003) as rms:

$$\sigma_{XS}^2 = \frac{1}{N}\Sigma_N^{i=1}(x-\overline{x})^2 - \overline{\sigma_i^2}$$

➡ **$\overline{\sigma}_{XS}$ & $\overline{Flux}$ moderate linear correlation in GeV & *R*-band.**

Search for multiplicative processes

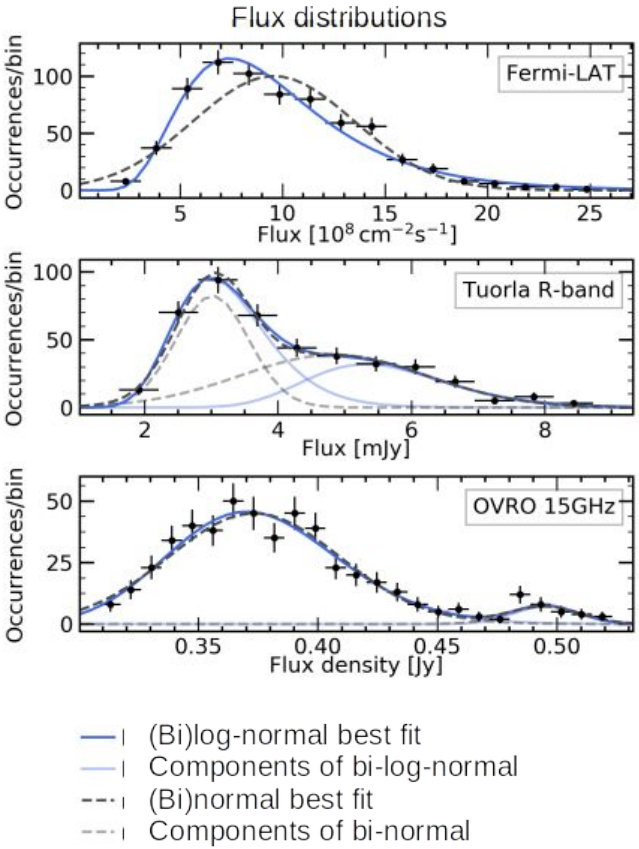

Claims of log-normality:

- BL Lacertae (Giebels & Degrange 2009).
- 1ES 1011+496 (Sinha et al. 2017), (Ackermann et al. 2015c).
- ~35 bright *Fermi* blazars (Shah et al. 2018).

- LAT: Log-normal (χ^2_{red}=1.42) provides much better fit than normal (χ^2_{red}=4.12) in LAT data >3σ.

- Radio & *R*-band:

  Double-peaked structure: Tuorla peaks consistent w/ states before & after t_{break}.

Duty cycle: FSRQs

ApJ 924 (2022) 95

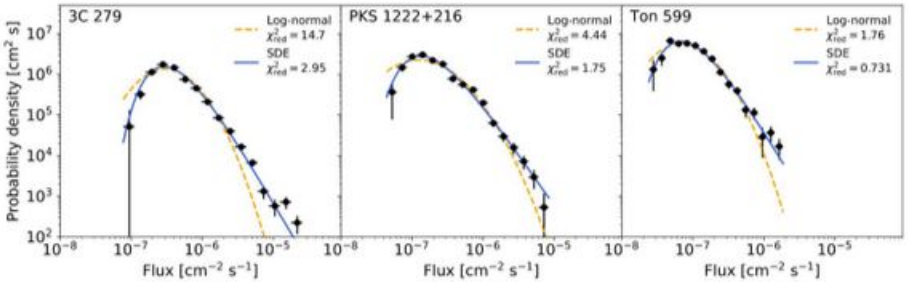

Model based on stochastic differential equation (SDE) by Tavecchio et al. 2020: Magnetic flux accumulation timescales in 3C 279, PKS 1222+216 and Ton 599, respectively, to be 200, 700, and 1800 r_g /c, respectively, within the magnetically arrested disk scenario.

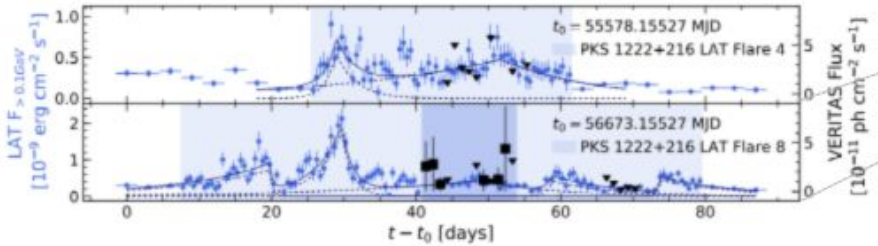

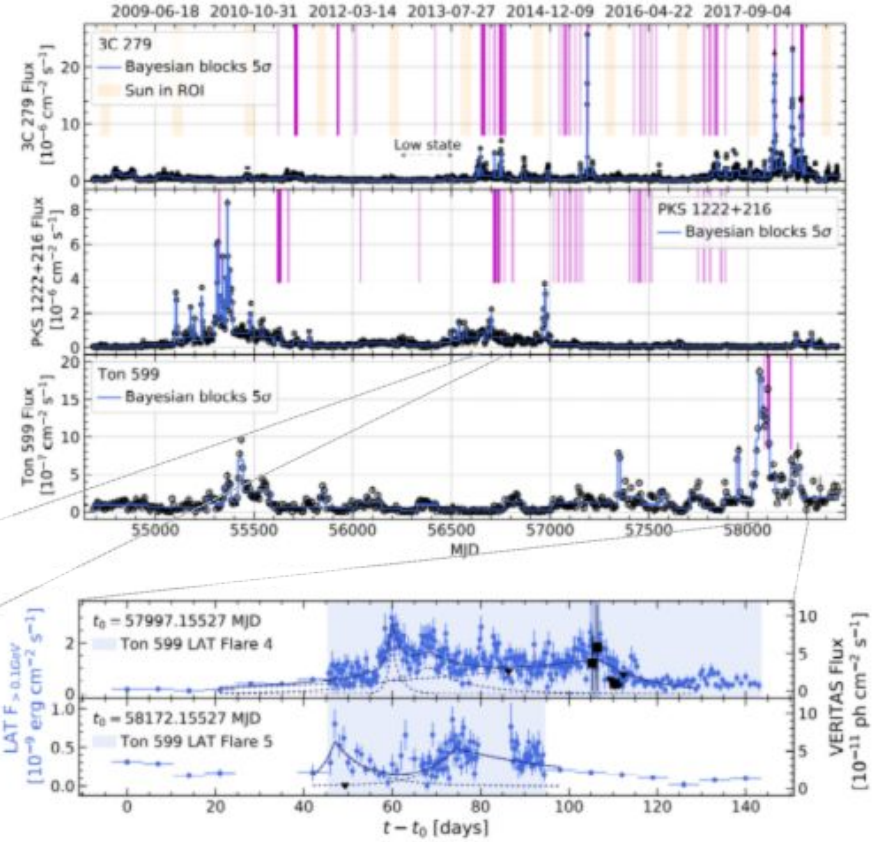

Duty cycle: FSRQs

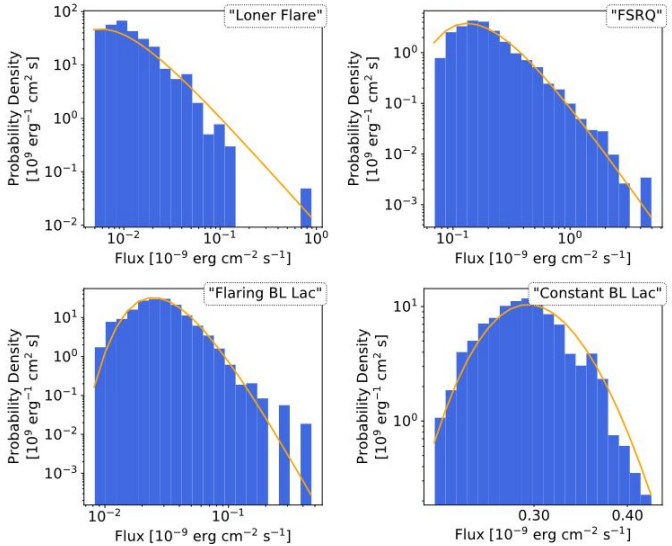

ApJ 936 (2022) 147

Inverse gamma distribution better describes a heavier-tailed distribution, which arises as a consequence of a shot-noise process. Discretes bursts averaged over bins. Model parameters: average burst rate burst fluence, timescale of long-term stochastic fluctuations

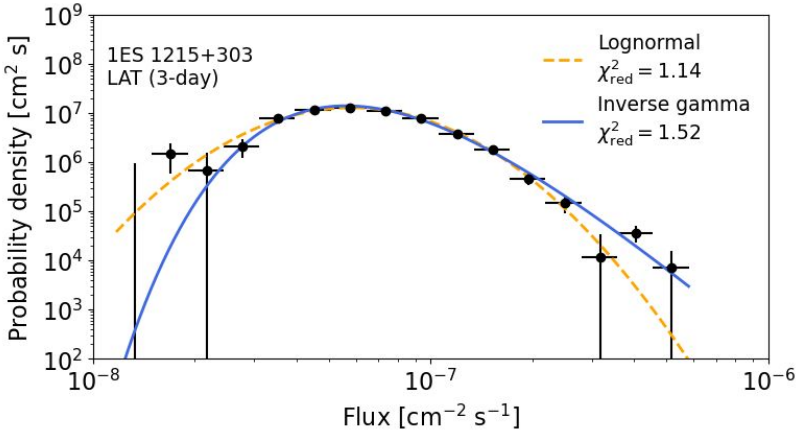

- Inverse gamma fit vs. Lognormal fit parameters → Accretion disk processes
- Magnetic flux Accumulation → 3 day timescale magnetic flux accumulation

Watch out for the Sun & Moon in the ROI!

[ApJ 924 (2022) 95]

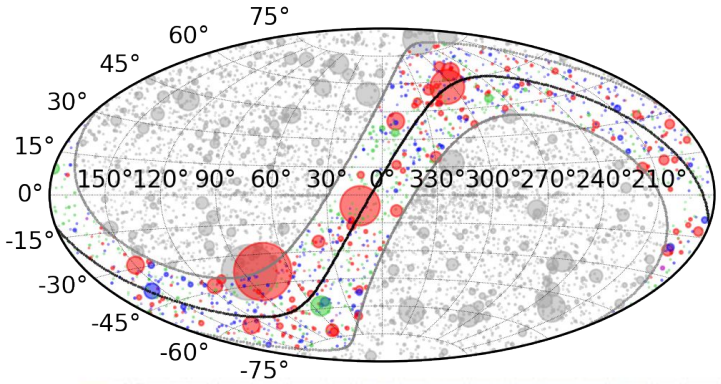

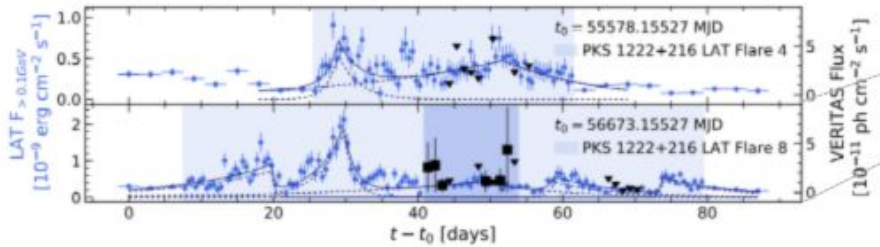

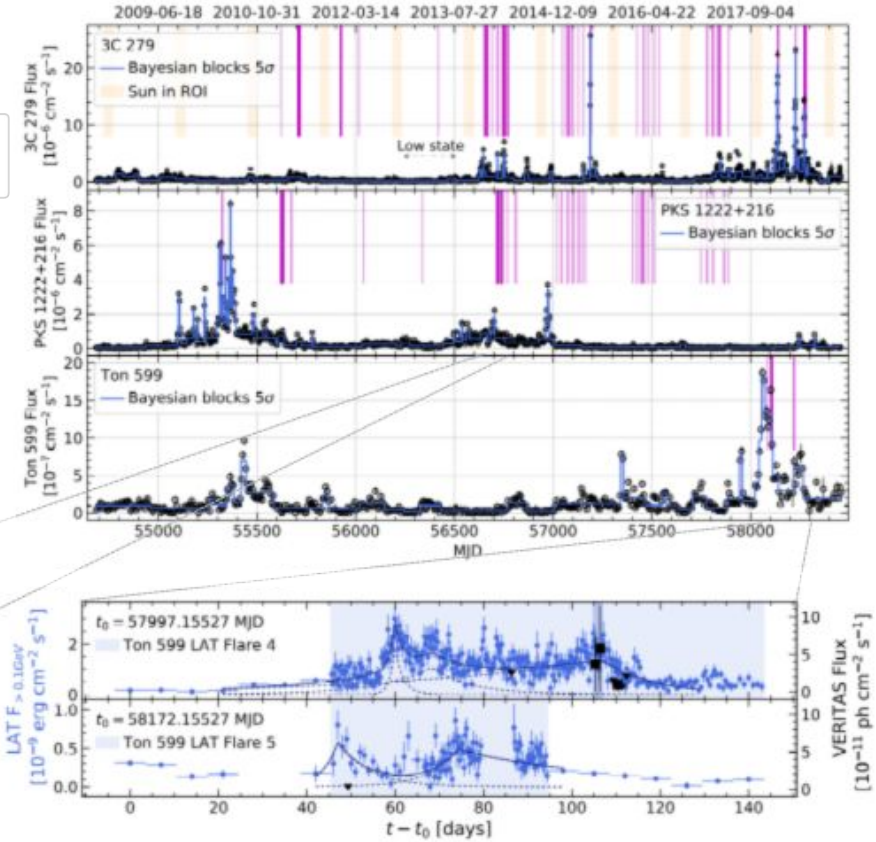

Careful with Solar and Lunar contamination!
3C 279 is 0.2 front the ecliptic.

Low vs flaring states: Spectral characteristics ➥ Acceleration mechanisms

[ApJ 891 (2020) 170]

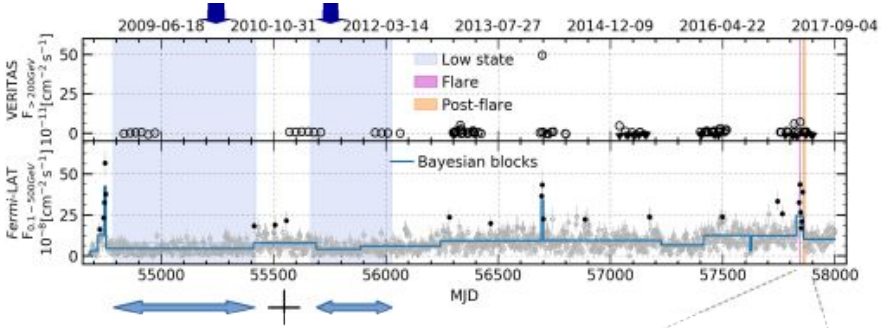

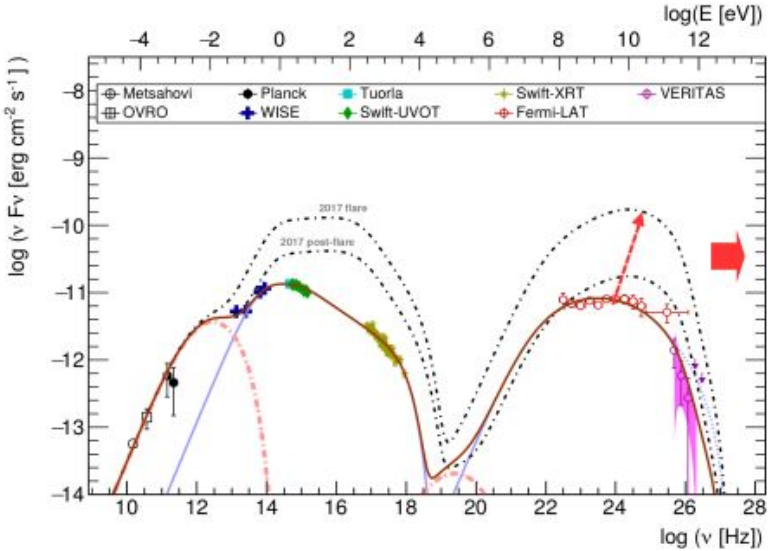

$K_1 \times 3$
$B \times 2.4$
$\gamma_{brk} \times 4.5$
$n_2 \times 1.2$

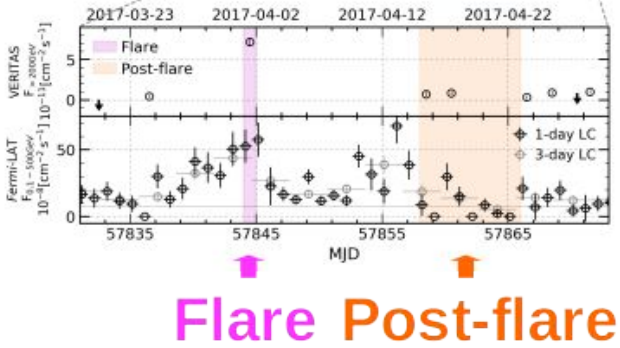

Flare **Post-flare**

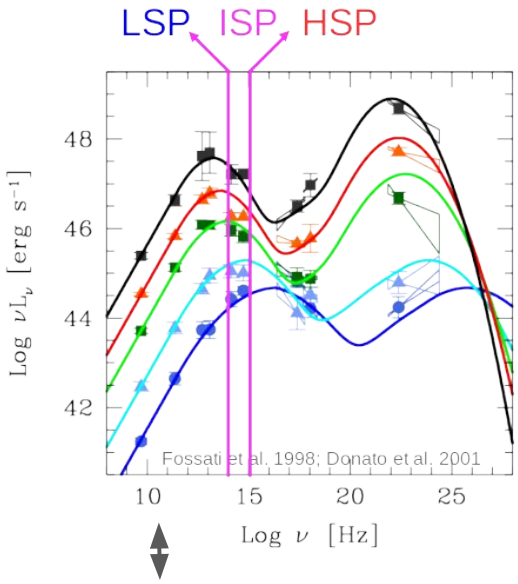

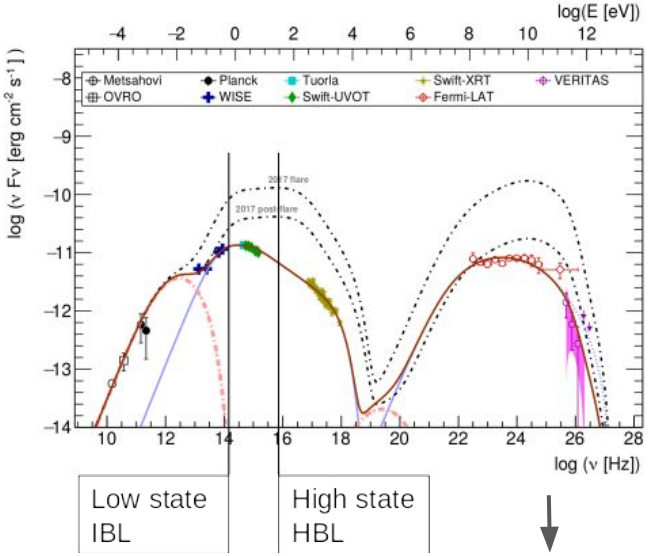

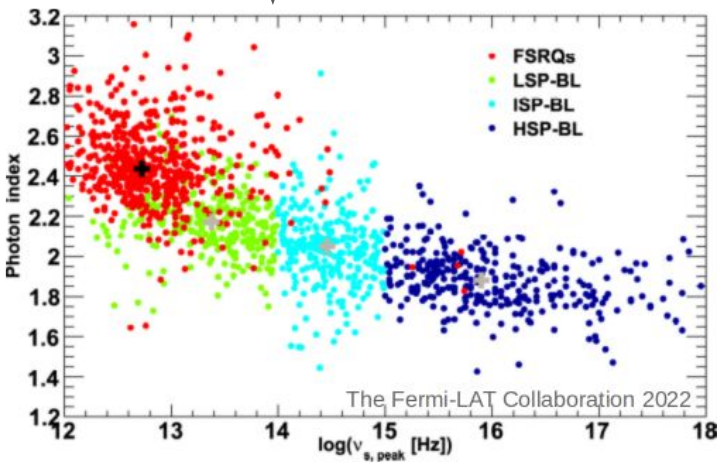

ApJ 891 (2020) 170

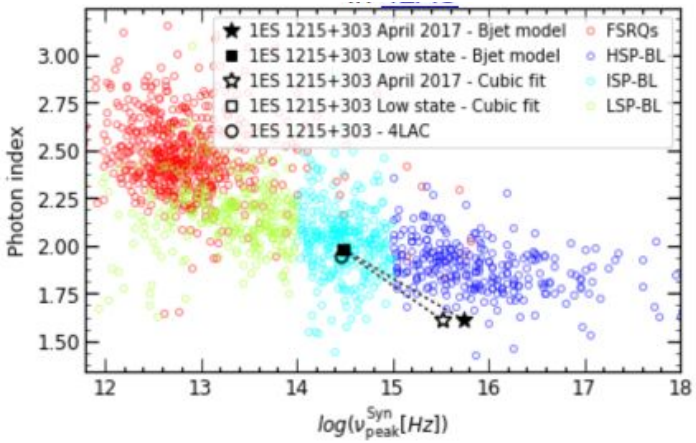

LCR
The Fermi Large Area Telescope
Light Curve Repository

https://fermi.gsfc.nasa.gov/ssc/data/access/lat/lcr/

ApJS (2023), 265, 31

Fermi
Gamma-ray
Space Telescope

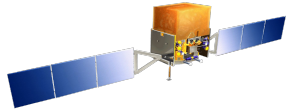

Fermi-LAT LCs.

Public database since Dec 2021.

Publication ready.

1525 sources (26% of 4FGL-DR2).

3-, 7- & 30-day cadence.

Spectral information.

Entire mission (> 16 years).

Continuously updated.

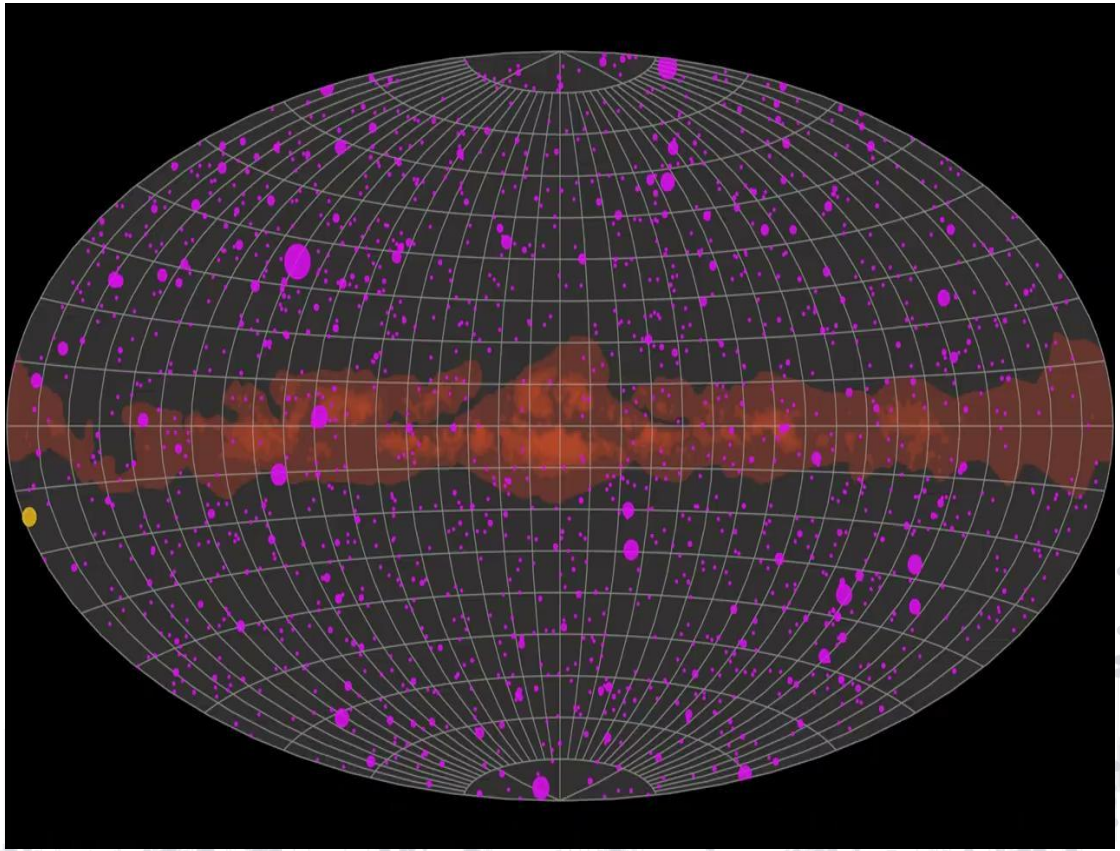

~90% AGN

Mostly blazars.

LCR population: ~90% Active Galaxies

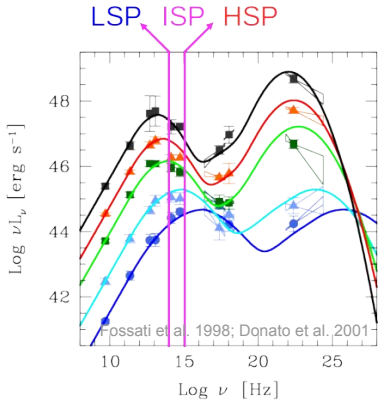

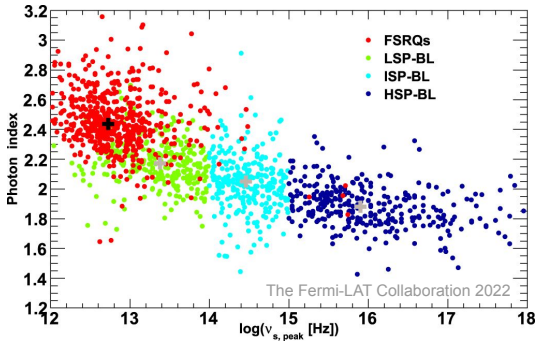

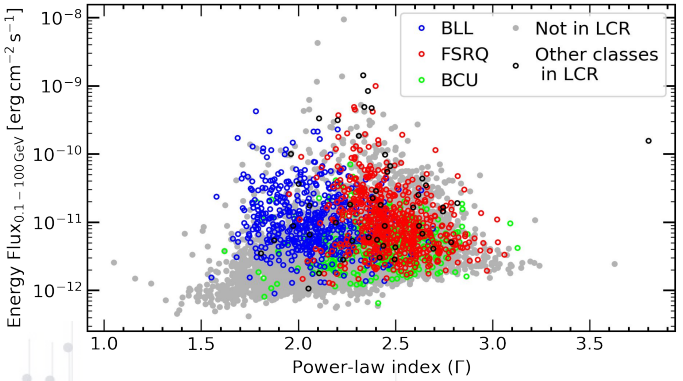

- 38% FSRQs, 31% BL Lac & 24% BCU of LCR sample, or 77%, 36% & 26% of their respective 4FGL-DR2 class.

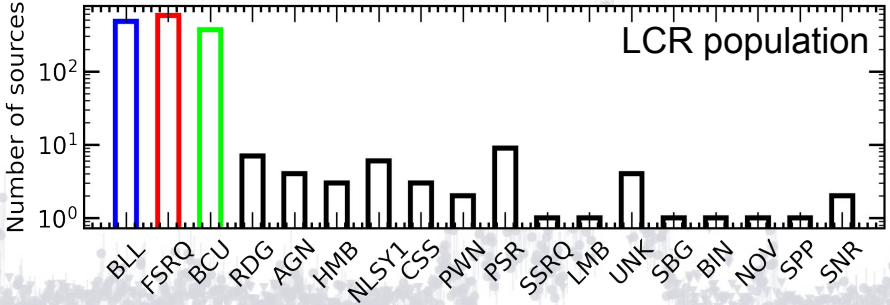

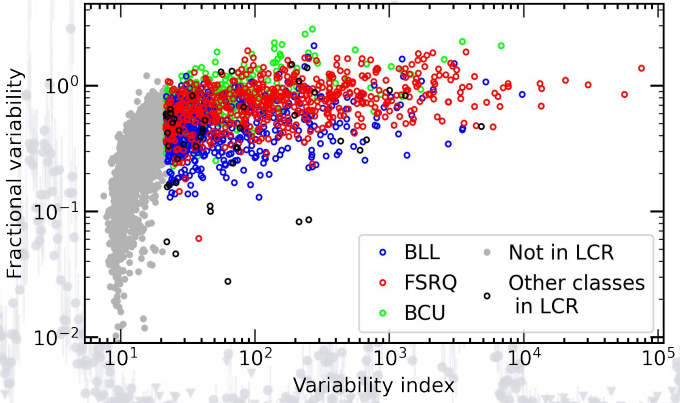

LCR paper: Diagnostic plots - Caveats

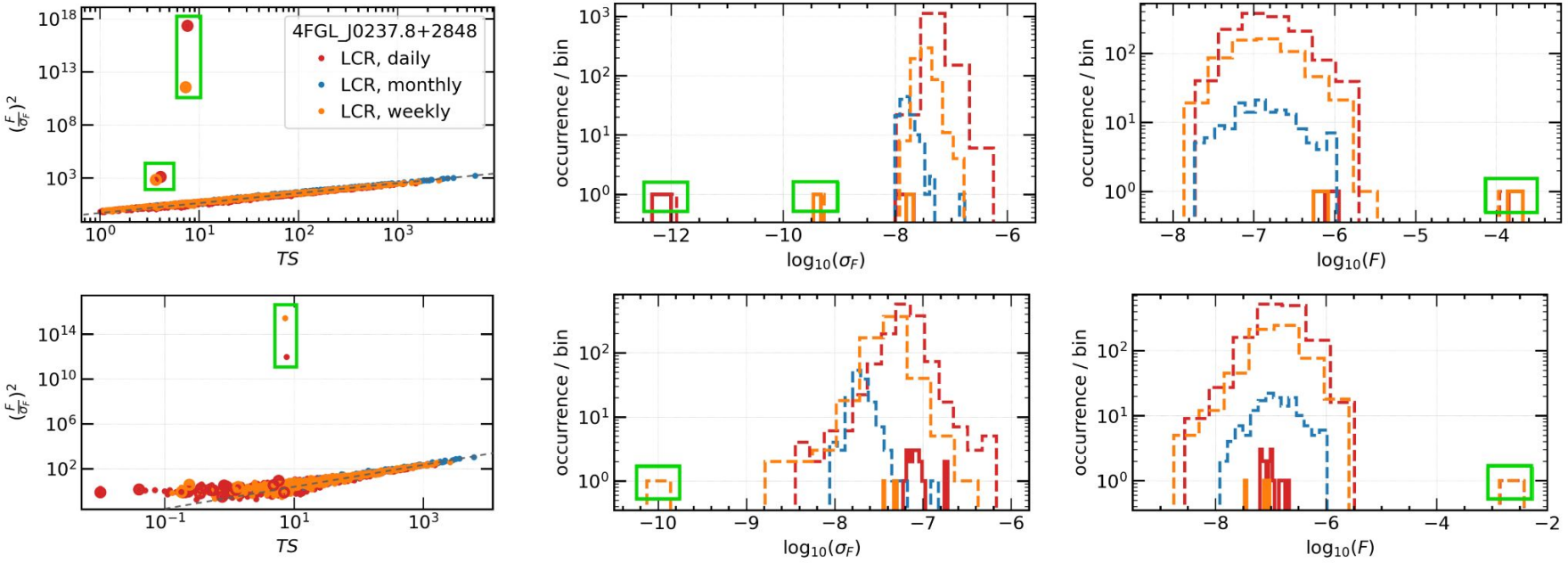

FSRQ 4C +28.07 (0.1–100 GeV): Top panels show the case for which the spectral index is fixed. The bottom panels show the case for which the spectral index is free to vary. The ratio of flux to flux uncertainty (left panels) is expected to be approximately proportional to the square root of the test statistics.

LCR paper: Exposure - Caveats

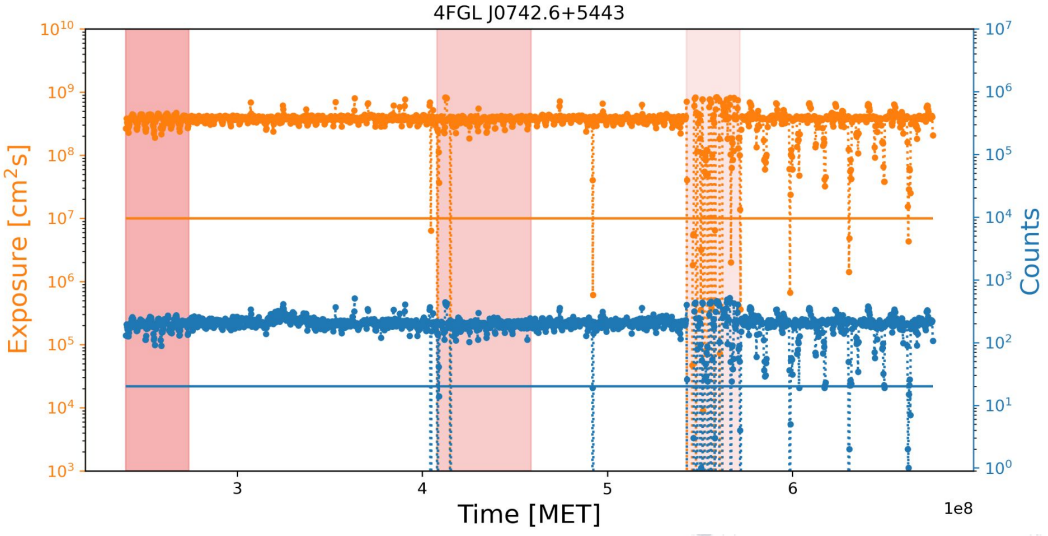

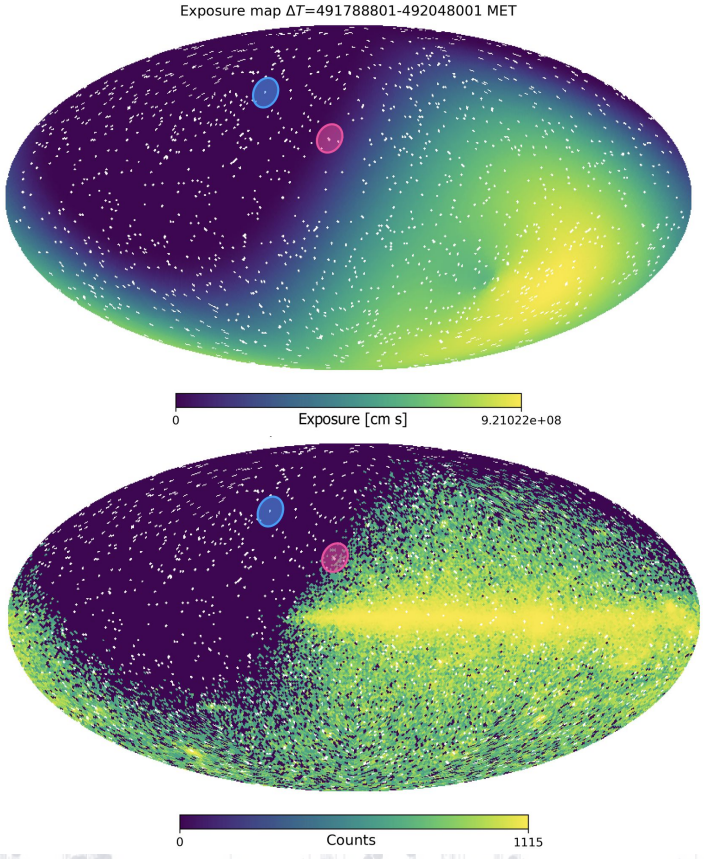

LCR pipeline does not save exposure files: Independent analysis to obtain all-sky exposure maps for each time range & estimate exposure for each LCR source ROI (i.e. 2.6K instead of 4M analyses). FSRQ GB6 J0742+5444 In the example above.

Scientific impact: Analysis methods

- Modeling weekly-timescale gamma-ray variability in blazars with self-supervised deep learning (Brill 2023, arXiv:2302.07700).
  - Model predicts the flux probability distribution at each time step.
  - Extract info on weekly-timescale flux distributions over time or between sources.

- LCR scientific impact discussions: arXiv.2210.12875, arXiv: 2308.12709.

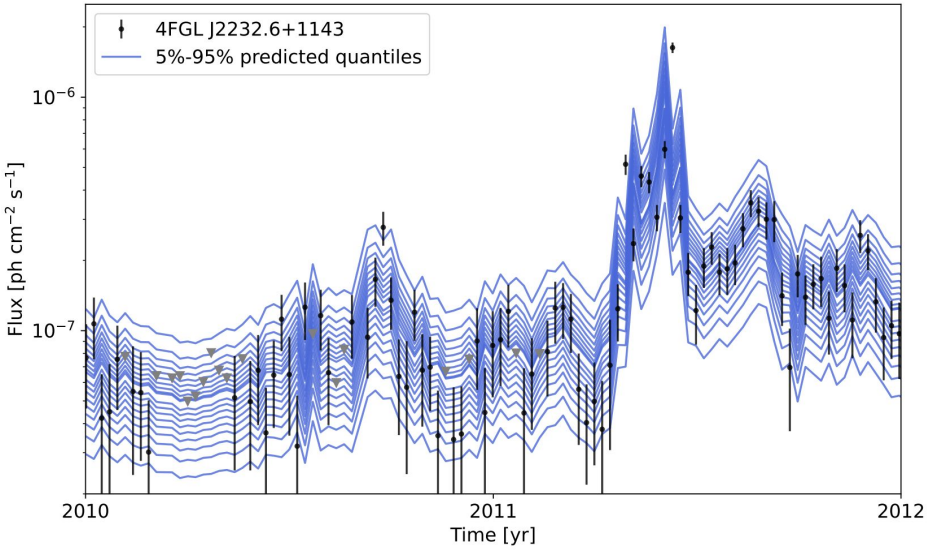

Scientific impact: Flaring and quiescent states

- Optical/γ-ray blazar flare correlations: understanding the high-energy emission process using ASAS-SN and *Fermi* LCs MNRAS 2023, 519, 6349.
- Proton synchrotron, an explanation for possible extended VHE gamma-ray activity of TXS 0506 +056 in 2017 (PhysRevD.106.123005).
- Spectroscopic reverberation mapping of Quasar PKS 0736 + 017: broad-line region and black-hole mass (MNRAS 2022, 516, 2671).

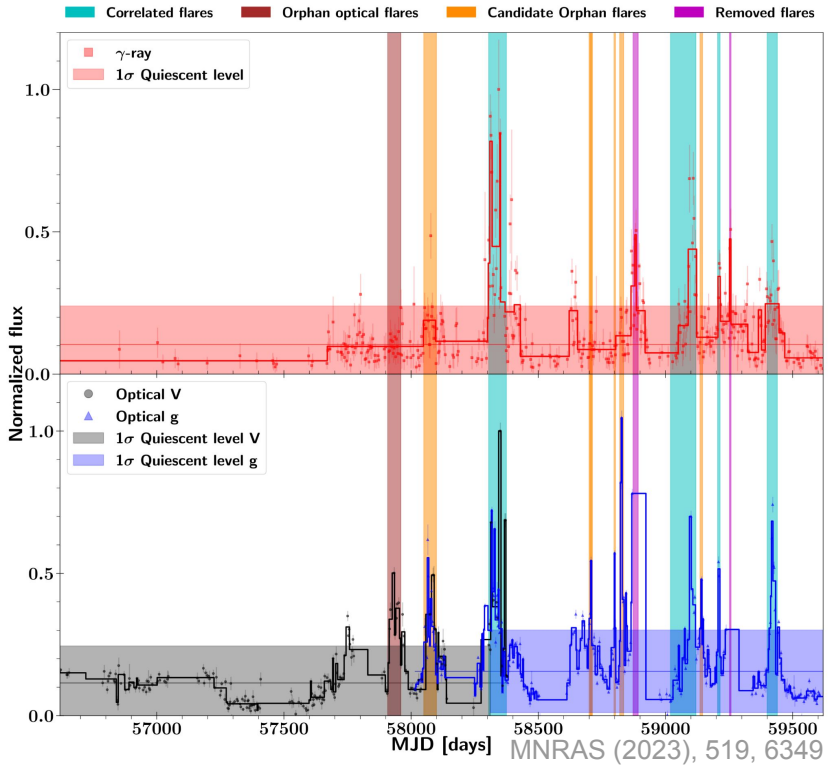

MNRAS (2023), 519, 6349

Scientific impact: Search for periodicity

- Quasi periodic oscillations (QPO) in AGN might indicate, e.g., the presence of supermassive black hole binary systems or a precessing jet.
- Possible QPOs in optical data. Possible jet precession in radio observations. No conclusive QPO detection in γ-rays.
- Analysis must include trial factors (look-elsewhere effect).
- QPO studies with LCR data:
  - MWL periodicity search in a sample of γ-ray bright blazars (MNRAS 2023, 518, 57880).
  - Detection of possible transient QPOs in the *γ*-ray LC of PKS 0244-470 & 4C+38.41 (ApJ 2023, 950, 173).
  - A 31.3 day Transient QPO in γ-ray emission from blazar S5 0716+714 (ApJ 2022, 938, 8).

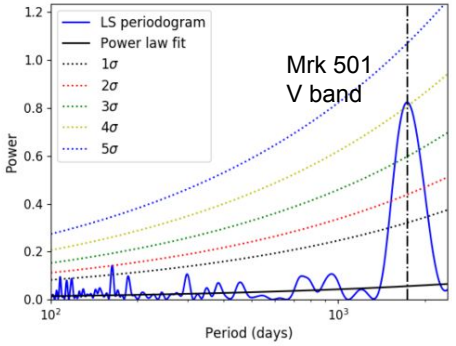

MNRAS 2023, 518, 57880

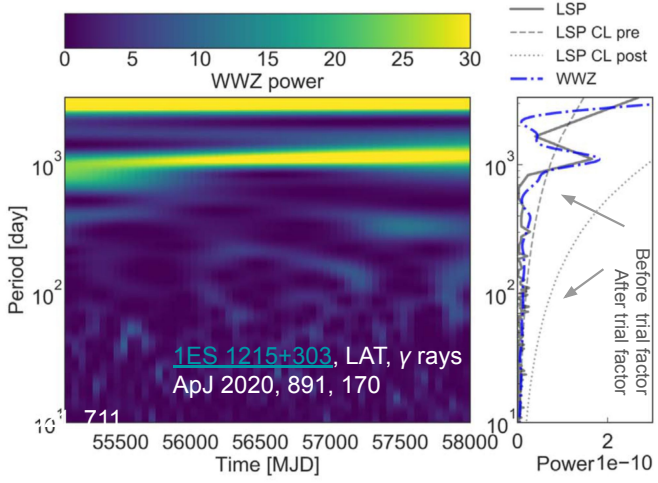

M 87

Search for periodicity: PG 1553+113

2.1 yr period with significance ~4σ against stochastic red noise in Fermi-LAT data.

Possibly arising from pulsational accretion flow in a sub-parsec binary SMBH system of elevated mass ratio, with orbital modulation of the supplied material and energy in the jet. Other: instabilities, disk & jet precession, rotation or nutation, & perturbations by massive stars or intermediate-mass BH in polar orbit.

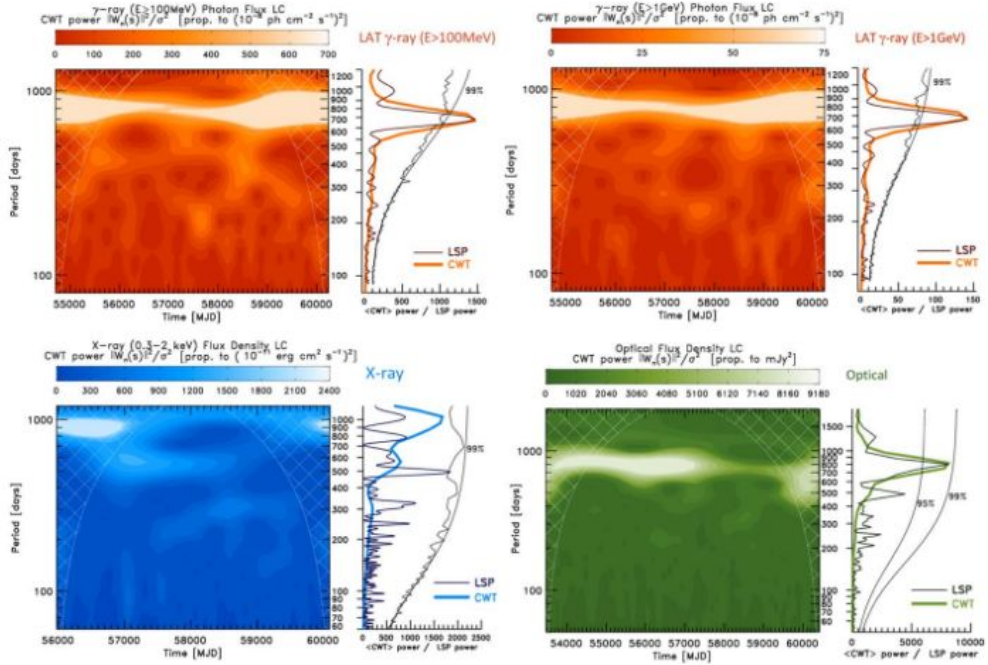

Figure 6. Top panels: 2D image filled (orange color scale) contour plots of the Morlet CWT gamma-ray power spectrum, the "scalogram," respectively for the Fermi-LAT $E > 100$ MeV and $E > 1$ GeV, 45 day bin, photon flux light curves of Figure 1. Side plots are the global CWT power spectrum averaged along the MJD epochs, and the one-dimension LSP power spectrum in the bias-corrected REDFIT implementation. The LSP power axis is rescaled to the scale of the global CWT comparing the relative main bumps. The 99% false alarm confidence level lines (parametric χ^2 and Monte Carlo) against the null hypothesis of an origin by pure stochastic AR(1)-noise process realization, are shown. Lower panels: 2D scalogram-filled color scale contour plot of the Morlet CWT (blue color scale) of the Swift-XRT integrated (0.3–2.0 keV) flux density (omitting the few, too sparse, XRT data prior to the year 2012), and 2D scalogram-filled color scale contour plot of the Morlet CWT (green color scale) of the optical flux density, corresponding to light curves presented in Figure 2. Cross-hatched regions in all the panels are the "cone of influence," where spurious edge effects caused by finite time series boundaries become important. Side plots are the corresponding global CWT and the LSP power with their false alarm confidence levels lines, scaled to the global CWT peak.

Scientific impact: Much more (ADS)

- IXPE and Multiwavelength Observations of Blazar PG 1553+113 Reveal an Orphan Optical Polarization Swing.
- X-Ray Polarization of BL Lacertae in Outburst.
- Discovery of X-ray polarization angle rotation in the jet from blazar Mrk 421
- Microquasar Cyg X-3 - a unique jet-wind neutrino factory?
- The spectra of IceCube Neutrino (SIN) candidate sources - IV. Spectral energy distributions and multiwavelength variability
- Repeated patterns of gamma-ray flares suggest structured jets of blazars as likely neutrino sources (jets composed of a fast spine and a slower sheath)
- Hunting Gamma-Ray-emitting FR0 Radio Galaxies in Wide-field Sky Surveys
- Comprehensive Study of the Blazars from Fermi-LAT LCR: The Log-Normal Flux Distribution and Linear rms-Flux Relation

Polarization

Neutrinos

Population search

Lognormality

Enabling science: Community alerts

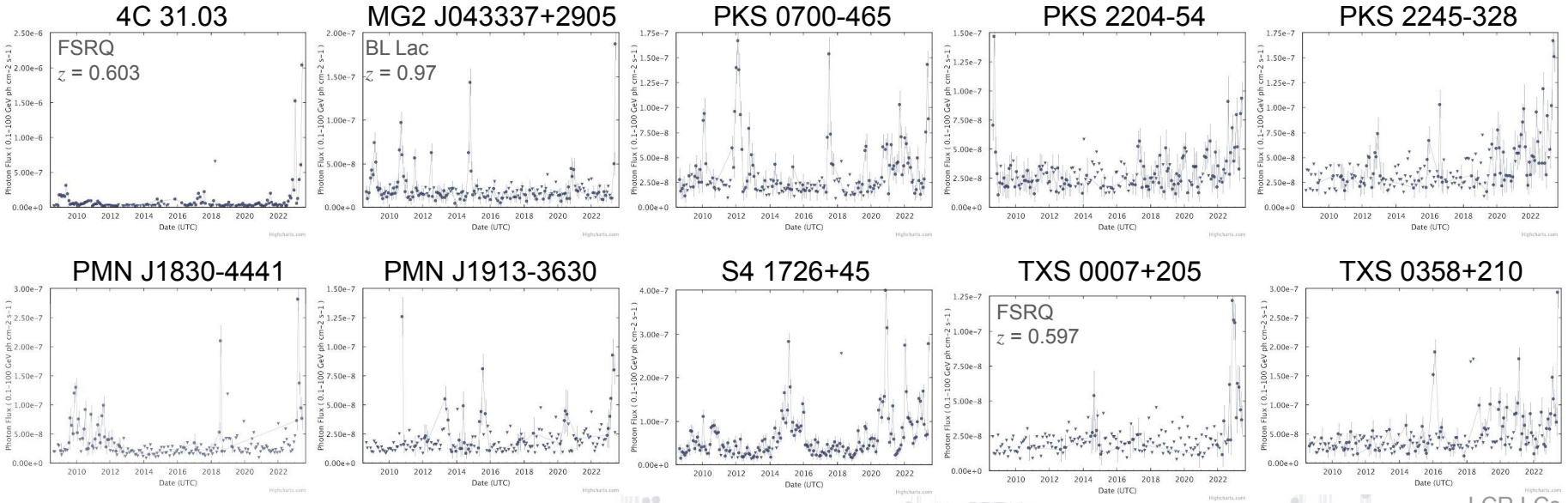

LCR LCs

- Cited by >76 papers (ADS).
- > 100 Astronomer's Telegrams and Gamma-ray Circular Notices: https://www-glast.stanford.edu/cgi-bin/pub_rapid.
- Now in astro-colibri.com and later CTAO.

Automating the validation process

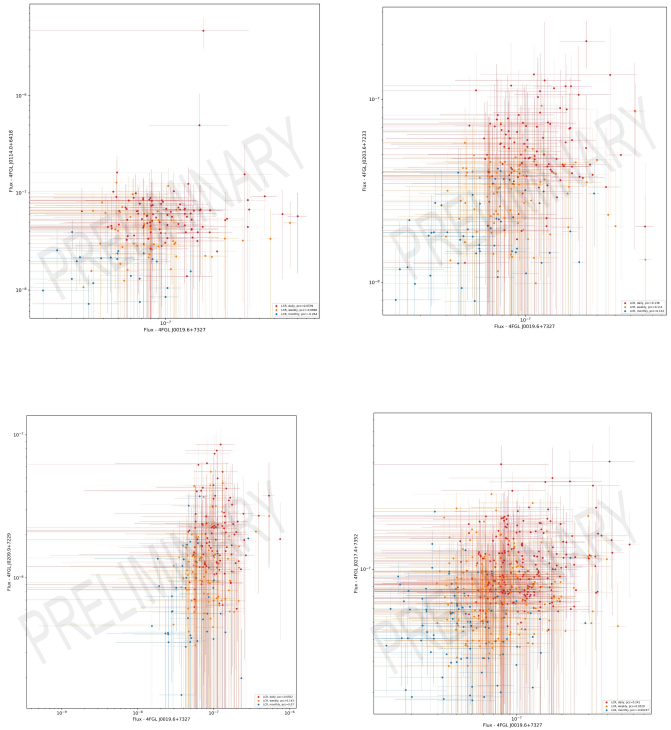

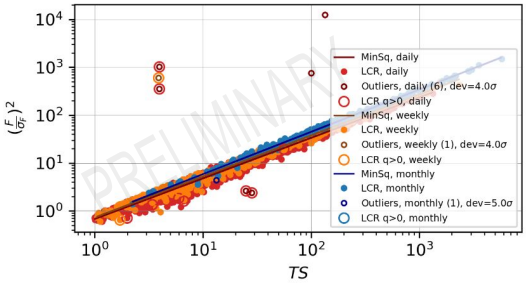

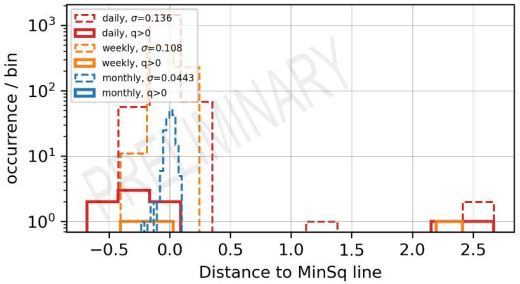

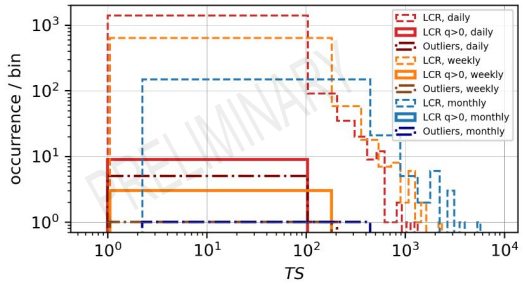

FSRQ 4C +28.07
4FGL J0237.8+2848
Index fixed

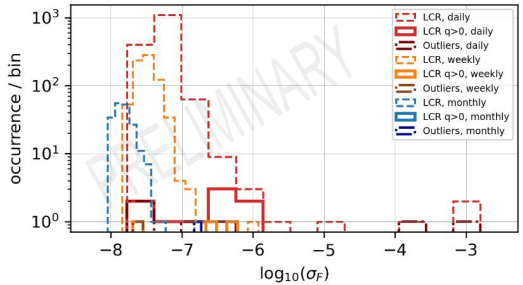

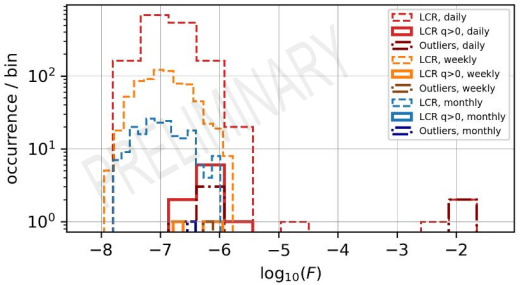

Automating the validation process

- Removes undesired data upfront:
  - With absent TS, flux, flux error, index or index error.
  - TS < 0.
  - Flux error or index error == 0.
- Excludes data from analyses that did not converge).
- Excludes outliers from significance proxies according to desired deviation thresholds.
- Prints distances to the Sun and Moon when closer than 12 deg.
- Examines possible correlations with light curves of variables sources within 12 deg from the target.

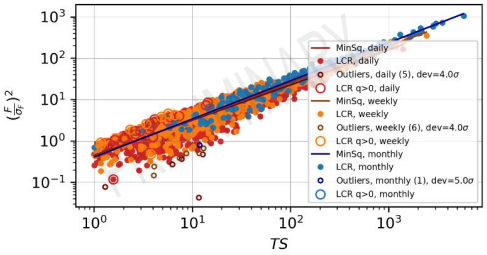

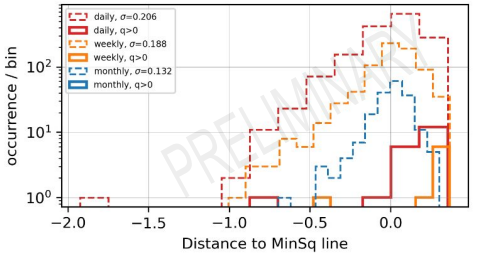

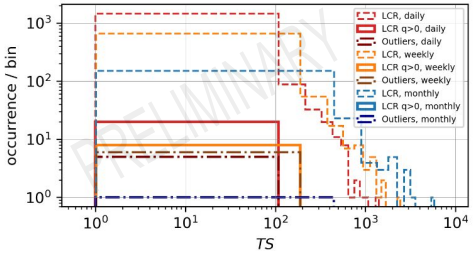

FSRQ 4C +28.07
4FGL J0237.8+2848
Index free

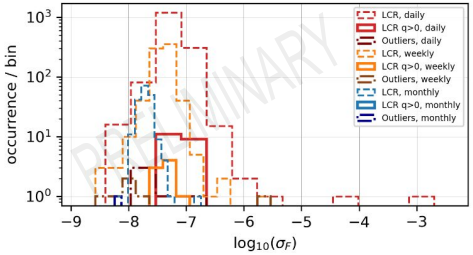

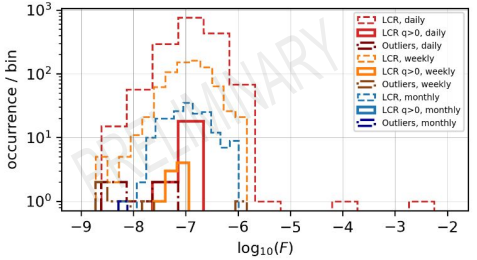

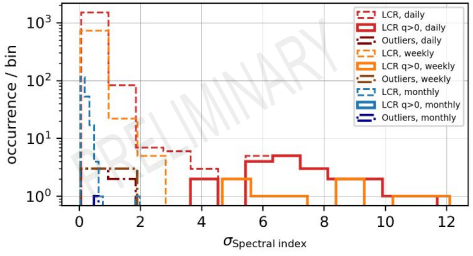

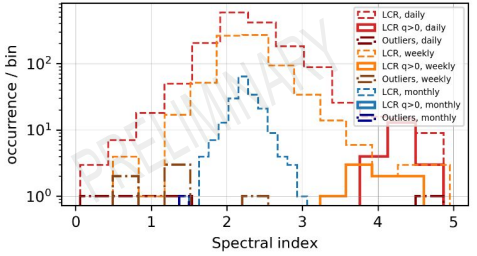

Duty cycle

Important to guide multi-wavelength observations. Exploits unique ability of the Fermi-LAT to scan the entire sky.

Procedure:

- Validate LCR light curves.
- Select light curves with >100 data points:
  - Daily: 1519 sources
  - Weekly: 1506 sources
  - Monthly: 775 sources
- Recursively fit a linear baseline.
- Select the threshold of activity. At >3 sigma:
  - Daily: 775 (out of 1519) sources
  - Weekly: 833 (out of 1506) sources
  - Monthly: 637 (out of 775) sources

Faint FSRQ: 4FGL J0004.4-4737

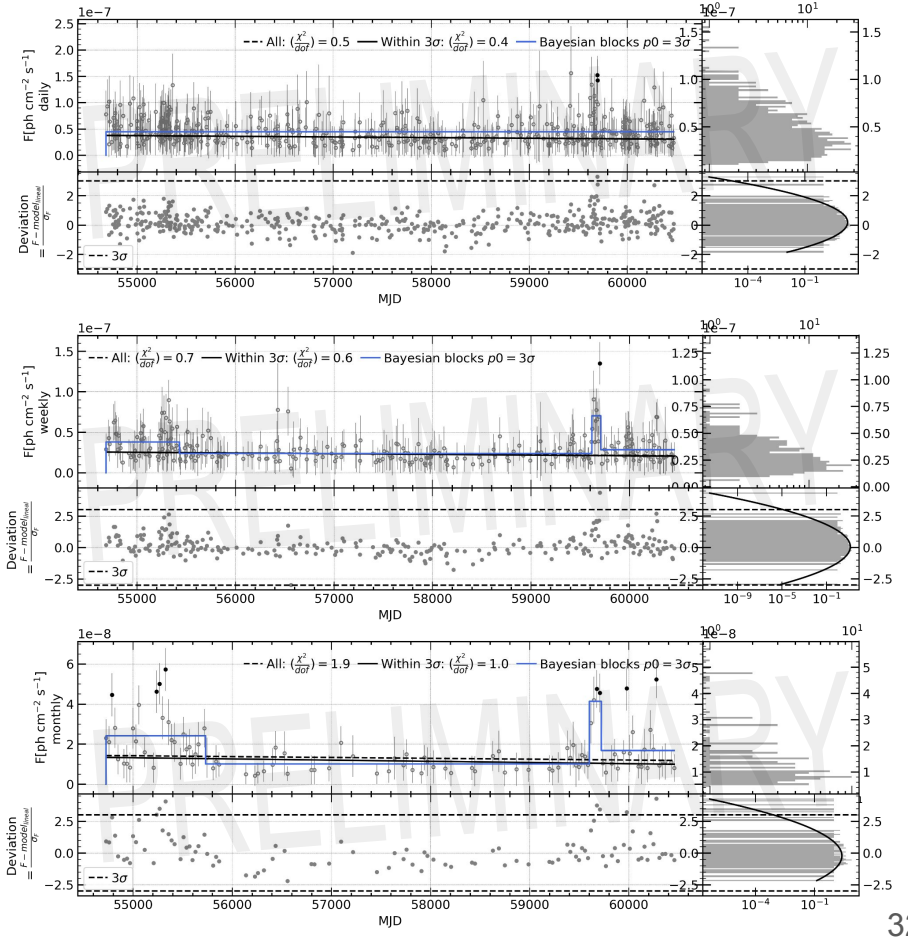

FSRQ 3C 279

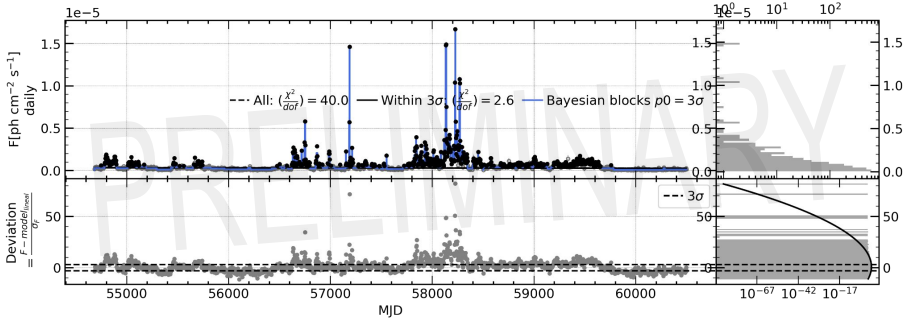

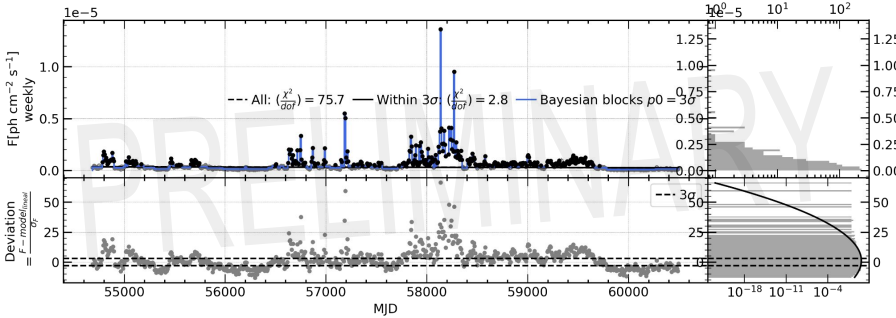

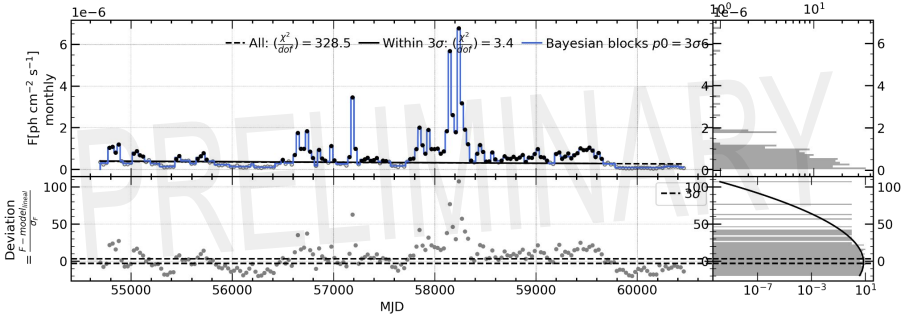

BLL PKS 0447-439 (HSP)

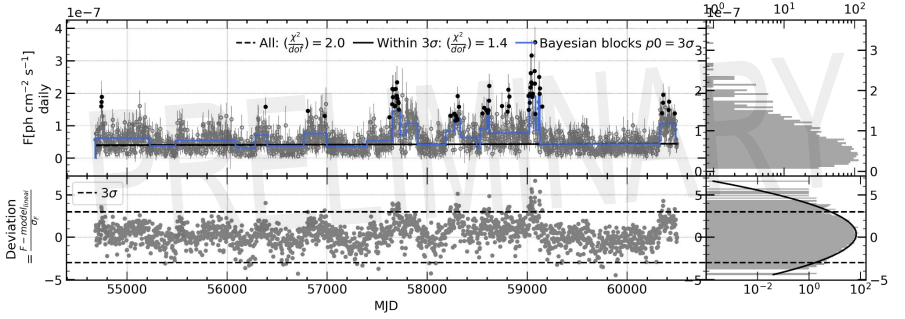

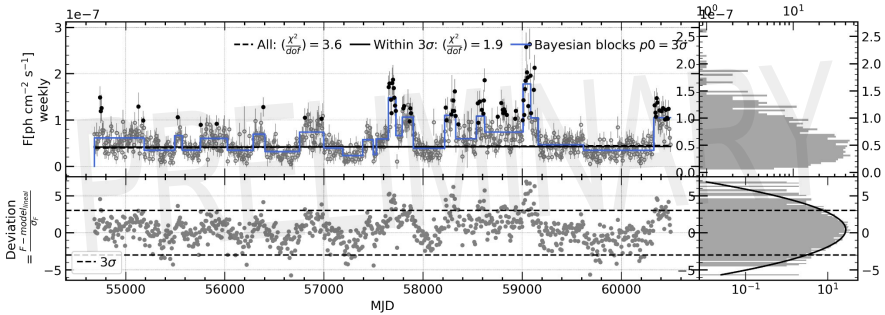

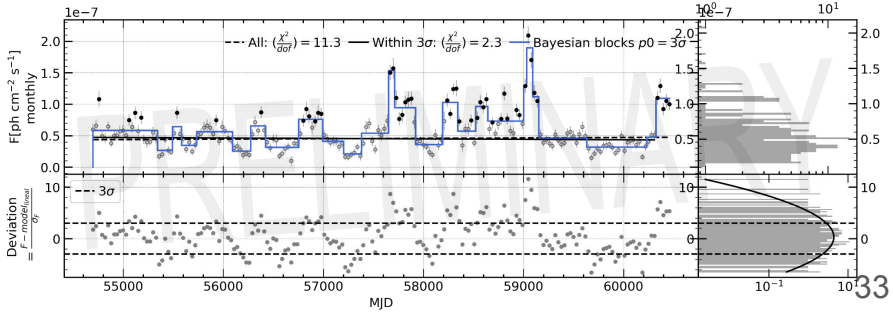

Blazar duty cycle

- 3-day: ~92% of LCR sources with >100 light curve data points. Of these, roughly 35% BLL, 41% FSRQ, 24% BCU.
- Weekly: ~92% of LCR sources with >100 light curve data points. Of these, roughly 34% BLL, 41% FSRQ, 24% BCU.
- Monthly: ~94% of LCR sources with >100 light curve data points. Of these, roughly 46% BLL, 46% FSRQ, 8% BCU.
- Blazars show activity at all timescales.
- ~100 sources flared only a few times during the mission at all cadences.
- Short timescale flares wash out at longer timescales.
- A baseline is less representative at longer timescales.
- FSRQs tend to reach longer duty cycles than BL Lacs.

LCR sources

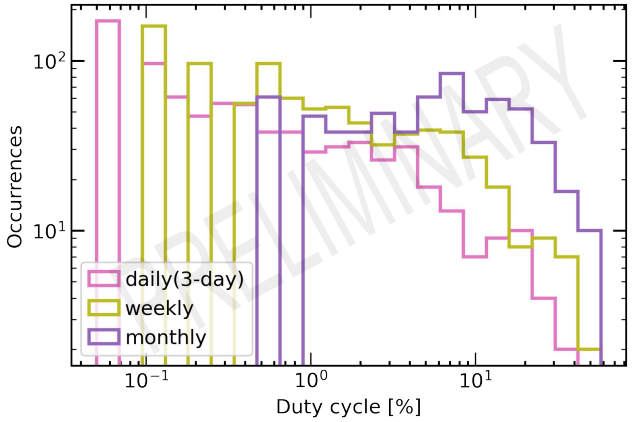

3-day blazars

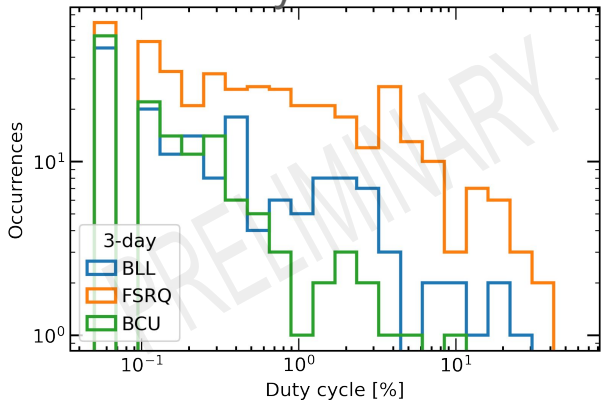

7-day blazars

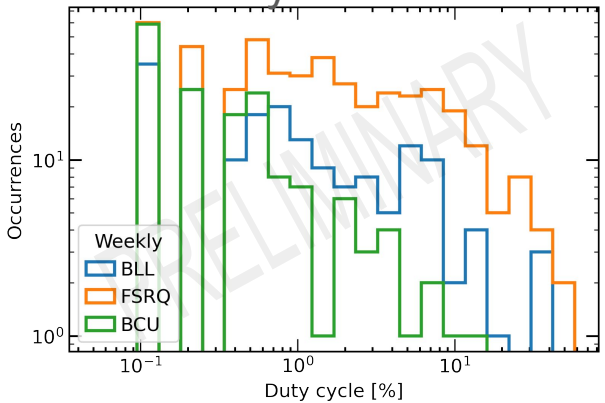

30-day blazars

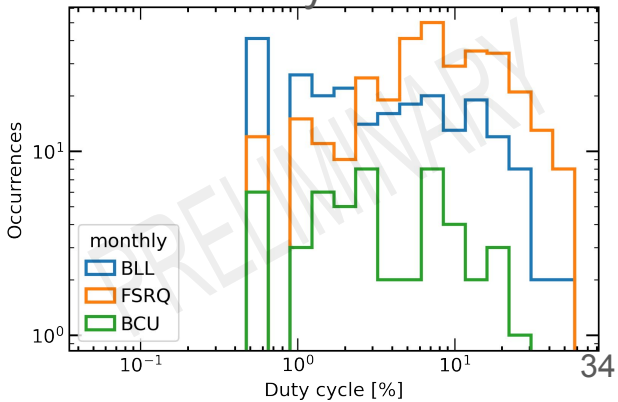

Ongoing & future work

- Fairly automated data validation.
- Duty cycle.
- Selection of flares.
  - Extract features & characteristics of flares according to the source type.
  - Can the selection be automated? ➥ Alerts!
- Implementation into Astro-COLIBRI & CTAO observing plan.
- Flux distributions.
- Spectral analysis.
  - Can we extract significant changes in the spectral slope and correlated with other spectral characteristics?

Contact: janeth.valverde@marquette.edu

Thank you!

Backup slides

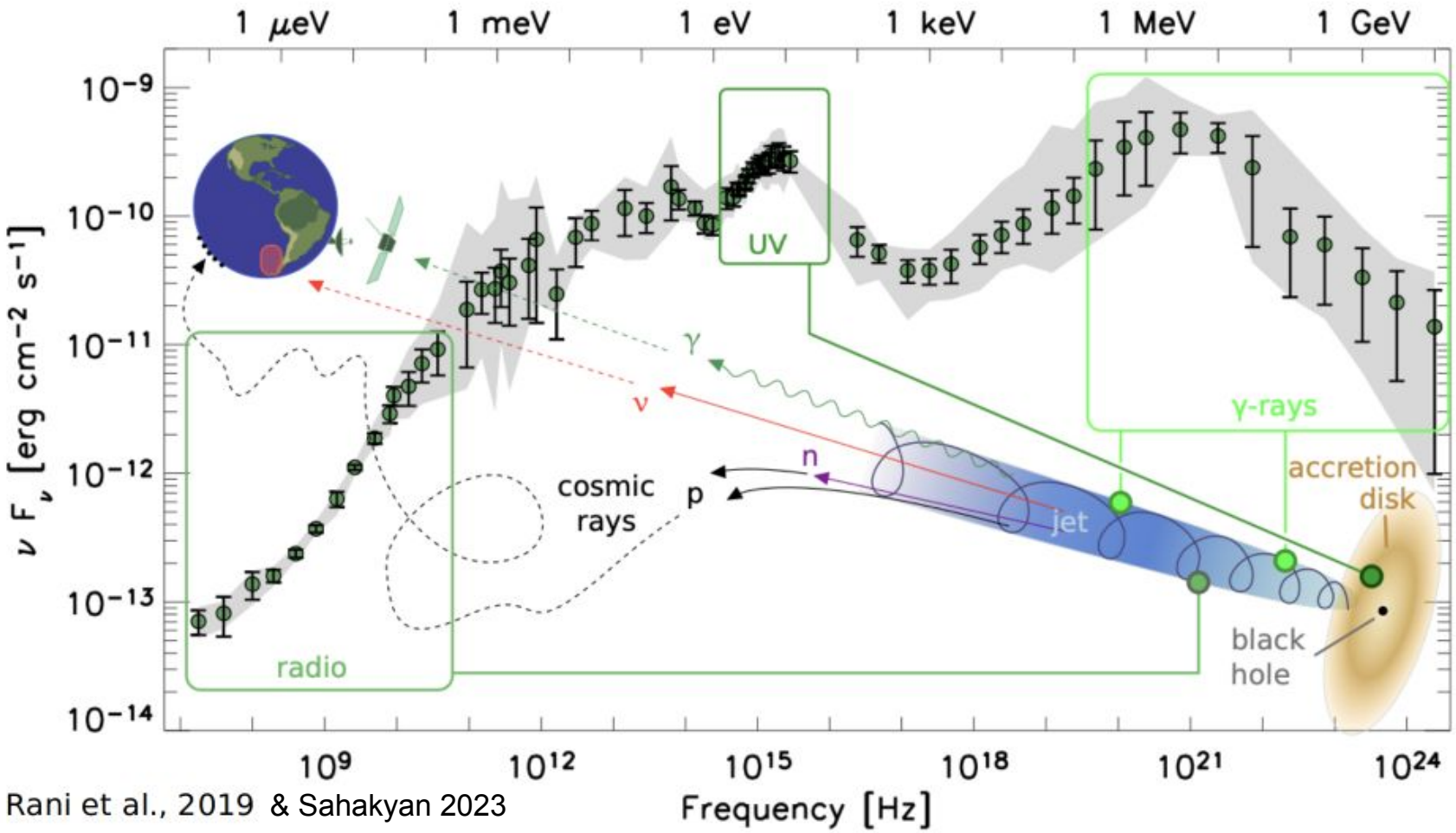

Rani et al., 2019 & Sahakyan 2023

Symmetry and fluence

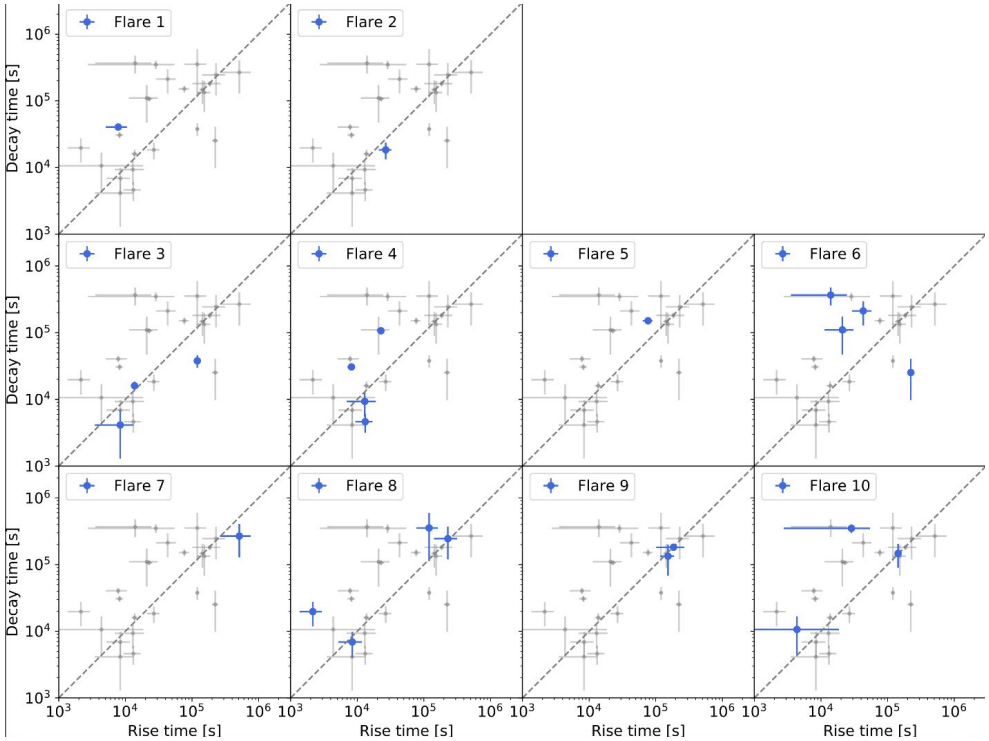

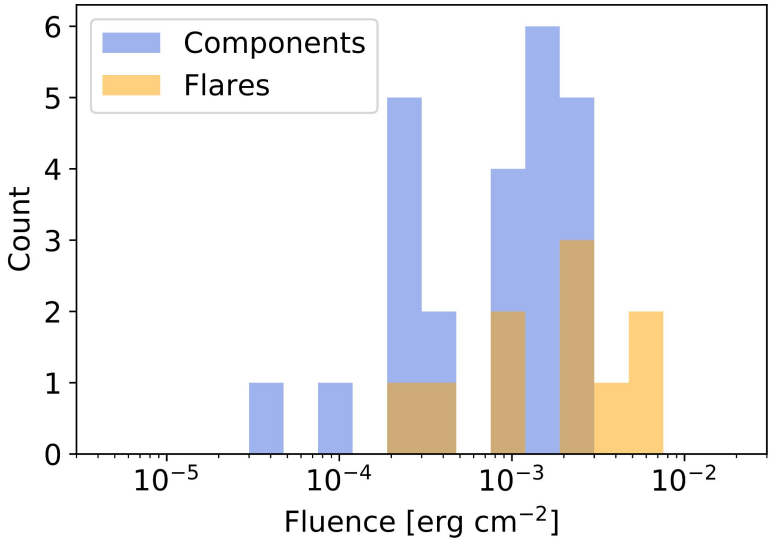

Fluence distributions of the individual flare components and flares resolved for 3C 279 during the first 11 years of the Fermi-LAT mission.

ApJ 924 (2022) 95

Constraints on size of emission region

ApJ 891 (2020) 170

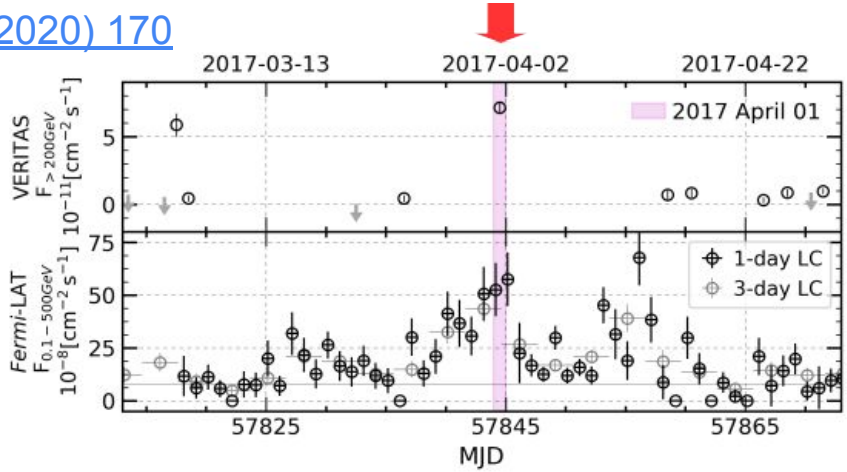

From unpublished data, strongest constraint given by flare 2017 Apr 01.

$$F(t) = F_0 + F_1 \times 2^{-(t-t_0)/t_{\mathrm{var}}}$$

$$R\delta^{-1} \leq t_{\mathrm{var}}/(1+z)$$

- GeV data, halving time: < 0.9 days.
- From SED modeling: $\delta \approx 25$.
- SMBH mass: $1.3\times10^{8} M_{\odot}$ => $\sim 3.9\times10^{11}$ m.
  (Woo & Urry 2002)

$$R \leq 1350 R_{\mathrm{S}}.$$

Senior Review: Alerts!

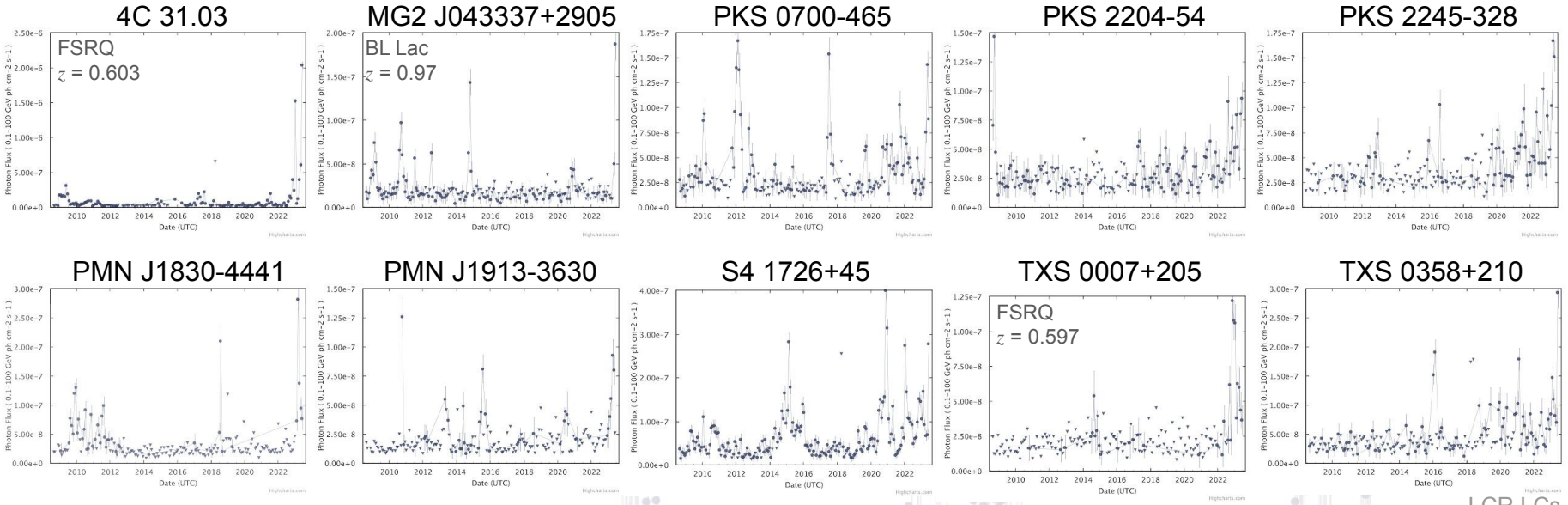

LCR LCs

- > 60 Astronomer's Telegrams and Gamma-ray Circular Notices: https://www-glast.stanford.edu/cgi-bin/pub_rapid.
- Soon in astro-colibri.com.

Flare selection

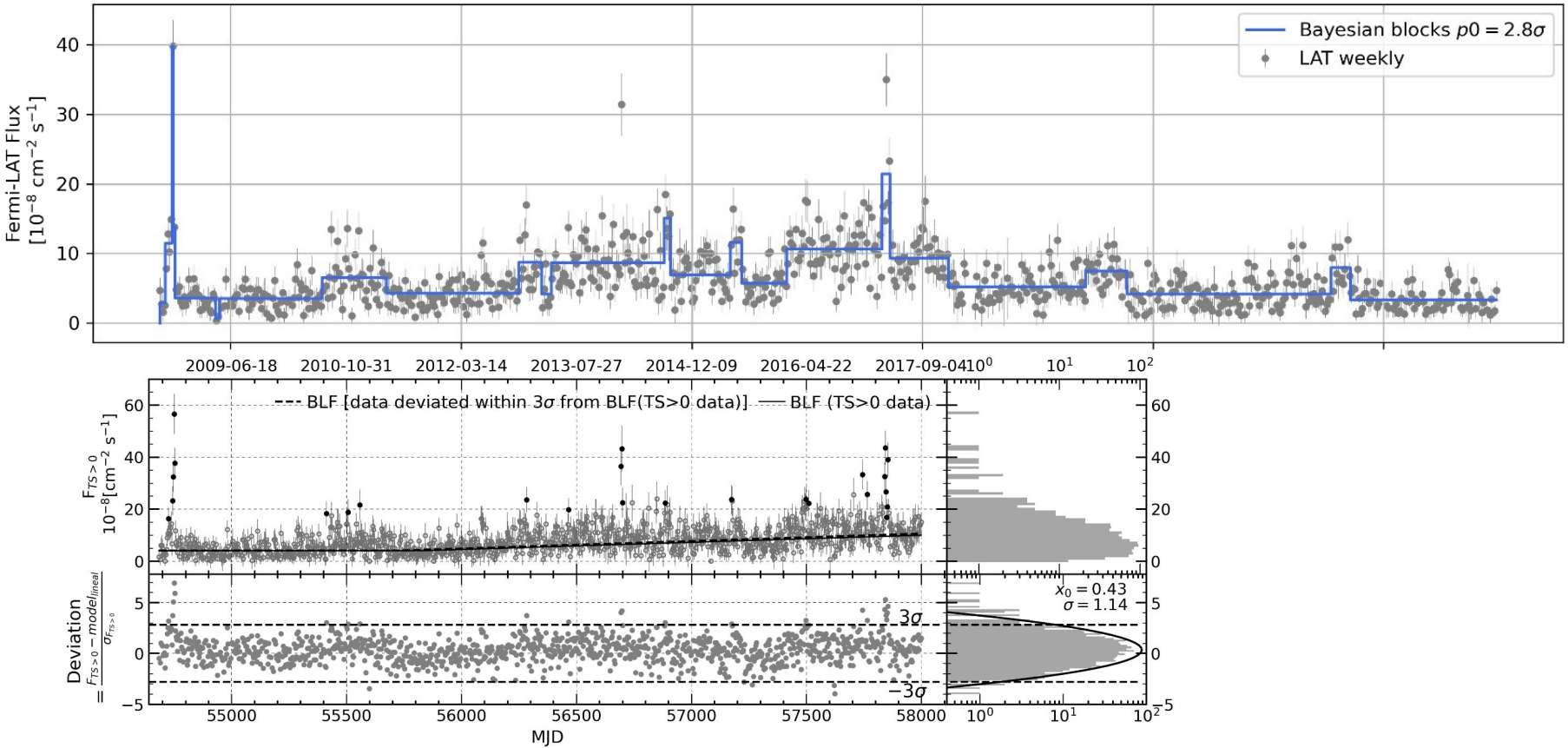

Leptonic vs hadronic production of flares

Eichmann et al. 2012

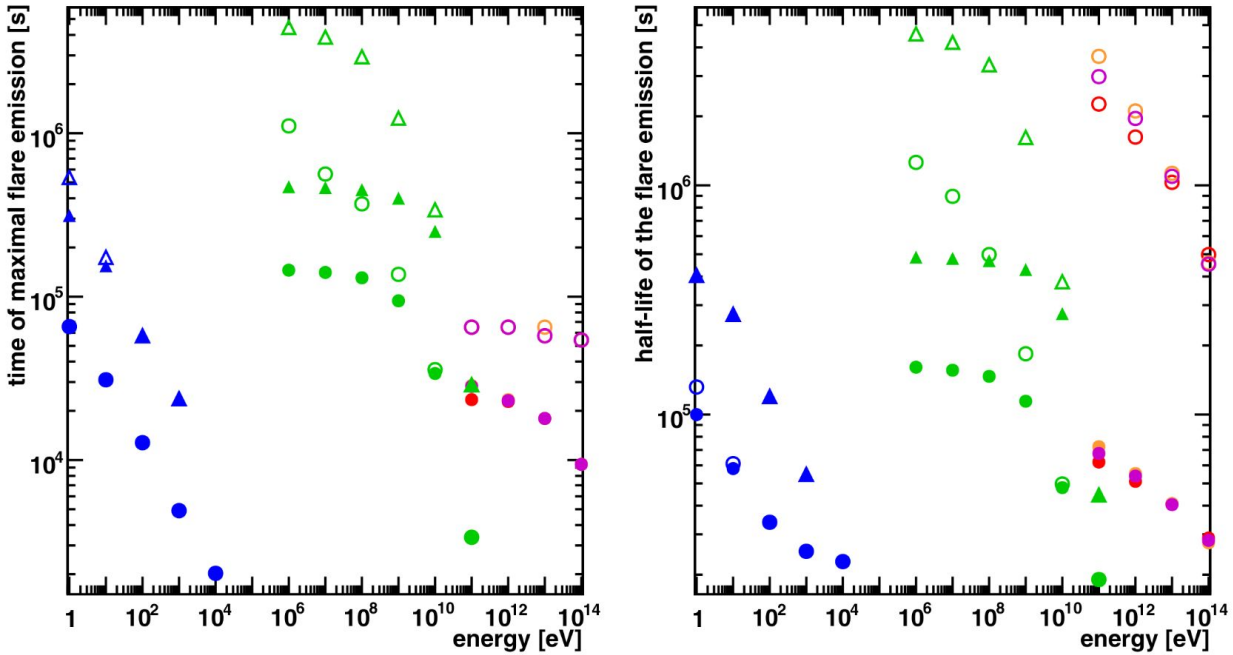

Figure 5. Characteristical temporal features of the emission of synchrotron photons (blue symbols), EC gammas (green symbols), as well as gammas (red symbols), muon-neutrinos (magenta symbols), and electron-neutrinos (orange symbols) by inelastic proton–proton interactions. The features are calculated by using two different plasma densities: $N_{10} = 0.1$ (non-filled symbols) and $N_{10} = 10$ (filled symbols) and in the case of the leptonic emission scenario we additionally vary the magnetic field strength, so that $b^2 + l_{\rm EC} \simeq 1$ (circles) and $b^2 + l_{\rm EC} \simeq 0.1$ (triangles), respectively. Furthermore, we used $\theta_1 = 1$, $\beta = 0$, $R_{15} = 1$, $\gamma_6 = 1$, and $q_{-4} = 1$ in the full diffusion limit.

Yoshida et al. 2023

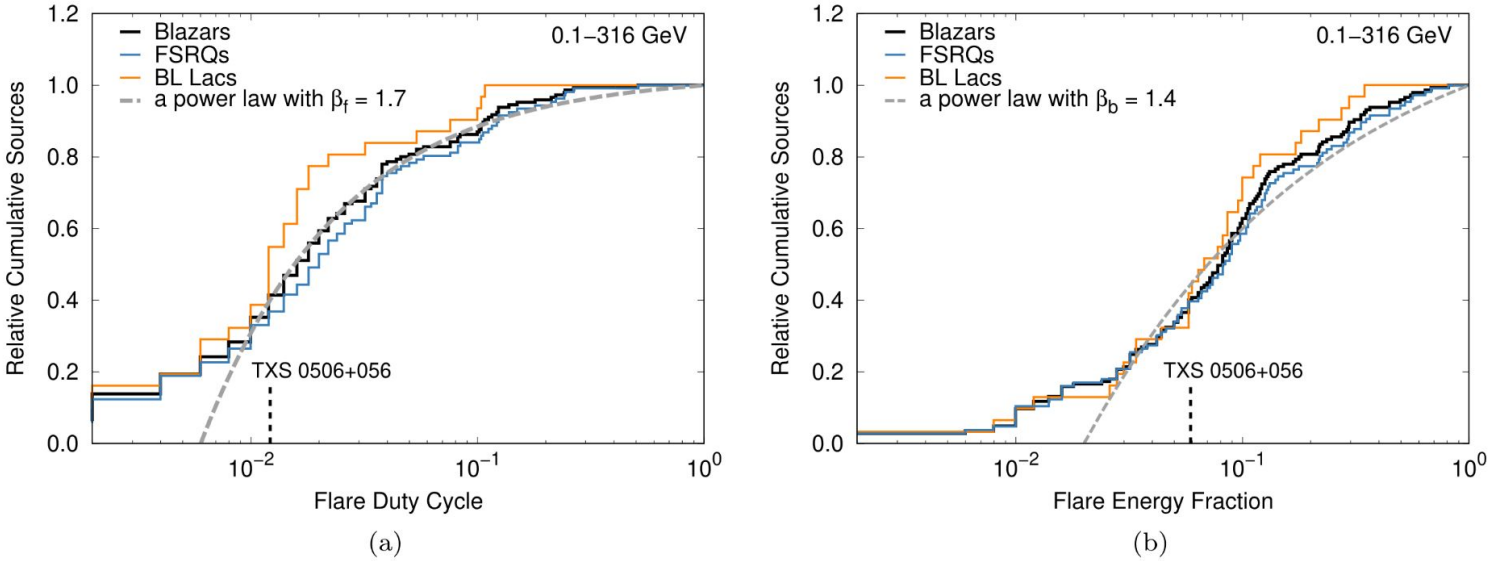

Figure 3. Cumulative histograms (normalized to one) of the 0.1–316 GeV gamma-ray flare duty cycles (a) and flare energy fractions (b) of 145 blazars (black solid histogram), 106 FSRQs (blue solid histogram), and 31 BL Lac objects (orange solid histogram). In both panels, the vertical dashed line indicates the values for TXS 0506+056 .The dashed gray lines depict cumulative power-law functions (see text for more details).

Time domain and multimessenger astrophysics

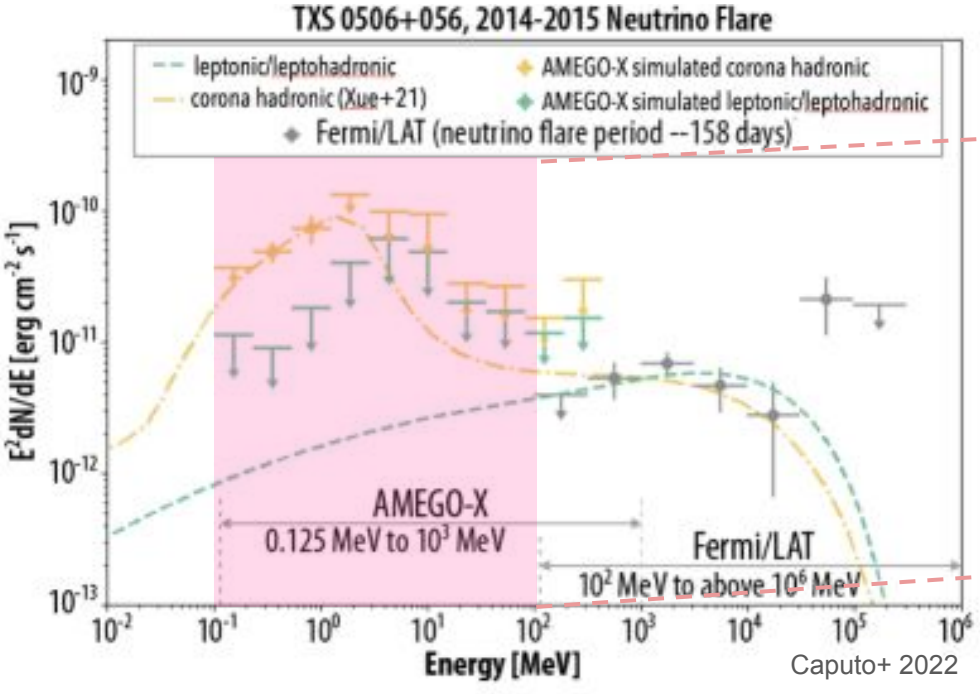

Caputo+ 2022

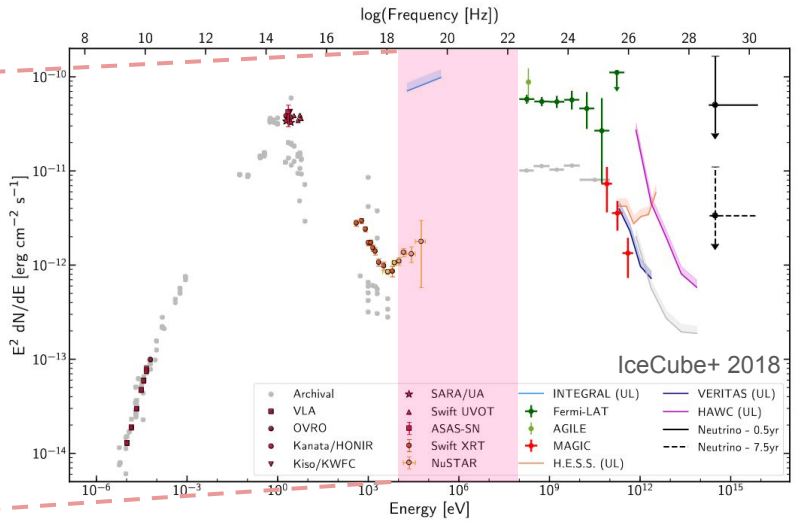

- Some hadronic models predict γ rays absorbed by jet photons, then processed into MeV photons that scape the jet.

Time domain and multimessenger astrophysics

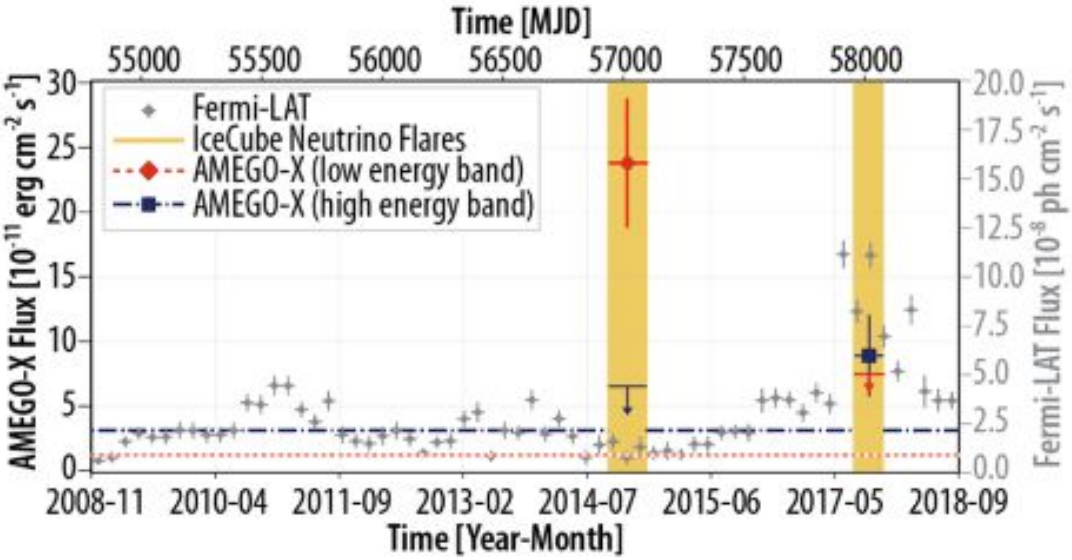

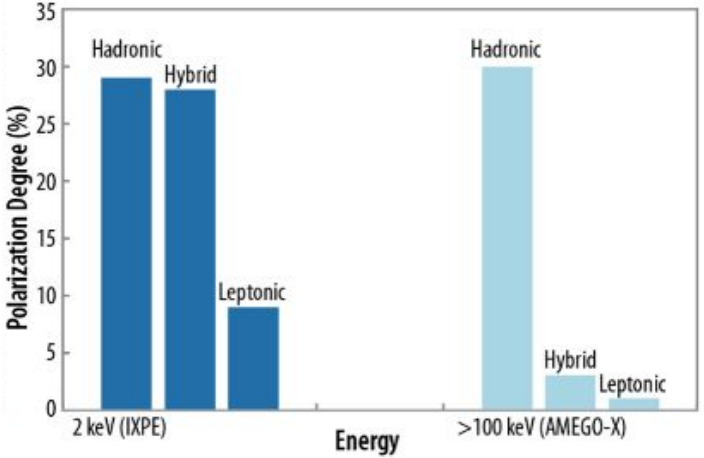

Caputo+ 2022

- Brightest ν events might not be detected by Fermi-LAT in γ because of opacity due to radiation fields.
- Powerful blazars crucial to determine their contribution to mysterious IceCube diffuse ν flux.
- MeV polarization prominent in hadronic scenario.

Time domain and multimessenger astrophysics

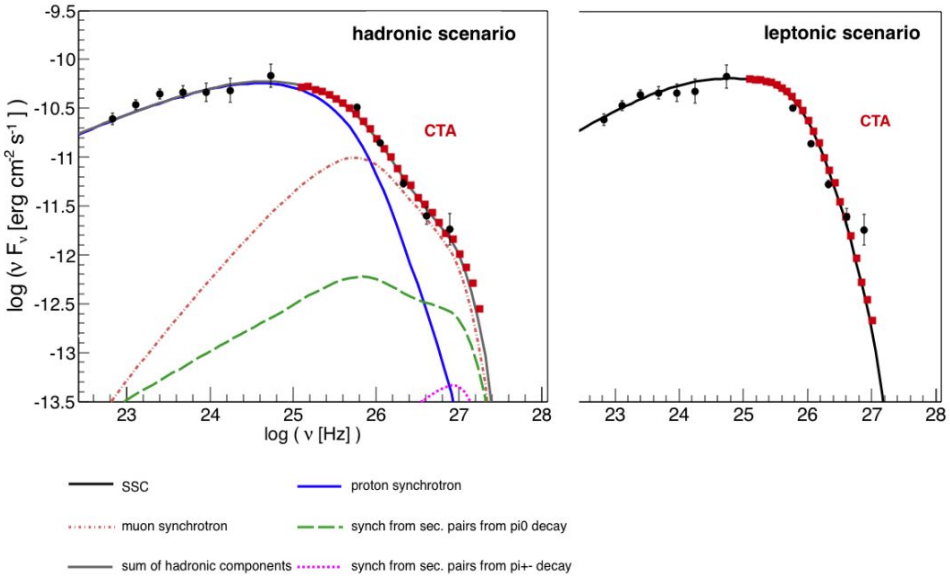

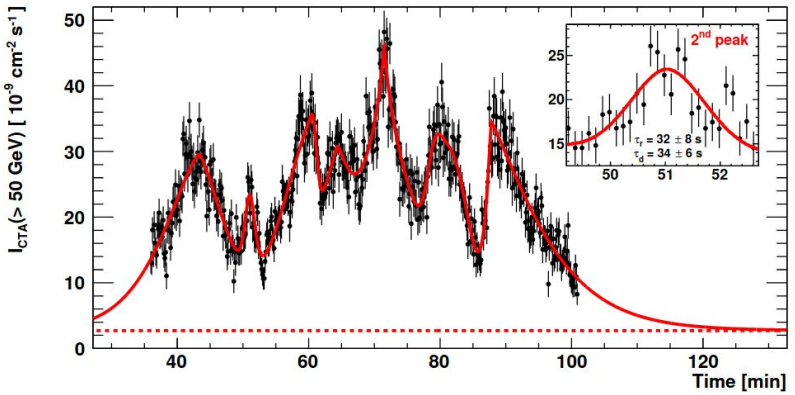

PKS 2155-304, extrapolated from 2006 flare.

- CTA might reveal features in the TeV spectra: Probe hadronic scenarios, ALPs, etc.
- CTA consortium 2018

The future is exciting!

- Time-domain era →LAT ideal for GW/ν. Lifetime of LAT orbit extends into mid-2030s.
- MeV unexplored→All-sky survey.
- CTA→EGal survey & ν follow ups.

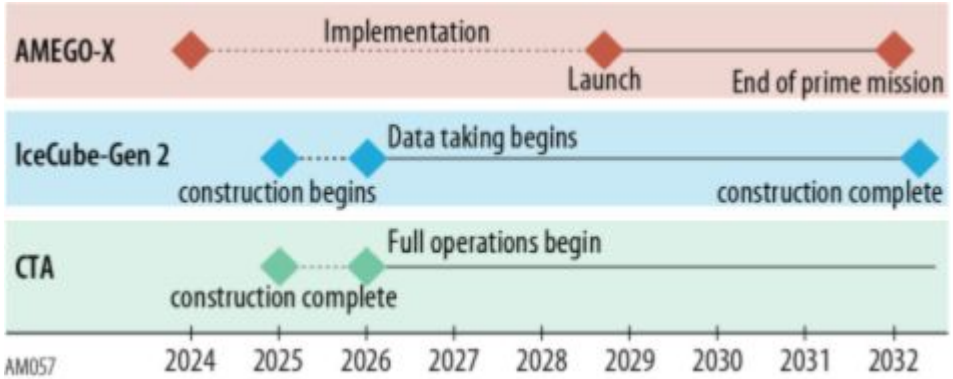

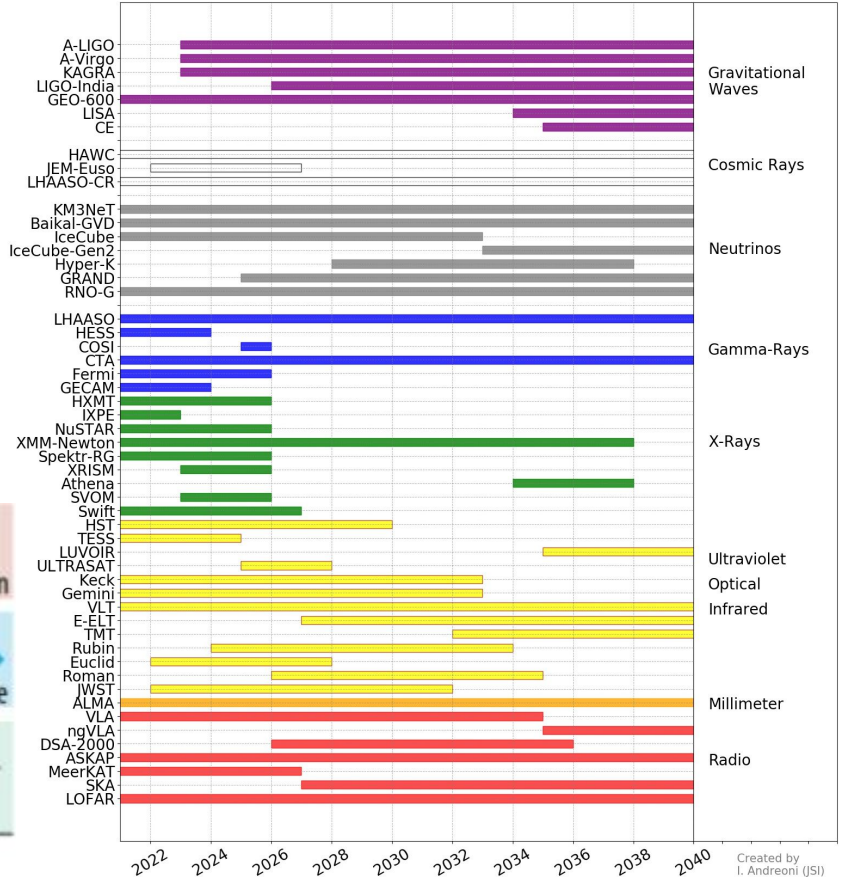

Blazar classification

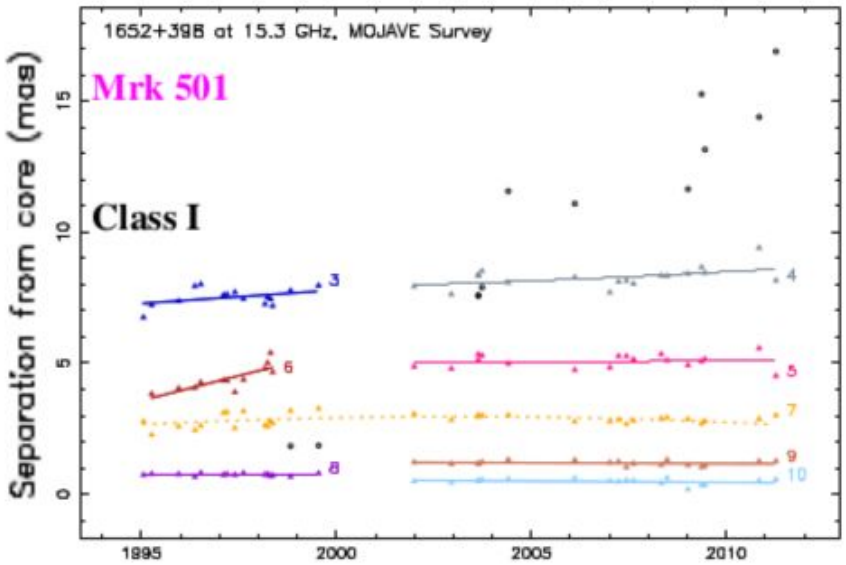

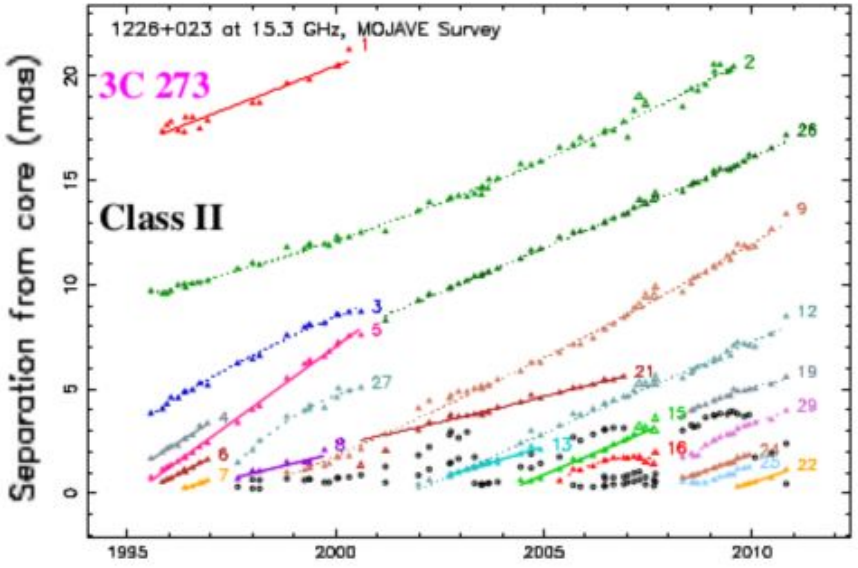

More recent classification based on the kinematics of jet radio components (Hervet et al. 2016):

- Class I: HBLs.
- Class II: FSRQs.
- Class I/II: IBLs, components close to the core in relative motion.

Blazar variability

- Variability timescales from years to minutes.
- Rapid variability challenge theoretical models:
  - Large δ ($\delta = \frac{1}{\gamma(1-\beta\cos(\theta))}, \quad \gamma = (1-\beta^2)^{-1/2}$)
  - Long cooling time in hadronic models
  - Can be produced by proton synch with very high energy protons & extremely large B.
- Possible quasi-periodic flux modulation.

PG 1553+113: Period ~2yrs?

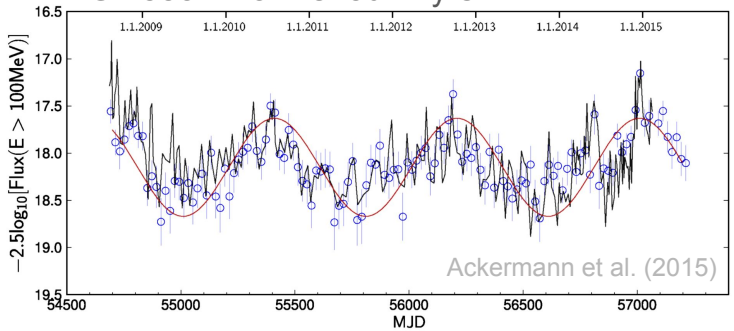

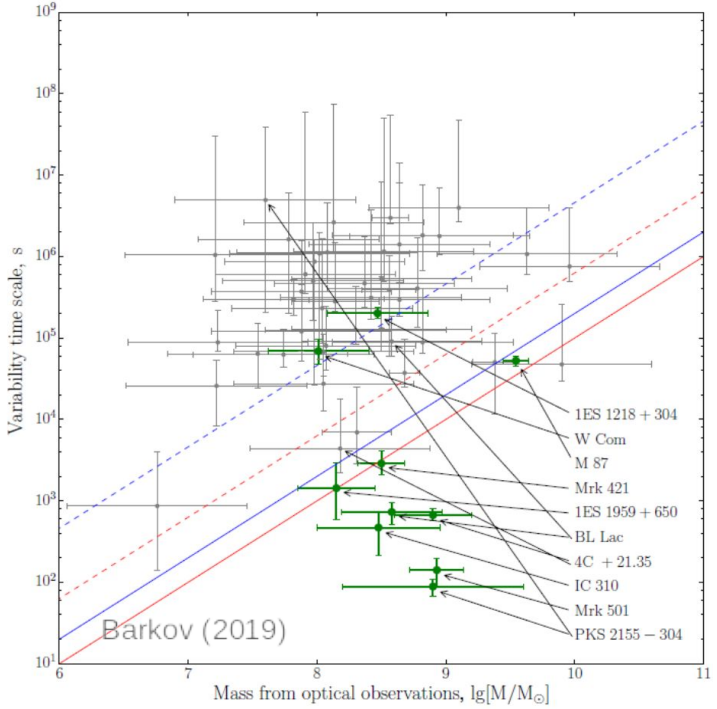

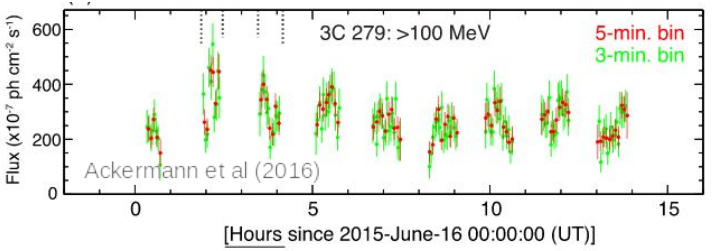

Fermi-LAT

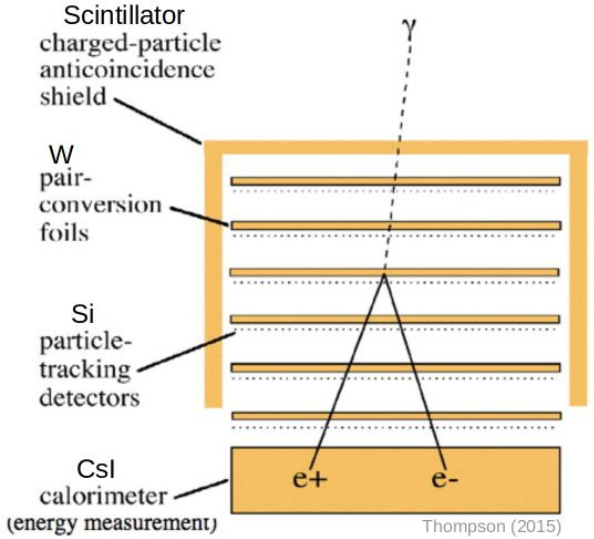

γ --> $e^+ + e^-$

ROI=Region of Interest 10º

Isotropic diffuse γ-ray emission.

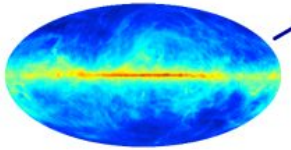

Galactic diffuse γ-ray emission.

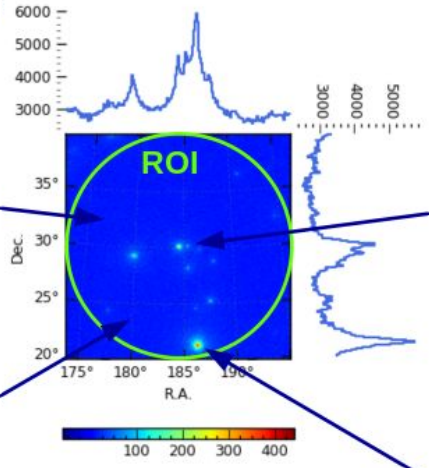

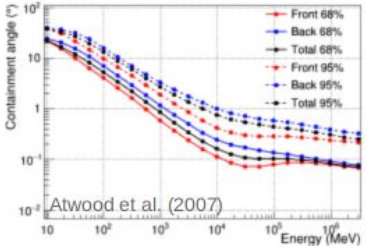

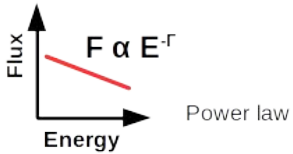

Emission from point-like sources.

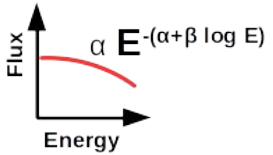

Light curve analysis

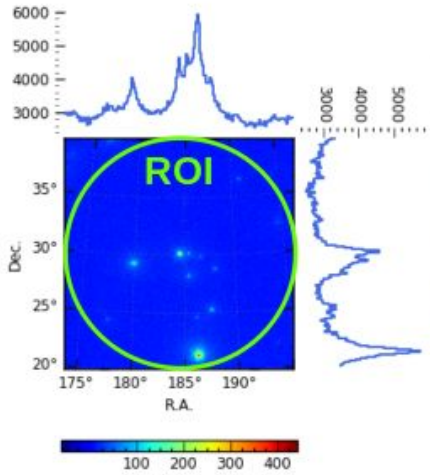

Cuts
Exposure
Cube maps
…
pre-calculations
Likelihood fit
Source maps
Sanity checks

Use fit model for SED/LC

Light curve: N time bins

Thousands if source is bright enough.

Sanity checks. Method validation. Run more refined LC if required by higher level analyses.

SED: M energy bins

a few dozens.

Sanity checks. Run SED for smaller time ranges as required by higher level analyses.

Strong long-term optical-GeV correlation

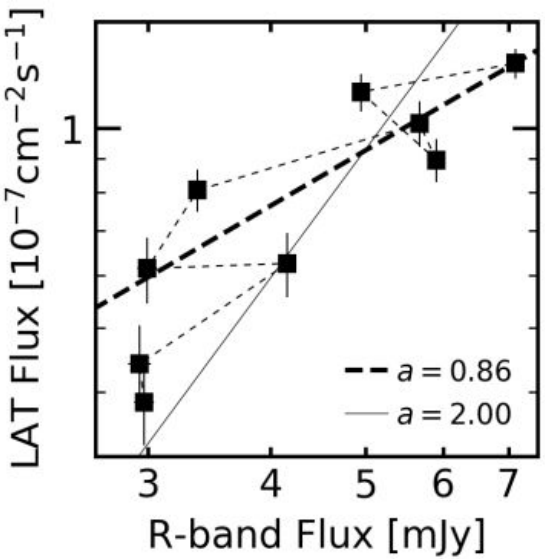

a= 1: in SSC, compatible with change of B & δ, does not favor a change of particle density
in EIC: compatible with increase of B or particle density, does not favor change of δ

a = 2: in SSC: compatible with a change of particle density
in EIC: compatible with a change of δ

- a = 0.86 ± 0.21
- Excluded a ≈ 2 (> 3.6 σ)
- No evidence of correlation between other bands.

- **Does not favor particle density change in SSC scenario**
- **Does not favor Doppler factor change in EIC scenario**

Jet structure: No evidence of precession

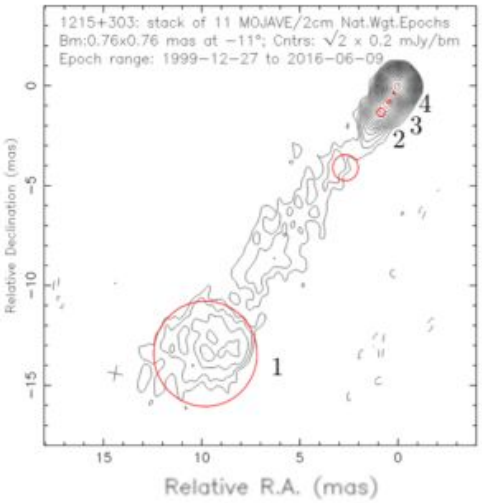

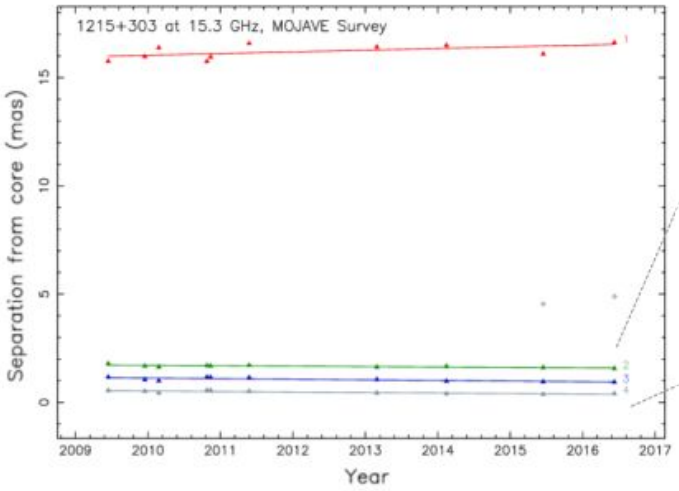

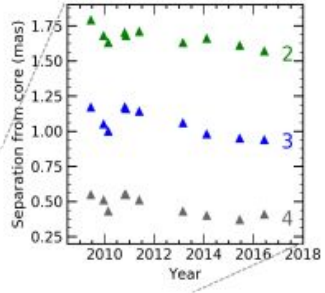

Knots 2,3,4 show similar inward motion ≈ 0.2c

(Lister et al. 2019)

Apparent inward motion possibly caused by long term power increase that would increase the distance (optically thin at larger distance) and size of radio core.

➡ **Fairly constant separation & stable jet.**

SED Modeling: Low state

[ApJ 891 (2020) 170]

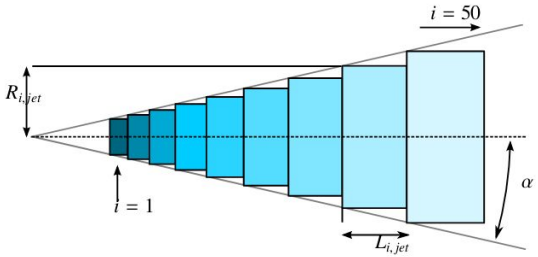

General considerations:

$$\Gamma_{blob} > \Gamma_{jet}$$
$$\rho_{blob} > \rho_{jet}$$
$$B_{blob} \geq B_{jet}$$
$$R_{blob} < R_{jet}$$
$$n_{1blob} \leq n_{1jet}$$

Blob-in-Jet model (Bjet)
(Hervet et al. 2015)

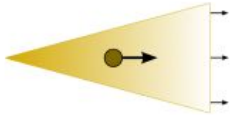

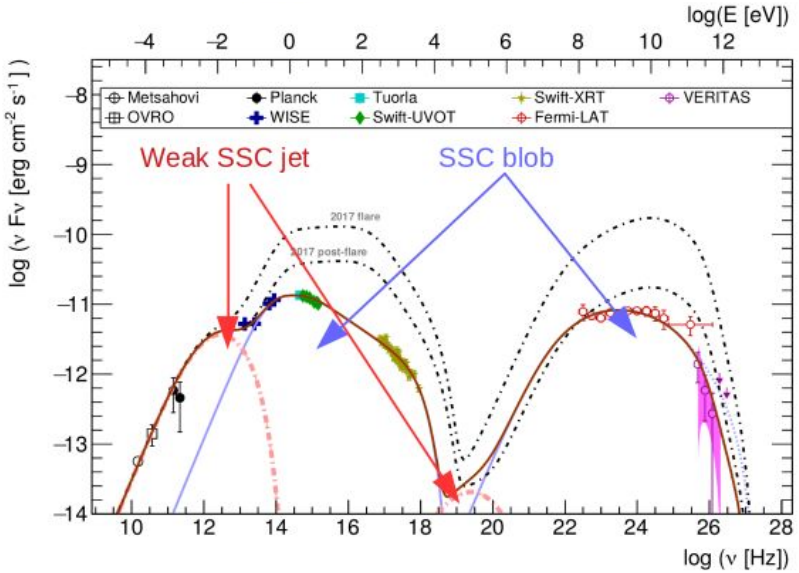

Particle energy distribution

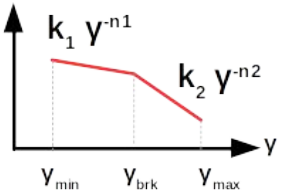

Parameter	Value	Unit
θ	2.0	(°)
Blob		
δ	25	–
K_1	1.5×10^6	cm^{-3}
n_1	2.82	–
n_2	3.7	–
γ_{min}	4.7×10^3	–
γ_{max}	6.5×10^5	–
γ_{brk}	2.0×10^4	–
B	2.0×10^{-2}	G
R	5.8×10^{16}	cm
Jet		
δ	15	–
K	51.3×10^4	cm^{-3}
n	2.82	–
γ_{min}	9.0×10^2	–
γ_{max}	3.5×10^3	–
B_1	3.5×10^{-2}	G
R_1	1.0×10^{17}	cm
L^*	1.0×10^2	pc
$\alpha/2^*$	2.4×10^{-1}	°

* *Host galaxy frame.*

Dramatic synchrotron peak shift

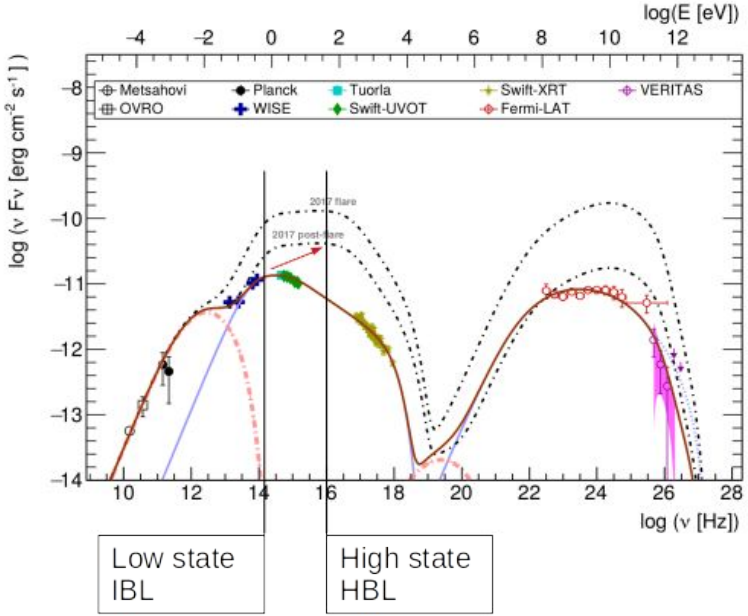

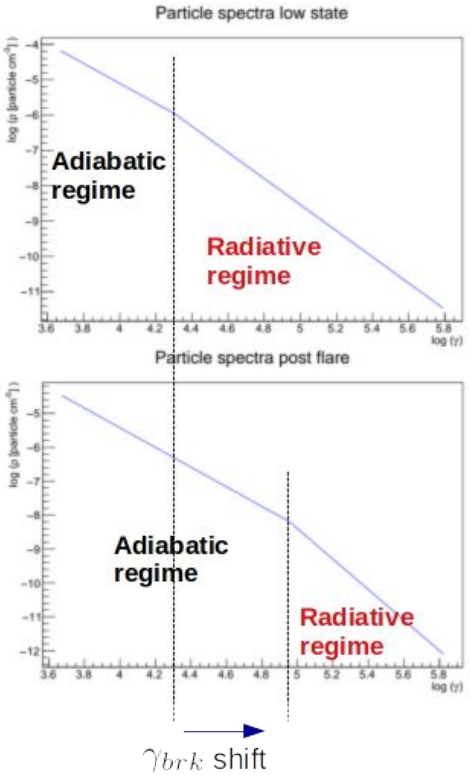

Relatively more efficient adiabatic/advective cooling during flare state

Synchrotron peak shift

VER J0521+211 (Archambault et al. 2013)
IBL => HBL

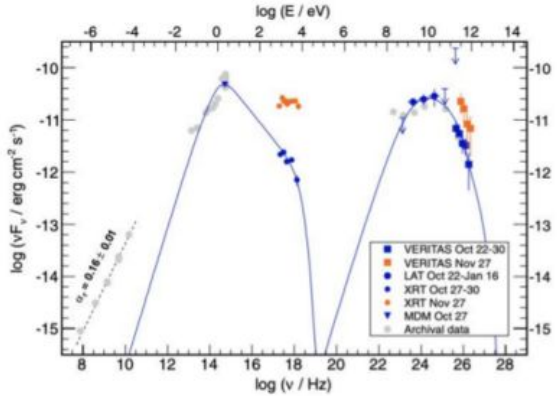

Figure 6. Spectral energy distribution of VER J0521+211 during the VERITAS detection. Optical, X-ray, GeV, and TeV data are shown for the low emission state (blue markers) and for the X-ray and TeV flare on 2009 November 27 (orange markers). Archival data points are shown in gray: radio (Cohen et al. 2007; Gregory et al. 1996; White & Becker 1992; Jackson et al. 2007; Condon et al. 1998), infrared (Wright et al. 2010; Cutri et al. 2003), optical (Monet et al. 2003; Drake et al. 2009), and gamma rays (Nolan et al. 2012). Archival radio data at 15 GHz is from the OVRO program (http://www.astro.caltech.edu/ovroblazars) and was obtained following Richards et al. (2011). Optical and infrared data are corrected for Galactic extinction using Schlafly & Finkbeiner (2011). A dashed black line shows the fit of the radio data to a power law with $F_\nu \propto \nu^{-\alpha}$. The solid blue curve represents a one-zone SSC emission model with parameters adjusted to describe the low-state data, assuming $z = 0.1$. Radio data points are not reproduced by the model, as they are expected to sample outer regions of the blazar jet, where the emission becomes optically thin to radio waves.

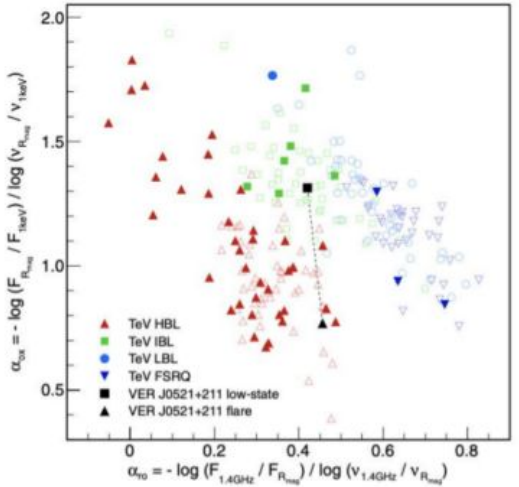

Figure 8. Spectral slopes of the synchrotron component for gamma-ray blazars. The effective spectral indices α_{ro} and α_{ox} are defined in the usual way between 1.4 GHz, 6590 Å, and 1 keV. SED classifications for the 47 known TeV blazars (filled markers) are taken from TeVCat (Wakely & Horan 2008). Multiband fluxes are obtained from Massaro et al. (2009) with the exceptions of RX J0648.7+1516, HESS J1943+213, and MAGIC J2001+435 (Condon et al. 1998; Monet et al. 2003; Voges et al. 1999; Bassani et al. 2009). Empty markers show GeV-detected blazars from Nolan et al. (2012) present in Massaro et al. (2009). VER J0521+211 is pictured in a "low-state" (2009 October 22–30) showing a spectral shape characteristic of IBLs, and in "flare" (2009 November 27), when it shows HBL-like properties.

Synchrotron peak shift

Mrk 501 (Pian et al. 1998)
HBL => EHBL

“For the first time in any blazar, the synchrotron power is observed to peak at hard X-ray energies. The large shift of the synchrotron peak frequency with respect to previous observations of Mrk 501 implies that intrinsic changes in the relativistic electron spectrum caused the increase in emitted power.”

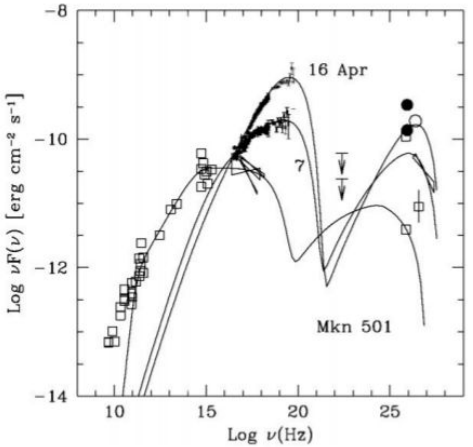

FIG. 3.—Spectral energy distribution of Mrk 501. The *BeppoSAX* data from 1997 April 7 and 16 are indicated as labeled. The nearly simultaneous Whipple TeV data (from Catanese et al. 1997) are indicated as filled circles, while the open circle (1997 April 13) and the TeV spectral fit (1997 March 15–20), along with its 1 σ confidence range, are from the HEGRA experiment (Aharonian et al. 1997a). Nonsimultaneous measurements collected from the literature are shown as open squares (radio: Gear et al. 1994; millimeter: Steppe et al. 1988, Wiren et al. 1992, Lawrence et al. 1991, and Bloom & Marscher 1991; far-infrared: Impey & Neugebauer 1988; optical: Véron-Cetty & Véron 1993 and Burbidge & Hewitt 1987; UV: Pian & Treves 1993; TeV: Quinn et al. 1996, Breslin et al. 1997, and Bradbury et al. 1997). X-ray spectral fits range in the low state are from Sambruna et al. 1994, Worrall & Wilkes 1990, and Comastri et al. 1997. Upper limits at 100 MeV are from Weekes et al. 1996 and Catanese et al. 1997. The solid lines indicate fits with a one-zone, homogeneous synchrotron self-Compton model. For all models, the size of the emitting region is $R = 5 \times 10^{15}$ cm, the beaming factor is $\delta = 15$, and the magnetic field is $B \sim 0.8$ G. For the “quiescent state,” the intrinsic luminosity (corrected for beaming) is $L' = 4.6 \times 10^{40}$ ergs s^{-1}, and electrons are continuously injected with a power-law distribution ($\propto \gamma^{-2}$) between $\gamma_{min} = 3 \times 10^3$ and $\gamma_{max} = 6 \times 10^5$. For the fit to the April 7 spectrum, $L' = 1.8 \times 10^{41}$ ergs s^{-1}, and the injected electron distribution ($\propto \gamma^{-1.5}$) extends from $\gamma_{min} = 1 \times 10^4$ to $\gamma_{max} = 3 \times 10^6$. For the fit to the April 16 spectrum, $L' = 5.5 \times 10^{41}$ ergs s^{-1}, and the injected electron distribution ($\propto \gamma^{-1}$) extends from $\gamma_{min} = 4 \times 10^5$ to $\gamma_{max} = 3 \times 10^6$. For the April 7 and 16 models, the seed photons for the Compton scattering are the sum of those produced by the assumed electron distribution plus those corresponding to the quiescent spectrum.

Synchrotron peak shift

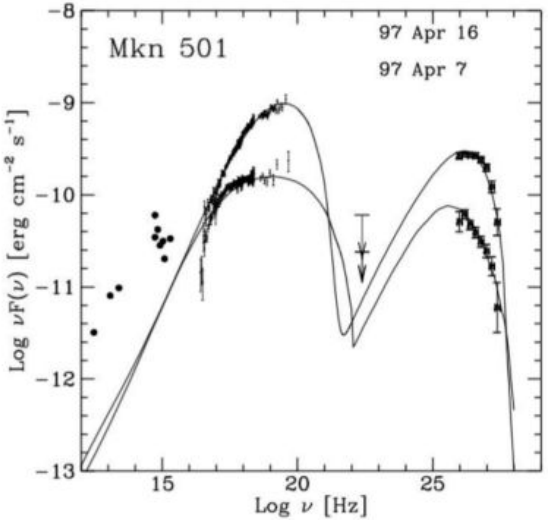

FIG. 6.—Overall SED of Mrk 501 in 1997 April. The CAT TeV spectra are from Djannati-Ataï et al. (1999). The solid line is the spectrum calculated with the homogeneous SSC model described in the text.

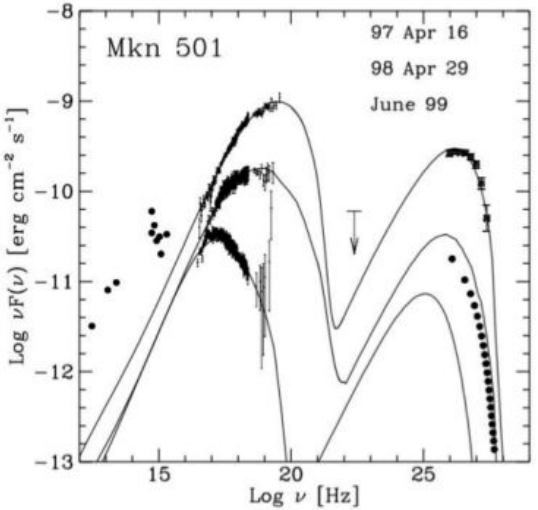

FIG. 7.—Overall SED of Mrk 501 of 1997 April 16, 1998 April 29, and 1999 June. The solid line is the spectrum calculated with the homogeneous SSC model described in the text. The filled circles are from the HEGRA 1998–1999 data (from Aharonian et al. 2001).

Tavecchio et al. (2001)

ZDCF

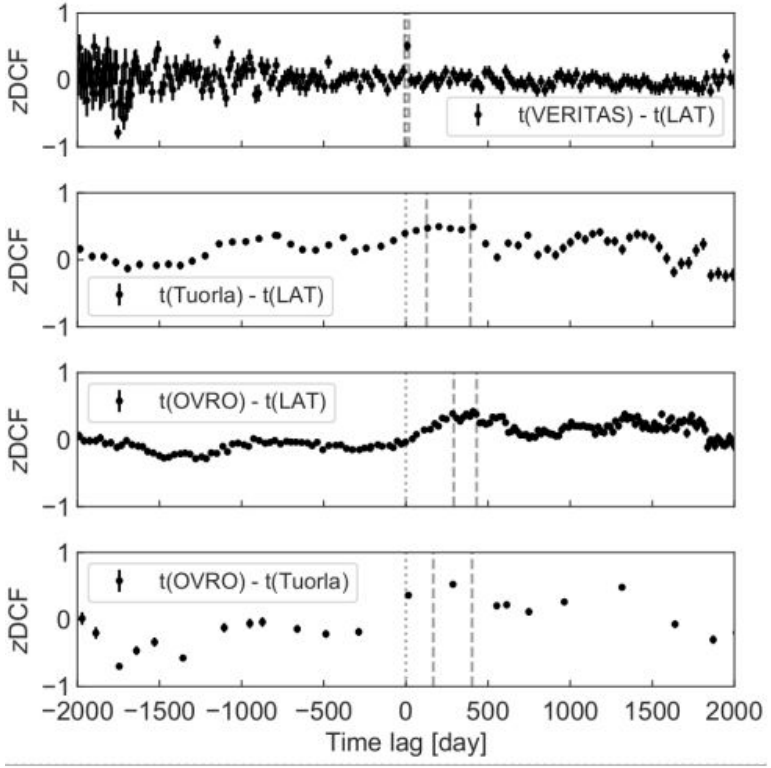

- A lag compatible with zero was found between the TeV and GeV gamma-ray fluxes, which would be consistent with the LC data presented in Slide 5.
- The absence of significant distinct peaks in the Z-transformed DCF-based LCs with 1–3 day binning intervals for the optical and gamma or the radio and gamma fluxes does not provide additional physical information.
- ZDCF uses Fisher's z-transform (Fisher 1921), minimum of 11 points/ bin & discards dependent pairs to avoid bias. Only the number of points/bin as a free param. (DCF has two). ZDCF does not depend on the number of observations, advantage for analysis of unequally sampled LCs.
- ZDCF out-performs the DCF & the interpolated CCF under wide range of conditions (Alexander 2013).

RMS-flux correlations

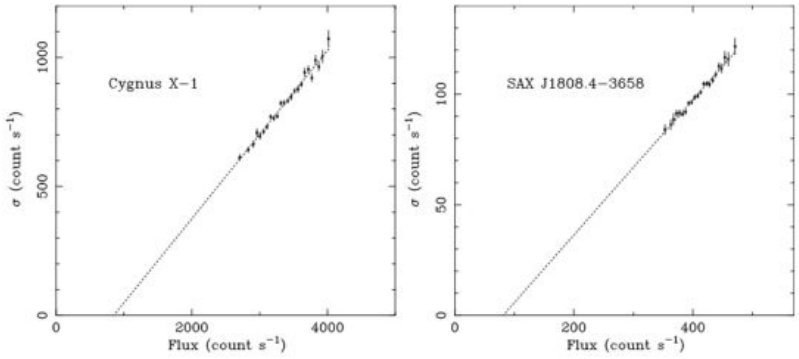

Linear relation in X-ray binaries (Uttley & McHardy 2001):

Lightcurves possibly made 'from the top down', due to large, long-time-scale variations on which the shorter-time-scale variations are later super imposed.For example, large-scale energy releases in the corona (e.g.through magnetic reconnection) might further sub-divide into a fractal structure, where the energy emitted by each sub-unit is proportional to the energy of its parent unit, but the time-scales for energy emission and the number of sub-units remain independent of total energy content (perhaps related to characteristic time-scales in the corona or disc).

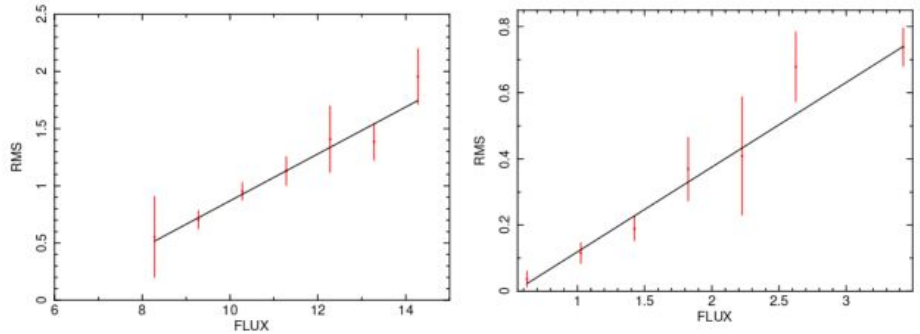

Suggested also in X-rays for 3C 273 (left) and 3C 279 (right) by McHardy (2008).

Search for quasi periodic oscillations

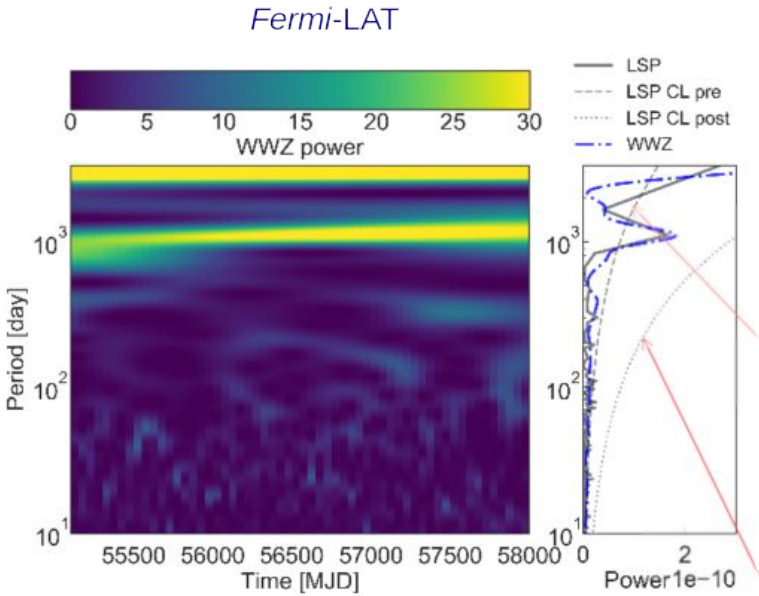

before trials

- Excess power @ ≈ 3-year period in both data sets.

after trials

- With trial factors, power < 90% C.L. [10^6 simulations (Emmanoulopoulos et al. 2013)]

➡ **No significant periodicity.**

WWZ = Weighted wavelet Z-transform
LSP = Lomb-Scargle periodograms

Extragalactic background light

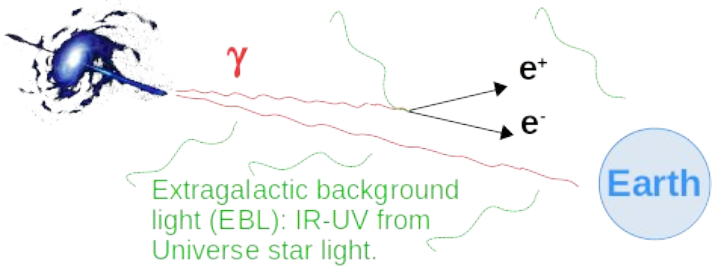

$\gamma(\sim TeV) + \gamma(EBL) \rightarrow e^+ + e^-$

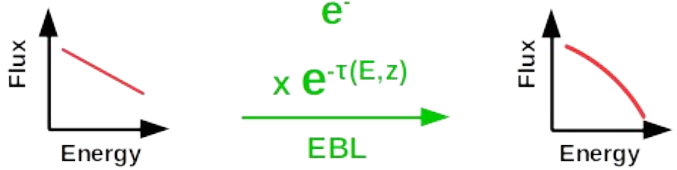

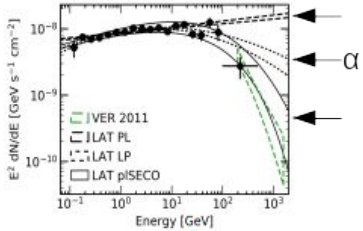

α $E^{-(\alpha+\beta \log E)}$

EBL

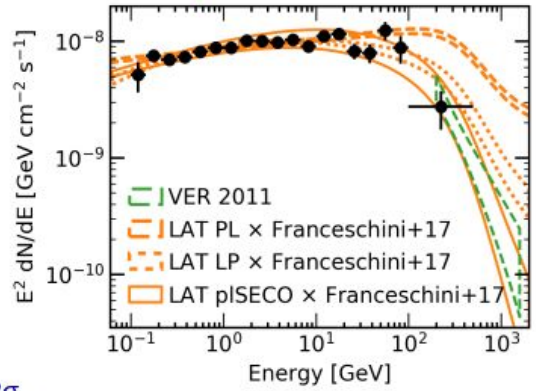

- Log-parabola (LP) preferred over power-law (PL) @ 7.2σ.
- Power-law sub-exponential cutoff (pISECO) preferred over PL @ 7.5σ. ➡ **Intrinsic curvature.**
- Other EBL models provide similar results.

Fermi-LAT Correlations

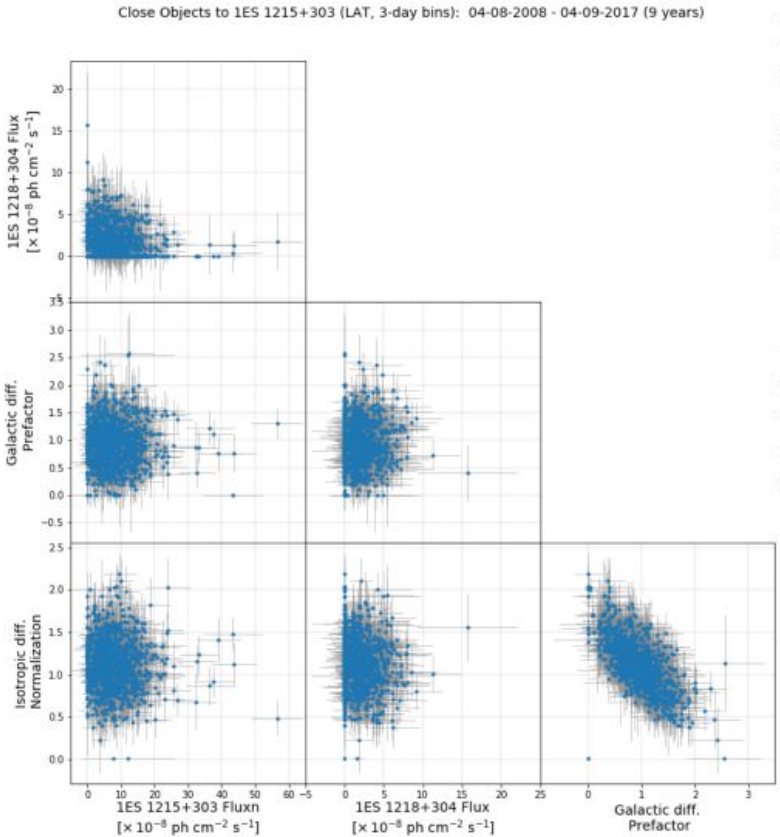

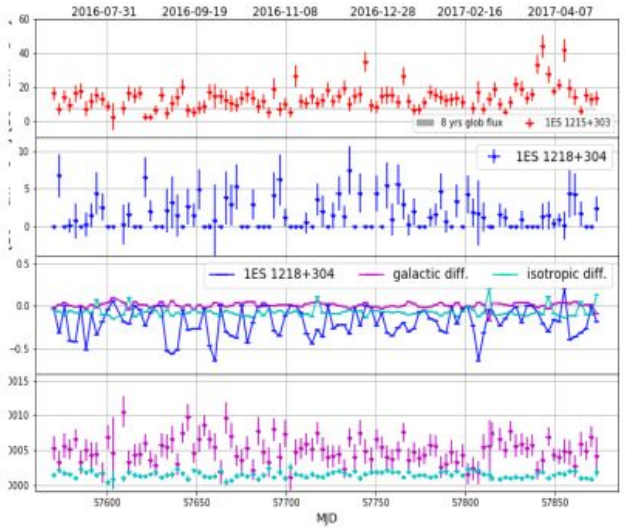

TeV FSRQs

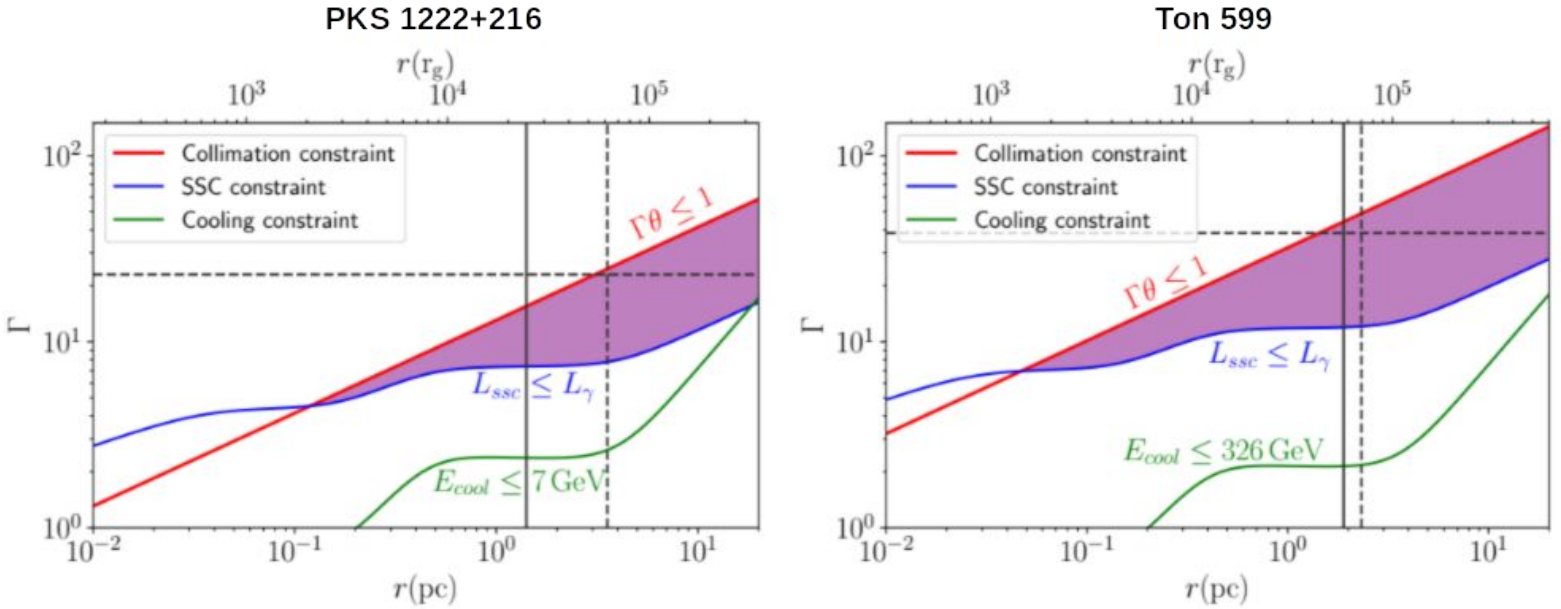

- Independent constraint on Lorentz factor & location of emission region. Black line: Opacity constraint from SED modeling.
- Strong constraint on Doppler factor >~40 for PKS 1222+216 & >~50 for Ton 599 to produce TeV emission dispite internal absoption. Emission region located a few parsecs from SMBH.

LCR computational strategy

A major challenge of producing likelihood light curves is the computational expense.

the LCR distributes the analyses of the light curve bins to separate nodes in a computer cluster hosted at the SLAC National Accelerator Laboratory.

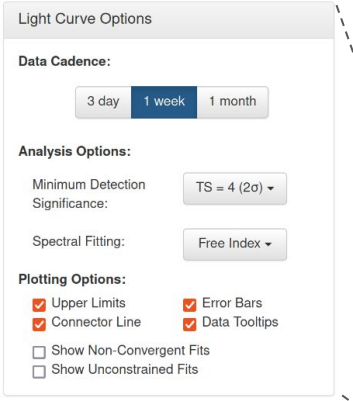

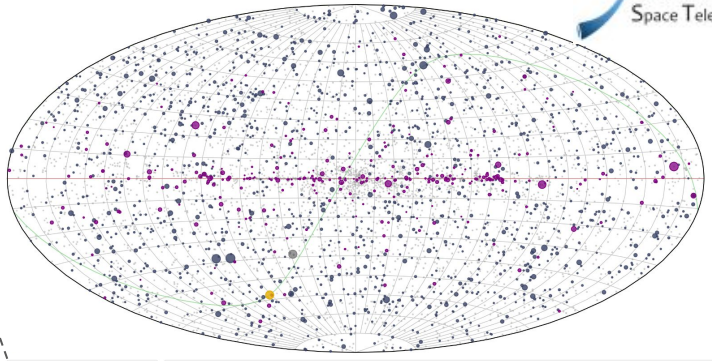

- Sources with variability index > 21.67 over 10 yearly points indicates <1% chance of being a steady source.
- Unbinned maximum likelihood, iterative, fit with decreasing tolerance [1, 1e-4, 1e-8].
- Only variable sources free in 12° ROI. Two-step fit strategy:
  - 1st fit: only normalization free & spectral index fixed to catalog value.
  - 2nd fit: normalization & a spectral index free; e.g. photon index for power-law or α for logparabola (β is fixed).
- Flux extracted when TS>1. 95% Bayesian ULs when TS<9.

Website

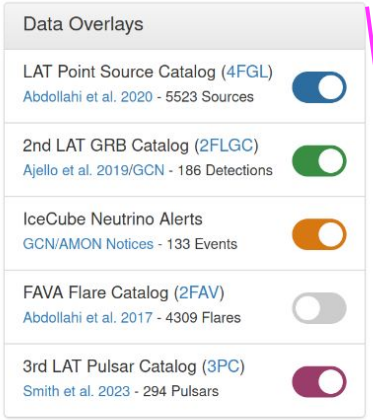

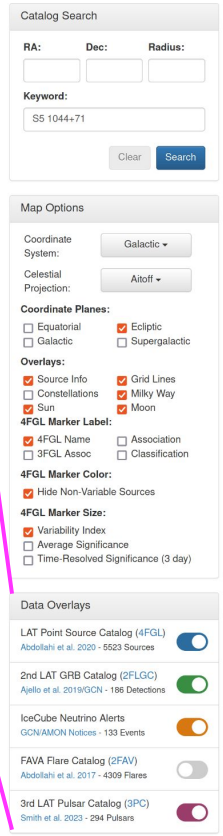

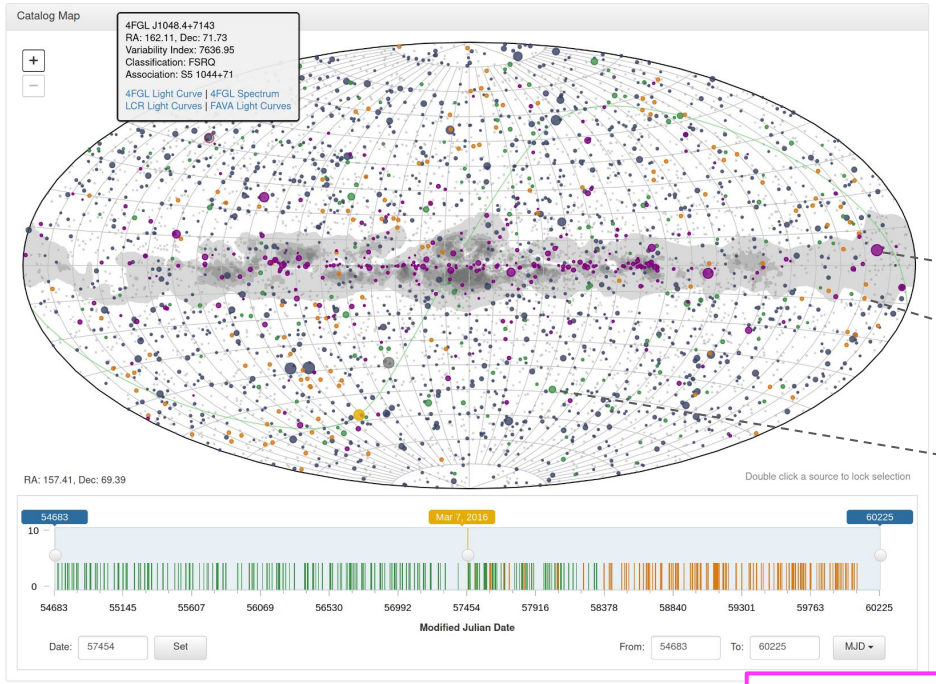

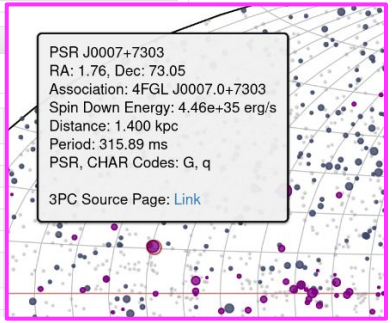

3PC source

IC error circle

2FLGC error circle

Link to main page

Analysis description & caveats

Download codes
Also pyLCR

Caveats: Exposure analysis

- Example of LC cleaning, by removing time bins with less than 200 counts in the ROI.
- Odd points with unphysical high flux and small error are cleaned up.

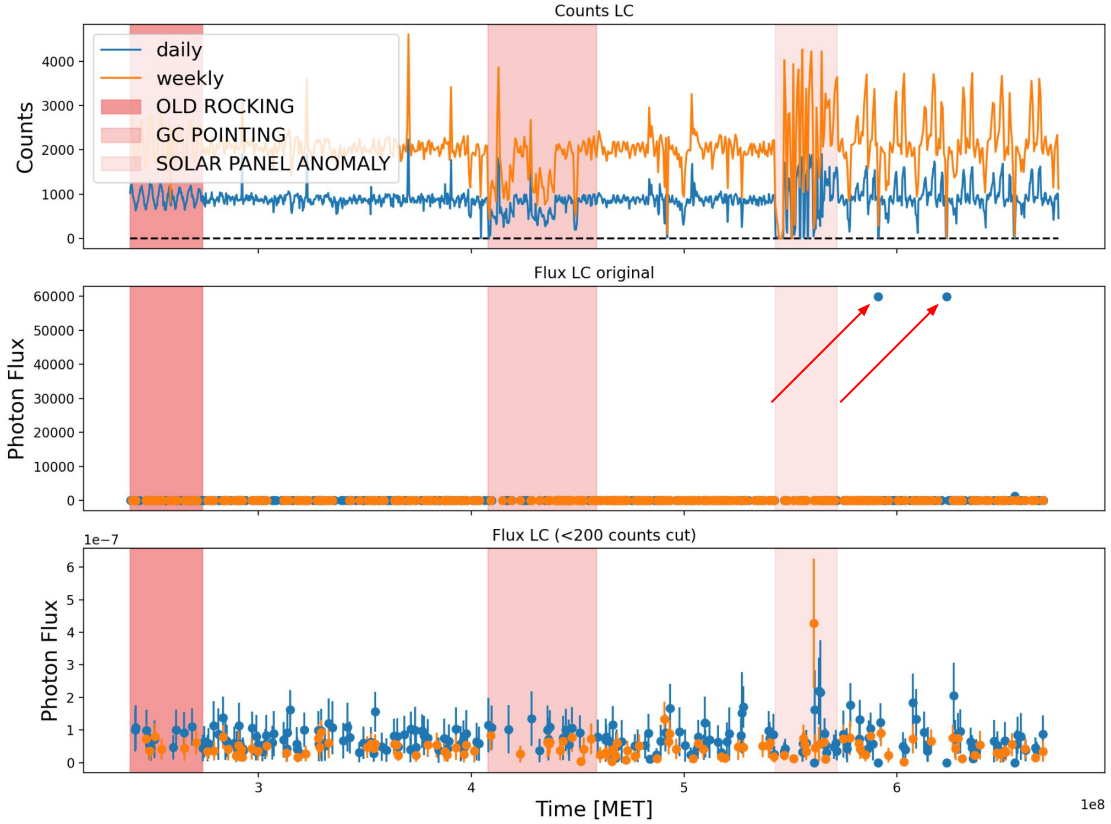

Caveats

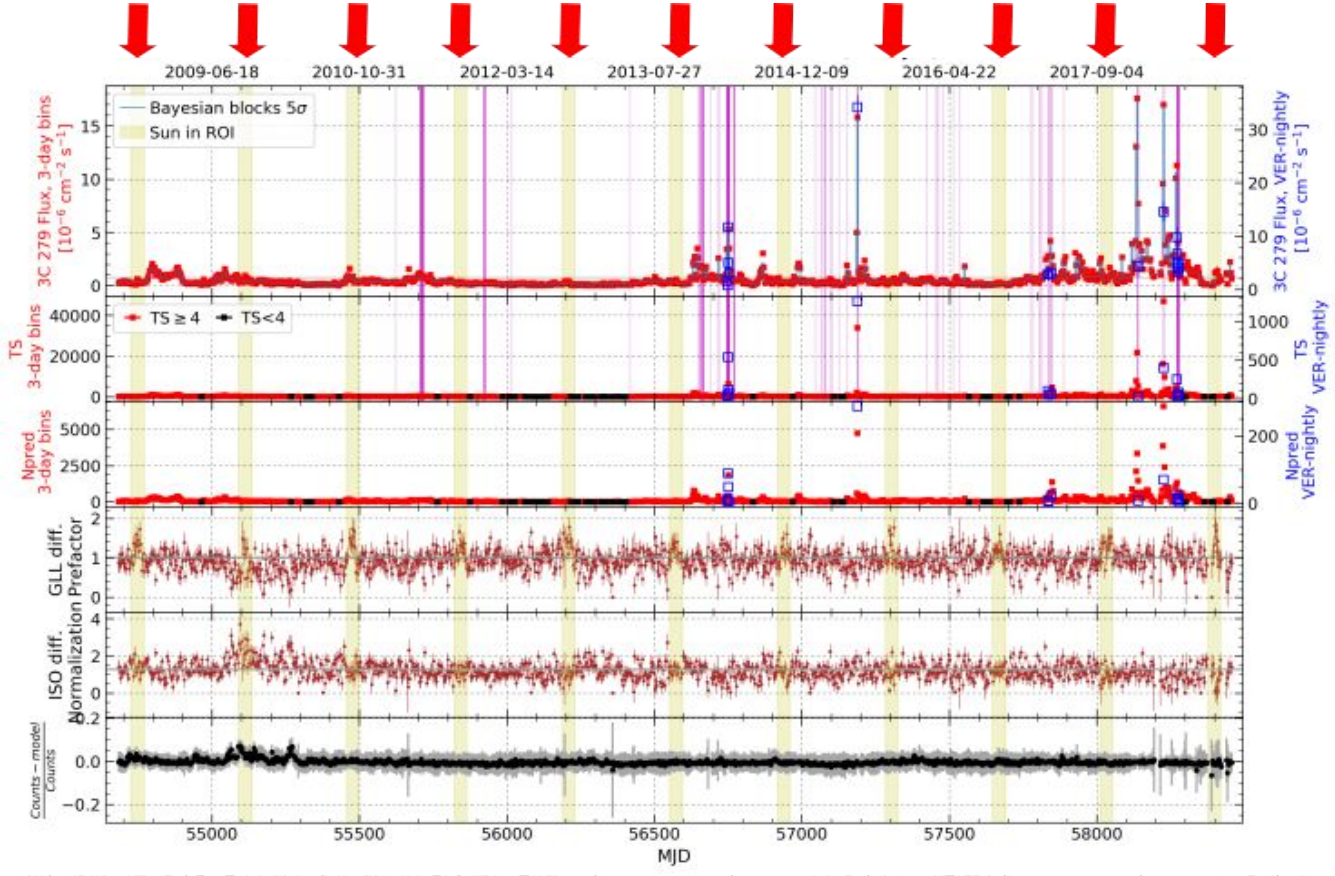

- ★ Possible contamination by the proximity of the quiescent Sun or Moon has not been accounted for, nor have those time ranges been excluded.
- ★ Happens for sources close to the Ecliptic during epochs of solar or lunar proximity (see e.g. Adams et al. 2022).
- ★ Yellow regions: Sun is < 20° from 3C 279 (quiescent Sun flux ~5×10^{-7} ph/cm^2/s).

Parameter Study of Self-Consistent Synchrotron Self-Compton (SSC) Theoretical Spectral Model

Model developed by Dr. Tiffany Lewis
Parameter study by Jordan Forman

Acceleration Mechanisms

- Shock Acceleration
  Particles gain energy from shock crossings in proportion to the energy they already have, and can pass through a shock region multiple times.

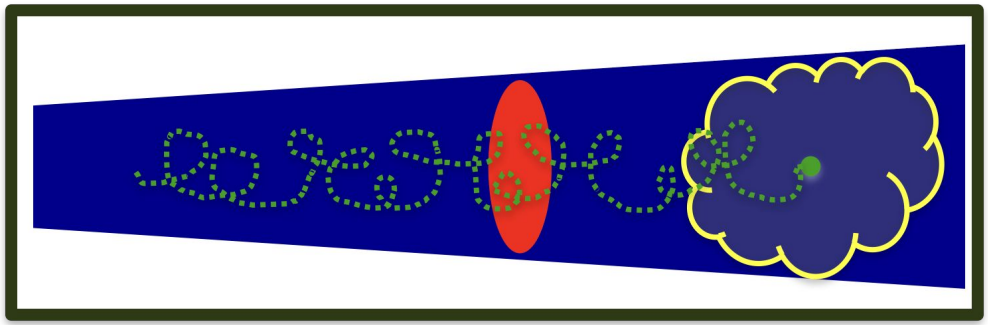

- Stochastic Acceleration
  Particles always gain energy from stochastic scatterings in the head-on approximation due to the bulk motions in the jet.

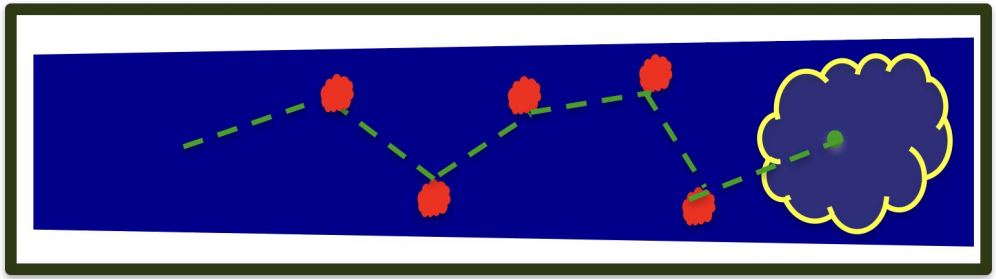

Parameter Study: Particle Injection Rate

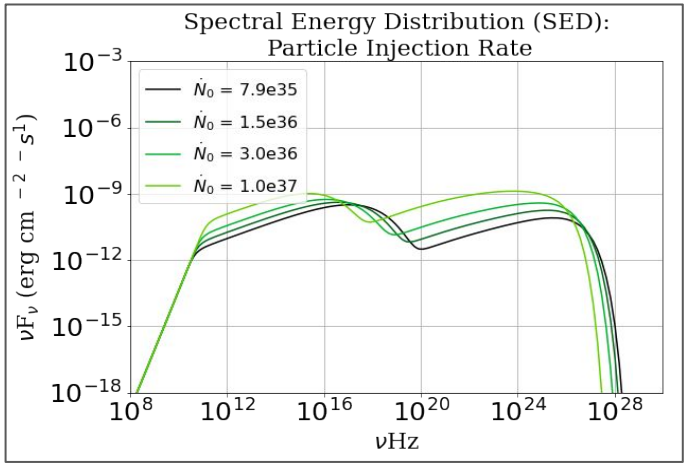

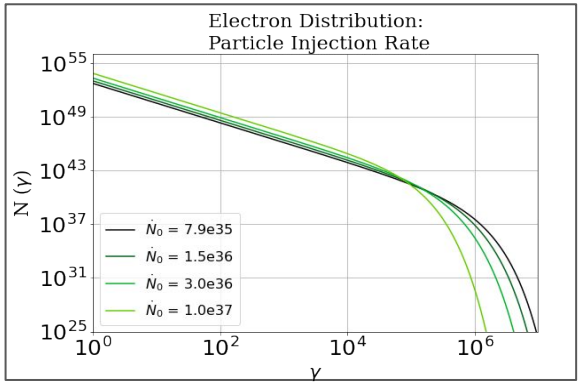

Particles may originate from near the black hole.

~ maybe Accretion disk?

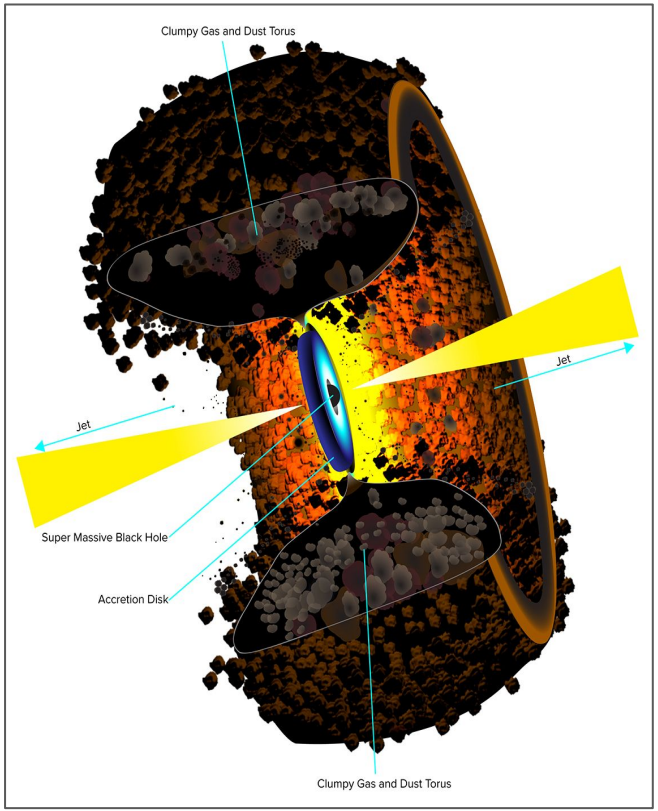

Parameter Study: Variability Timescale & Doppler Factor

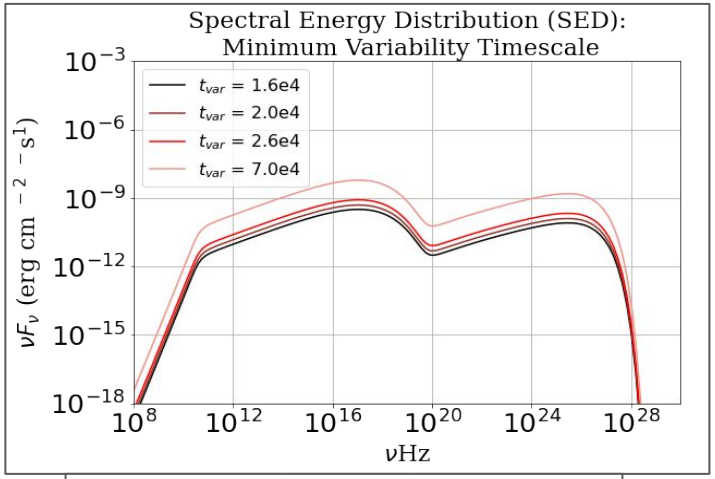

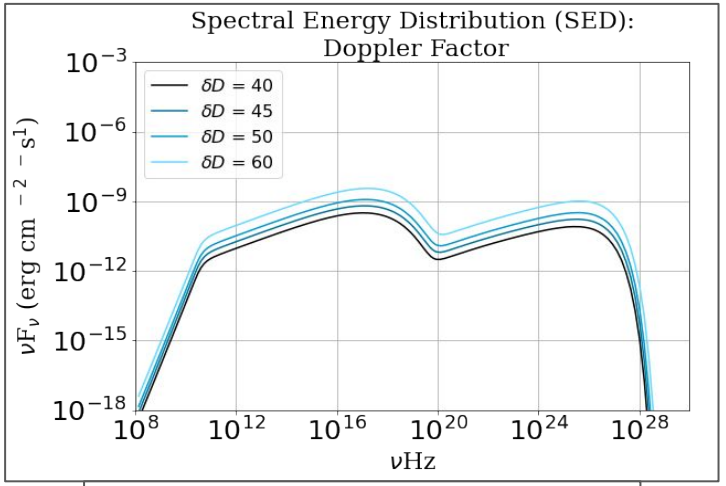

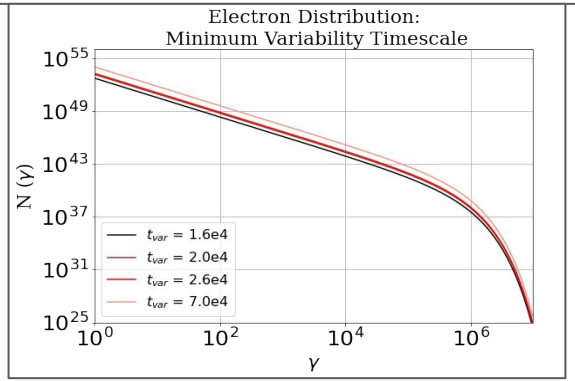

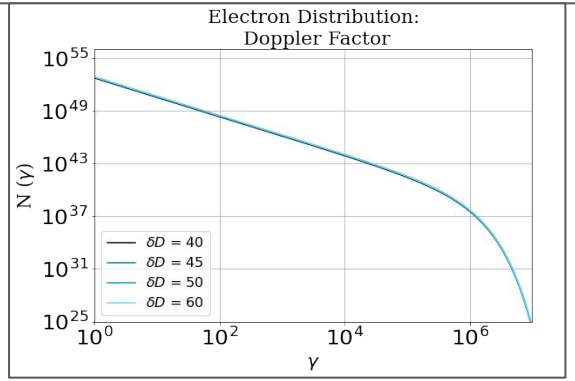

Parameter Study: Fermi-II Acceleration

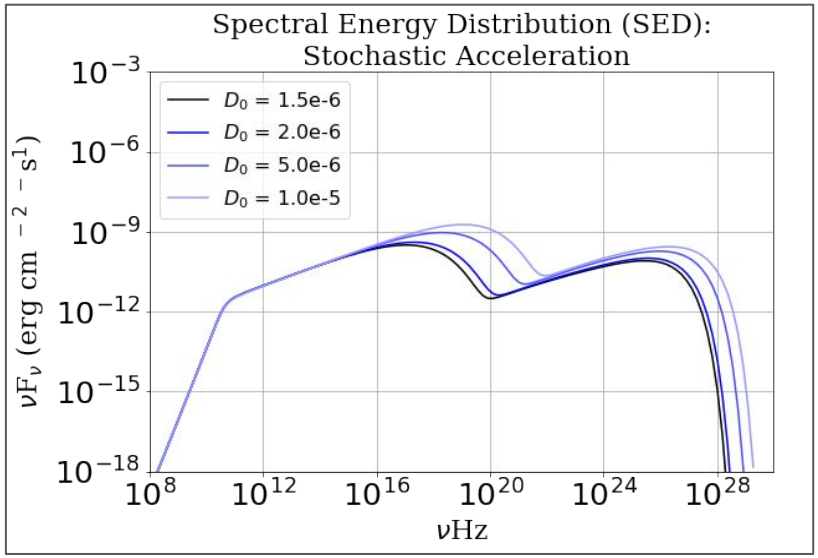

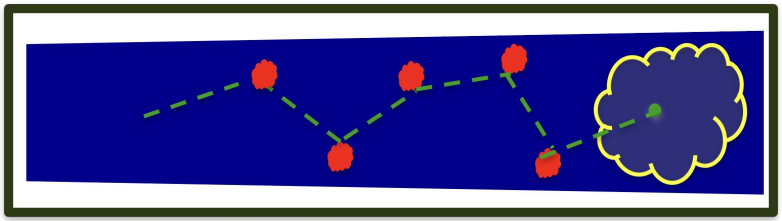

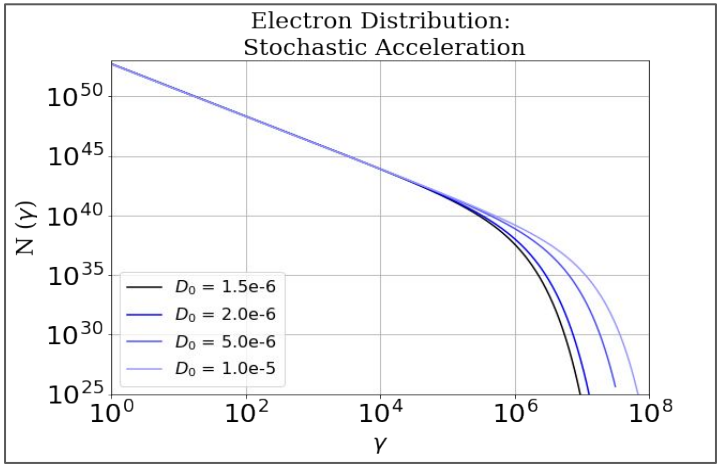

Particles always gain energy from stochastic scatterings in the head-on approximation due to the bulk motions in the jet.

Parameter Study: Fermi-I Acceleration

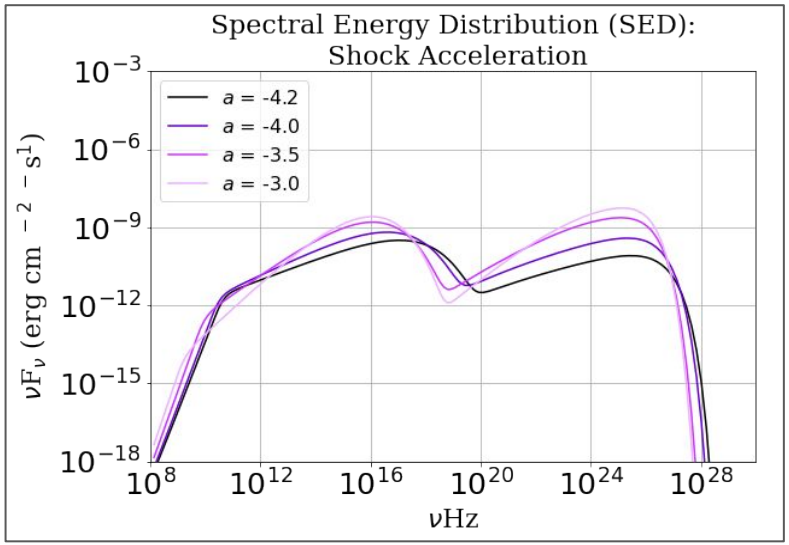

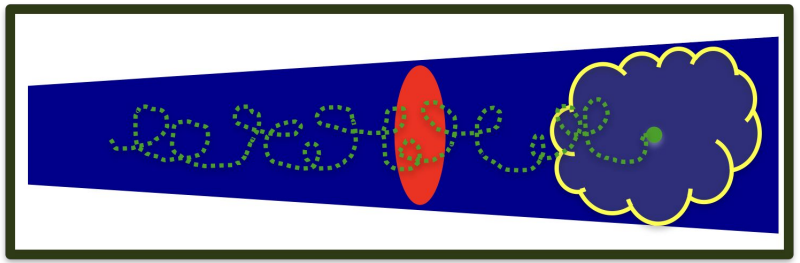

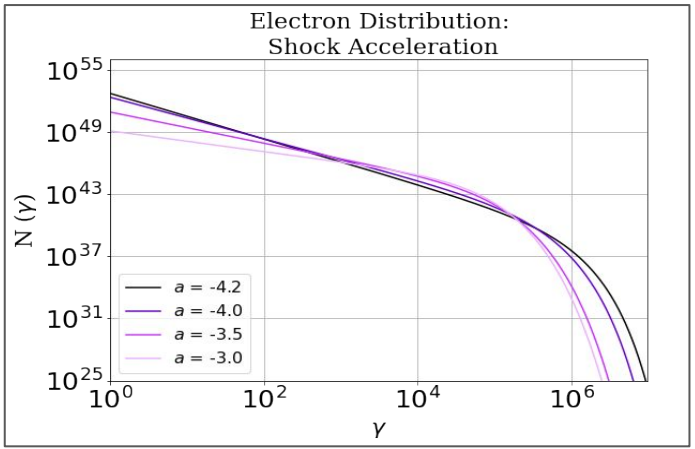

Particles gain energy from shock crossings in proportion to the energy they already have, and can pass through a shock region multiple times

Parameter Study: Magnetic Field

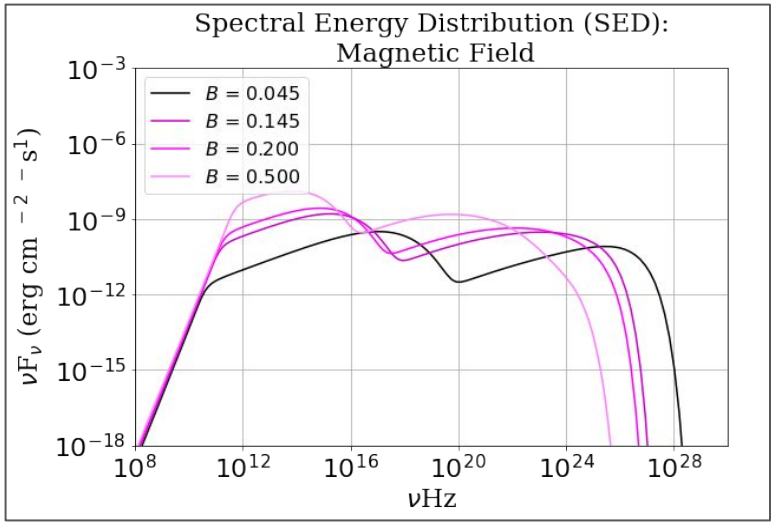

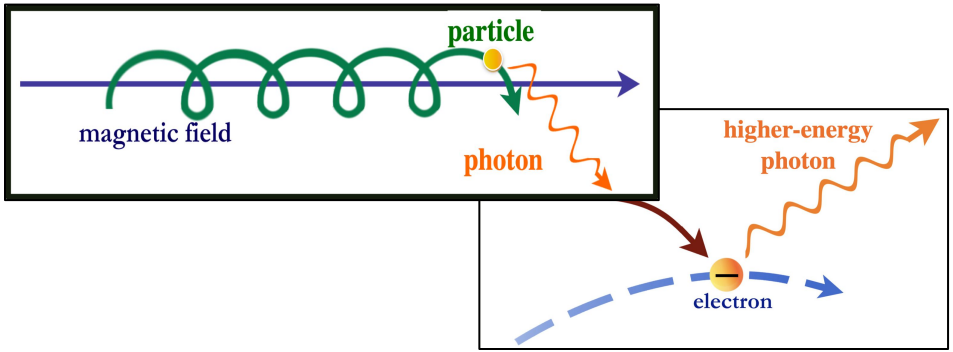

- Synchrotron emission
- Synchrotron Self-Compton (SSC) emission

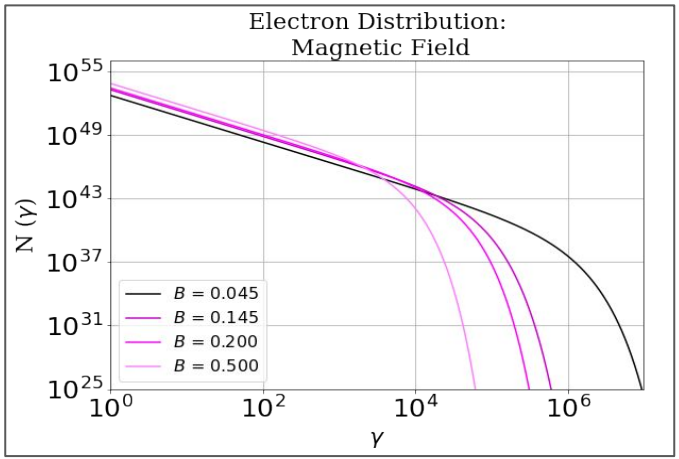

New Multiwavelength Campaign: Preliminary Light Curve

TeV γ-rays

GeV γ-rays

X-rays

UV / Optical